Master thesis : Deepwater Mooring Analysis for a 15 MW Seme-submersible FOWT located at the Morro Bay Wind Energy Area, California

Auteur : Taze, Ibrahim Engin
Promoteur(s) : 18519
Faculté : Faculté des Sciences appliquées
Diplôme : Master : ingénieur civil mécanicien, à finalité spécialisée en "Advanced Ship Design"
Année académique : 2021-2022
URI/URL : http://hdl.handle.net/2268.2/16568

Deepwater Mooring Analysis for a 15 MW Semi-submersible FOWT located at the Morro Bay Wind Energy Area, California

submitted on 31 August 2022

by

TAZE Ibrahim Engin | 3108 Castle Heights Av. | 90034 Los Angeles | California | USA |
engin.taze@alumnos.upm.es
Student ID No.: S202982

First Reviewer:

Prof. Hervé Le Sourne

ICAM

35, Avenue du champ de manœuvres,

44470 Nantes,

France

Second Reviewer:

Dr. Tomás López Olocco

UPM

Av. de la Memoria, 4,

28040 Madrid

Spain

EMship+
Advanced Design

CONTENT

LIST OF FIGURES

LIST OF TABLES

DECLARATION OF AUTHORSHIP

I declare that this thesis and the work presented in it are my own and have been generated by me as the result of my own original research.

Where I have consulted the published work of others, this is always clearly attributed. Where I have quoted from the work of others, the source is always given. With the exception of such quotations, this thesis is entirely my own work. I have acknowledged all main sources of help. Where the thesis is based on work done by myself jointly with others, I have made clear exactly what was done by others and what I have contributed myself.

This thesis contains no material that has been submitted previously, in whole or in part, for the award of any other academic degree or diploma.

I cede copyright of the thesis in favor of the Polytechnic University of Madrid (UPM) and the University of Liege (ULiège)

Date: 31.08.2022   Signature:

ACKNOWLEDGEMENTS

x

ABSTRACT

Mooring cables are crucial components of Floating Offshore Wind Turbine (FOWT) platforms. This study aims to analyze the mechanical behavior of a mooring system that is designed for a state-of-the-art floating offshore wind turbine structure that will operate in a deep-sea location ($> 1000\ m$). To achieve this, the loading demands have been characterized by the environmental conditions of a specific region on the coast of central California (Morro Bay wind energy area). Afterward, these loading demands have been used to examine the long (fatigue) and short-term responses of the mooring system through high-fidelity coupled fluid-structure computational simulations followed by vortex-induced vibrations and multi-objective optimization studies.

The proposed study begins with a brief presentation of the environmental, structural, and theoretical aspects of the mooring analysis. It is followed by an appraisal of various commercial and open-source simulation tools. Benchmark problem design and simulations have been carried out with a few software for different parts of the study. Firstly, a basic design demonstration has been made to cover the key concepts. A 5 MW spar type FOWT (Hywind) has been used as a reference. Uncoupled time domain analyses have been conducted in AQWA (ANSYS). Afterward, a preliminary mooring system has been designed for the state-of-the-art 15 MW semi-submersible (UMaine VolturnUS-S reference platform) floating offshore wind turbine. Then, coupled dynamic time domain simulations have been carried out in OrcaFlex (Orcina). Guidelines of the American Bureau of Shipping (ABS) and American Petroleum Institute (API) have been followed for the design and analysis of the mooring system. Pre-processing, processing, post-processing, and automation of these simulations have been explained. Results for the initial mooring design showed that the lines were over-conservative for the short-term damages, however, fatigue simulations showed that the upwind mooring line cannot reach the design life. Moreover, a 2D computational fluid dynamics (CFD) study has been conducted in Lily Pad software (Weymouth) to present the vortex-shedding characteristics for the designed mooring system in the ocean current. This part of the study aimed to highlight the vortex-induced phenomenon, which contributes to fatigue damage in the mooring systems. Finally, a multi-objective optimization study has been made with OrcaFlex and modeFRONTIER (ESTECO SpA) coupling via Python scripts. The purpose of this part of the study was to increase the fatigue life of the upwind mooring line. Initial solution sets presented high platform offsets; however, several improvements have been proposed for complete optimization.

1 INTRODUCTION

Energy crises and sustainable development are some of the main current global changes around the world. The emergency of climate change calls for a quick change of traditional energy solutions to replace them with renewable energy technologies. The global goal by 2050 is to supply 70% to 85% of the total energy must be supplied from renewable technologies (Vanegas-Cantarero et al., 2022) to limit global warming by 1.5 °C (IPCC, 2022). Thus, countless projects are in development for innovative solutions and target efficiency enhancements for renewable energy technologies.

Currently, 40% of the world population (around 2.4 *billion* people) are living within 100 *km* of the coast (Bennett, 2019). Therefore, offshore (and onshore) renewable energy solutions are good options for the mitigation of climate change. The main ocean energy sources are currents, waves, and wind. According to Petracca et al., (2022), the theoretical potential ocean energy resource is more than double the current global demand.

In the last two decades, wind power has seen spectacular growth (Zhu et al., 2022). According to the yearly report of the Global Wind Energy Council, in 2021, around 94 *GW* of wind power was added, and global cumulative wind energy surpassed 837 *GW*, which corresponds to 12% yearly growth (GWEC, 2021).

Of the various possible options of wind energy solutions, floating offshore wind is a strong energy source (IRENA, 2016). State-of-the-art for wind energy is the floating offshore wind turbines due to their numerous advantages which are further explained in the following chapters.

The Bureau of Ocean Energy Management (BOEM) in the United States published candidate geographical areas for offshore wind energy development on the United States coasts. Various projects are under development for locations with high potential for both the East and the West coast of the US.

On the West Coast, the Morro Bay energy area is one of the aforementioned areas. This area is significantly deeper (>1000 *m* depth) than the average commercial offshore wind farms that have been built. Therefore, some engineering challenges are present in this project. The project is in development, and it is not finalized at the time of this thesis. Thus, the study involves some assumptions regarding the possible project.

The focus of the thesis is to prepare a preliminary mooring system design study for a candidate floating offshore wind turbine structure that could be constructed in the given area. Since the

area is deeper than average commercial projects, the mooring system requires specific attention. Further chapters cover the preliminary design stages of the mooring system and mooring analyses.

To carry out these analyses, various considerations must be taken regarding the environment, structure, and simulation setup. Since the environmental parameters are the key contributors to the forces acting on the structure, adequate data must be found and utilized.

Moreover, state-of-the-art for floating offshore wind turbine structures must be followed since the floating wind technology is still in the development phase. There are many kinds of floating offshore wind structure designs with different numbers of columns and arrangements, it is important to choose a suitable structure for the area.

Another important aspect is to choose the simulation software with respect to theory, methodology, and the classification society (for this study, American Bureau of Shipping) rules and guidelines.

Afterward, simulations must be set with respect to the environmental data and classification rules. Mooring lines are crucial components for offshore structures. Therefore, there are specific standards and guidelines for carrying out the simulations and evaluating the simulation results. As mentioned, this study aims to carry out a preliminary design for a floating offshore wind turbine structure that is going to be located in the Morro Bay wind energy area. Therefore, the first few chapters have been dedicated to the required data for the mooring analyses and one chapter has been dedicated to the design of the floating offshore wind turbines to highlight some key design considerations that are connected to the mooring lines. Afterward, coupled dynamic analyses have been carried out for the limit state and fatigue life calculations. A small chapter was dedicated to the vortex-induced vibrations phenomenon which can contribute to fatigue damage. Finally, a multi-objective optimization was carried out to complete the preliminary design cycle for the chosen structure and the location.

2 MORRO BAY WIND ENERGY AREA PROJECT, CALIFORNIA

The Morro Bay wind energy area (Fig. 1) is a designated area for an offshore wind farm project that is in development. The area is located about 20 *miles* from the coast of Cambria and San Simeon, Central California. The area covers around 807 km^2. (Hodgson, 2022)
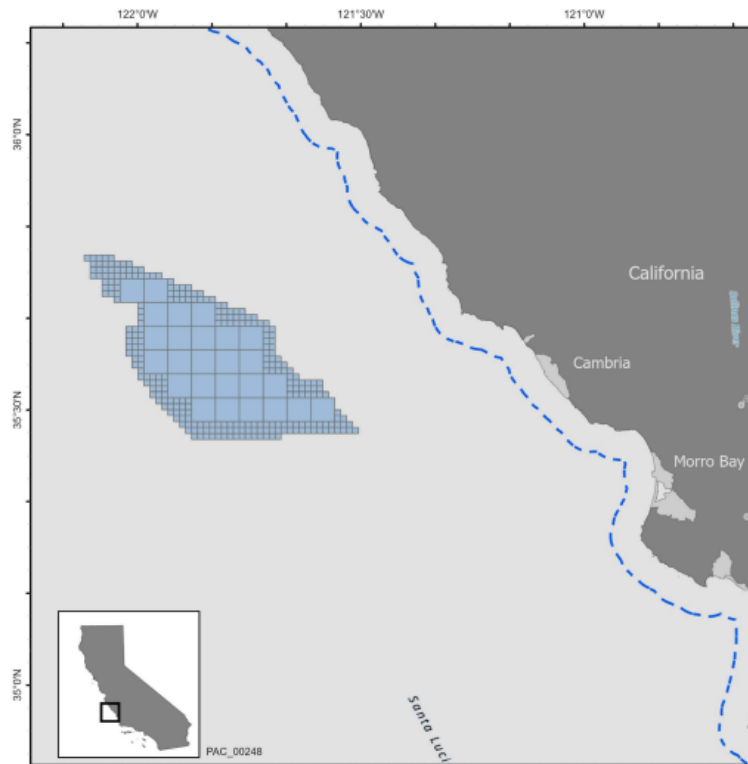
Figure 1. Morro Bay Area (BOEM, n.d.)

According to the scale provided by the Bureau of Ocean Energy Management (BOEM), the weighted average of the offshore wind potential for the Morro Bay Area is 8.01 out of 10, which corresponds to "excellent potential". It is expected that this area will support 787,771 houses annually with a 2.9 *GW* production goal. (BOEM & NOAA, n.d.-b)

2.1 Metocean Data for the Morro Bay Wind Energy Area

The mean depth of the target area is around 1 *km* (1046 *m*). There is not much data available about the seabed topology at the time of this report, however, in general, Pacific slopes are steeper than the Atlantic slopes (Britannica, n.d.). In the following chapters, oceanographic data for the Morro Bay area that is going to be used in the analyses have been divided into categories.

The main sources of the metocean data are MarineCadastre ocean reports, National Oceanic and Atmospheric Administration (NOAA), and the COREWIND project (2019).

MarineCadastre tool is developed by BOEM and NOAA. Users can either review the available ocean reports for numerous locations or draw custom areas to have an overview of Metocean data and offshore wind potential for a desired location on the US coasts.

The COREWIND (cost reduction and increase performance of floating wind technology) project, on the other hand, is an EU-funded project that targeted cost reductions and investigated performance enhancements by detailed mooring and anchoring system optimizations along with dynamic cables. Their reports are publicly available and one of the target locations is the Morro Bay wind energy area. (COREWIND, 2019)

2.1.1 *Wave Conditions*

In simple terms, significant wave height approximately corresponds to the highest one-third of the waves in the desired location and a given period. It is a major characteristic parameter of the statistical distribution of ocean waves. Also, it is a wave climate index at the local level. (BOEM & NOAA, n.d.-a) Below, Fig. 2 represents the wave rose which belongs to the Morro Bay wind energy area.
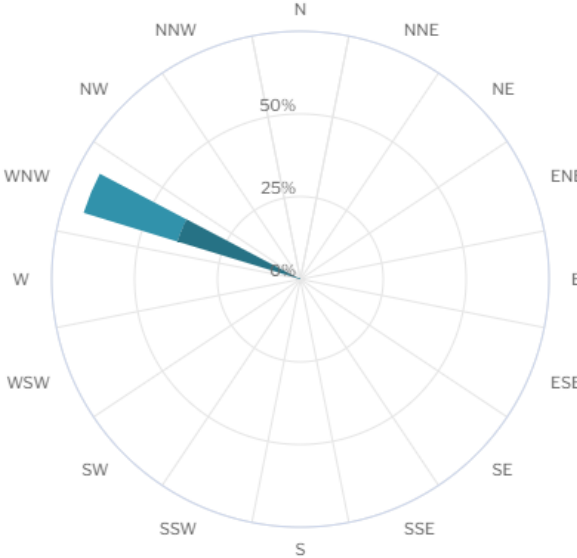
Figure 2. Wave rose (BOEM & NOAA, n.d.-a)

National Renewable Energy Laboratory (NREL) and Virginia Tech. have developed a resource assessment project and created a dataset underneath. They derived this dataset to obtain the significant wave height and direction. Required data was created by using monthly averages of the climatological data between 1980 to 2009. (BOEM & NOAA, n.d.-a)

4

2.1.2 Prevailing Wind Speed and Direction

Winds that have consistent flow in a particular direction over a region are defined as prevailing wind (Hanania et al., 2019). The following Fig. 3 represents the wind rose which shows the direction of the wind and the wind speed in the Morro Bay area.
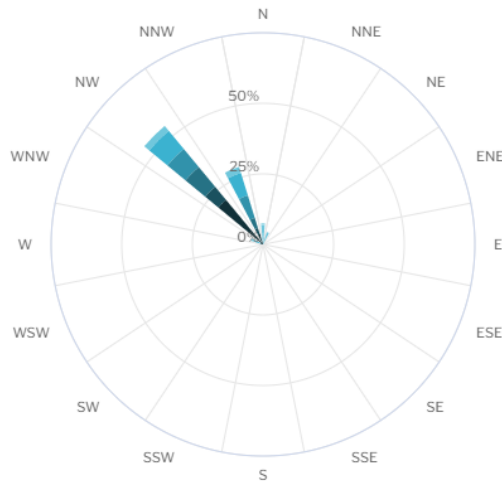
Figure 3. Wind rose (BOEM & NOAA, n.d.-a)

To create the wind rose in Fig. 3, monthly climatological average data files between 1979 to 2010 were used. The derived data comes from the Climate Forecast System Reanalysis (CFSR) dataset. (BOEM & NOAA, n.d.-a)

2.1.3 Current Speed and Direction

Ocean currents are continuous, directed, and predictable flows of seawater driven by water density, wind (Coriolis Effect), and gravity (National Geographic Society, n.d.). The current rose is provided in Fig. 4.
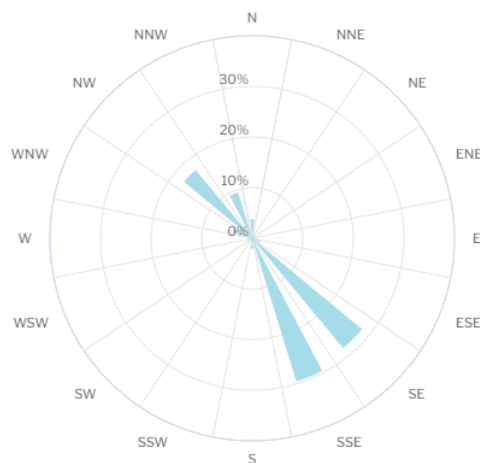
Figure 4. Current rose (BOEM & NOAA, n.d.-a)

The data required to create the current rose were derived from the Navy Coupled Ocean Data Assimilation (NCODA) and Hybrid Coordinate Ocean Model (HYCOM). Fig. 4 shows annual average values. (BOEM & NOAA, n.d.-a)

2.1.4 Water Properties

Water properties such as water temperature and salinity values are important for the simulations. The MarineCadastre Ocean Reports show that the water temperature and the salinity values are varied with the depth (BOEM & NOAA, n.d.-a). Therefore, the average value of the water temperature and the salinity between the sea surface and the mean depth of Morro Bay Area which is around 1-1.05 *km* has been found from the provided reports. The average salinity has been calculated as 34.16 *PSU* and the average temperature is calculated as 6.2 ℃.

2.2 Seabed Conditions

According to the U.S. Geological Survey surficial sediment database, the surficial sediment texture of the area is 80% mud and 20% mud & sand mixture (BOEM & NOAA, n.d.-a). The technical report that NREL published in April 2022 is provided below in Fig. 5, an average of 1° seabed angle has been found appropriate for the simulations.
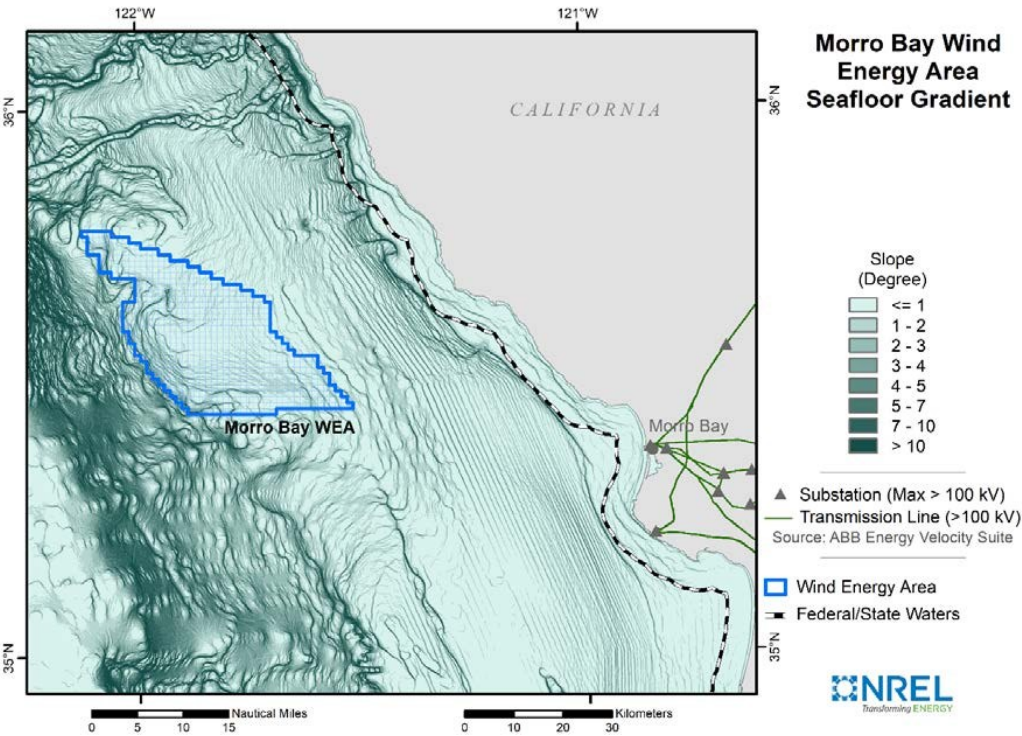
Figure 5. Seafloor gradients of the Morro Bay WEA and surrounding region (Cooperman et al., 2022)

3   FLOATING OFFSHORE WIND TURBINES

Offshore winds are stronger and have directional consistency when compared to onshore winds. For this reason, fewer wind turbines are needed for the same energy production at offshore wind farms (McCloy, 2019). This is the main reason for floating offshore wind farm constructions. Additionally, they are more advantageous in terms of visual impacts, land, and land transportation requirements, also it is easier to increase the scale of the turbines for economic benefits (X. Wang et al., 2018).

Currently, the Levelized Cost of Energy (LCOE) is decreasing each year for the FOWT with technological development. Offshore wind LCOE has declined by 28% to 51% between 2014 and 2020, it is also anticipated that this trendline of decrease will be continued in the future therefore it is predicted that the availability will be much higher (Wiser et al., 2016).

In simple terms, Floating Offshore Wind Turbines (FOWT) are composed of wind turbines that are located on top of floating structures. These floating structures are stabilized by their adequate mass and weight distribution by their structural design and by mooring lines and anchors which fixate the structure to the ocean bottom. Stability is crucial for energy harvesting. For an efficient energy harvesting process, the movement of the FOWT should be minimized. There are different design solutions for FOWT structures that aim for enhanced efficiency (IBERDROLA, n.d.). These different types are further analyzed in the next chapters.

3.1   Floating Offshore Wind Turbine Structure Types

In general, there are many custom designs for FOWT structures, however, these designs can be analyzed under four main concepts. Four main FOWT foundation types are widely used in the industry, which are Barge, Semi-submersible, Spar, and TLP (Tension-Leg Platform). The following Fig. 6 represents these types (Ha et al., 2021). A summary is provided in Table 1 for different design concepts.

Semi-submersible structures contain multiple pontoons and columns. These columns provide stability to the structure while the pontoons provide additional buoyancy. It has numerous applications in the industry, generally starting from 40 *m* of depth. It is the most common type of floating offshore wind turbine in the industry. The installation and transportation processes are simple when compared to the Spar and TLP types. In general, the cost of the anchoring system is cheaper than the cost of the TLP type. (Tacx, 2019; Du, 2021)

The Barge structure is an extension of the Semi-Submersible type. The shell of the hull is made from steel or concrete. A shallow draft design is present which supports the wind turbine. The floating barge contains a square and ring-shaped floating platform with a central pool to absorb the wave loads and dampen the motions. As a result of the shallow draft design, transportation and installation are easy for this type. (Chuang et al., 2021)
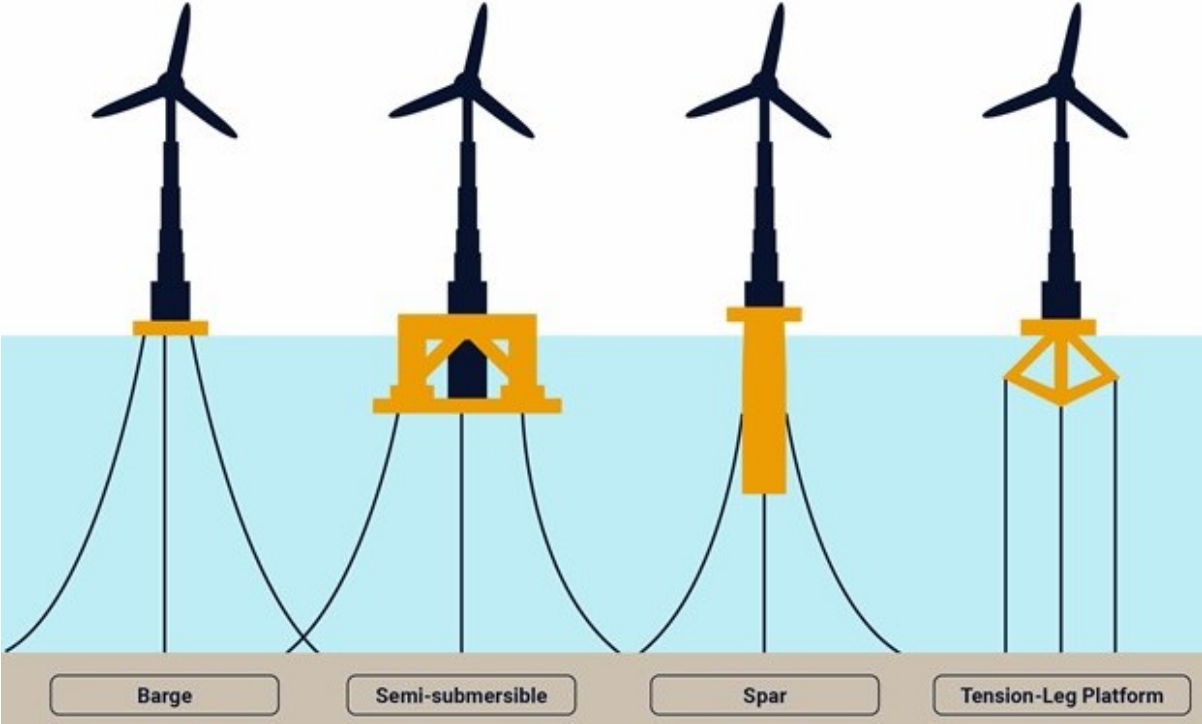
Figure 6. FOWT structure types (Hankins, 2021)

The Spar type is a vertical buoyant cylinder with a large diameter. It contains ballast at the bottom to provide stability with the draft. In general, the "deep draft" design of the Spar type makes it more stable when compared to the Semi-submersible. The configuration is simpler than all the other types and anchoring system costs are generally lower than TLP. However, because of the deep draft design, transportation and installation processes are more complex for the vessels, and it is not useable for shallow water depths, it is functional for water depths deeper than $100\ m$. (Tacx, 2019; Du, 2021)

The TLP type also contains pontoons and columns. These columns have a unique structure for this type. The mooring arrangement and the system for the TLP are unique as well, which are made by vertical tensioned tendons. This provides stability to the structure; the motion is highly restricted. It is the most stable type of all. However, the high stiffness design makes the structure vulnerable to high-frequency dynamic loads which can produce resonance in heave and pitch

8

motions. These motions are extremely harmful to the structure. They may lead to fatigue damage in tendons or total structural failure. (Tacx, 2019; Du, 2021)

Table 1 summarizes the characteristics of the main archetypes of the FOWT structures.

Table 1. Comparison of the design concepts (Chuang et al., 2021)

	Spar	Semi & Barge	TLP
Water Depth (m)	>100	>50	>50
Nb. of Mooring Lines	3-4	3-5	5-7
Seabed Condition	Unlimited	Unlimited	Limited
Footprint	Large	Large	Small
Assembly	Offshore	Port-side	Port-side
Capital Expenditures (CAPEX)	High	Low	Medium
Technology Readiness Level (TRL)	8	7	4

3.2 Mooring Lines & Anchoring Systems

It was mentioned in the earlier chapters that because of the ocean topography on the west coast, the depth is bigger than the average commercial projects in northern Europe for the offshore wind areas. Therefore, mooring, and anchoring system design is of high priority for the Morro Bay Wind Energy Area.

3.2.1 Mooring Lines

The main purpose of the mooring lines in floating systems is to keep the structure at an adequate position to ensure efficient behavior under operating conditions, as mentioned in the earlier chapters, it is important for energy production for the FOWT, and to withstand the loads under extreme conditions of the marine environment (Azcona et al., 2017). Additionally, mooring systems are utilized in the installation stage of the FOWT for station-keeping (Ha et al., 2021). Mooring line components include wires, chains, anchors, buoys, etc. depending on the application. The chain is the commonly used material for depths up to 300 m, for deeper seas, wire ropes are more appropriate because of it is superior flexibility and lightness. The synthetic fiber rope is the lightest, and it is generally used in mooring systems in ultra-deep waters (>1500-2000 m) with a combination of other types. (Azcona et al., 2017)

The point where the platform and the lines are connected is called "fairlead". The fairlead location varies depending on the application. The most common configuration for the mooring lines is the catenary mooring system. A chain or cable is hanging underwater, the lines are relatively longer than the depth of water since some of the parts are laid on the seabed which affects the cost. Therefore, the only forces that the anchor experiments are the horizontal forces. On the other hand, in taut mooring systems, the lines are pre-tensioned, and the axial stiffness of the mooring lines mainly procreates the restoring forces. It has more linear stiffness compared to the catenary systems which allows a better platform offset control under mean load. Also, the mooring lines must be elastic enough not to avoid overloading under the platform motions induced by the waves. Semi-taut and taut mooring systems have shorter lines and less space on the seabed when compared to the catenary. Additionally, semi-taut mooring systems are used on some platforms. It is a hybrid between the catenary and the taut systems. (Azcona et al., 2017)

The following Fig. 7 represents the mooring line configurations.
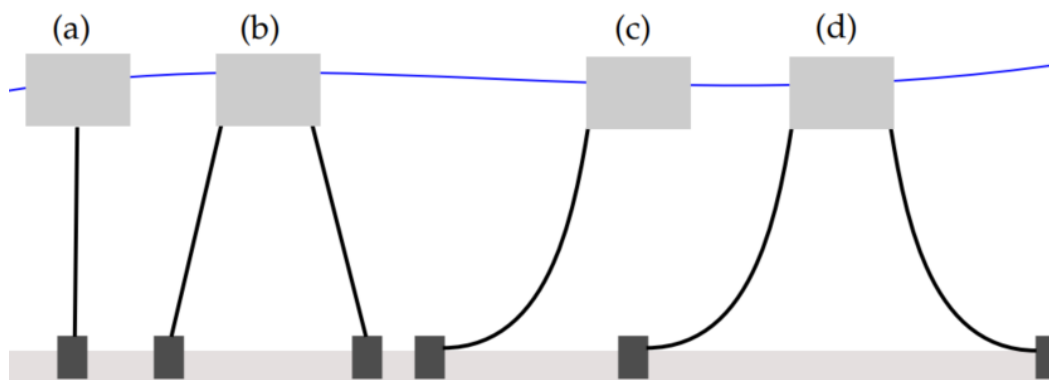
Figure 7. Taut (a,b) and Catenary (c,d) configurations (Davidson & Ringwood, 2017)

Another classification for the mooring systems is the number and distribution (Fig. 8) of the lines. Spread moorings are commonly used for offshore wind applications. It usually has a symmetrical distribution with several lines connected to the fairlead on multiple locations, the lines can be grouped or equally spread. This system limits the rotation due to wind, waves, and currents in the horizontal plane by maintaining an almost constant heading for the structure. Grouped mooring arrangements have superior redundancy characteristics against the failure of a line. There is also another approach which is called a single point mooring. Catenary Anchor Leg Mooring (CALM) and Spread Anchor Leg Mooring (SALM) are examples of this approach. It has stiffness against every horizontal motion which are displacements and rotation. A turret with bearings is sometimes used for the connection of all the mooring lines, the turret

allows the structure rotation. This configuration allows the system to minimize the loads in vigorous multi-directional environments by adjusting to the prevailing environment. Thus, it is mainly used when a prevailing direction is present. It is convenient for Wave Energy Converters (WECs).(Azcona Armendáriz, 2015)
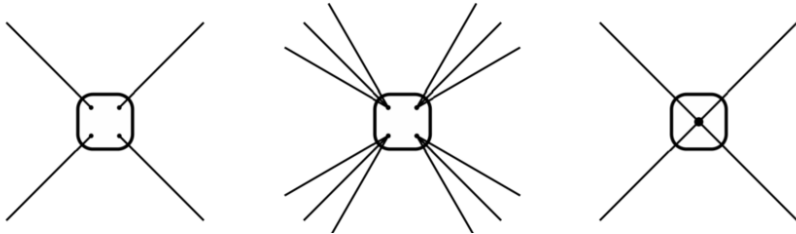
Figure 8. Respectively, equally spread, grouped spread, and single point distributions (Azcona Armendáriz, 2015)

3.2.2   Anchoring Systems

Anchors secure mooring lines and keep the structure at the desired position. They are located on the seafloor. Various types of anchoring systems are available for offshore applications, differences between them are how they achieve the capability to maintain the position. General criteria for the selection of anchoring systems are holding capacity, soil type, usage (relocation capability required or not), weight, (installation) equipment, directionality, and performance (Sound and Sea Technologies, 2009).
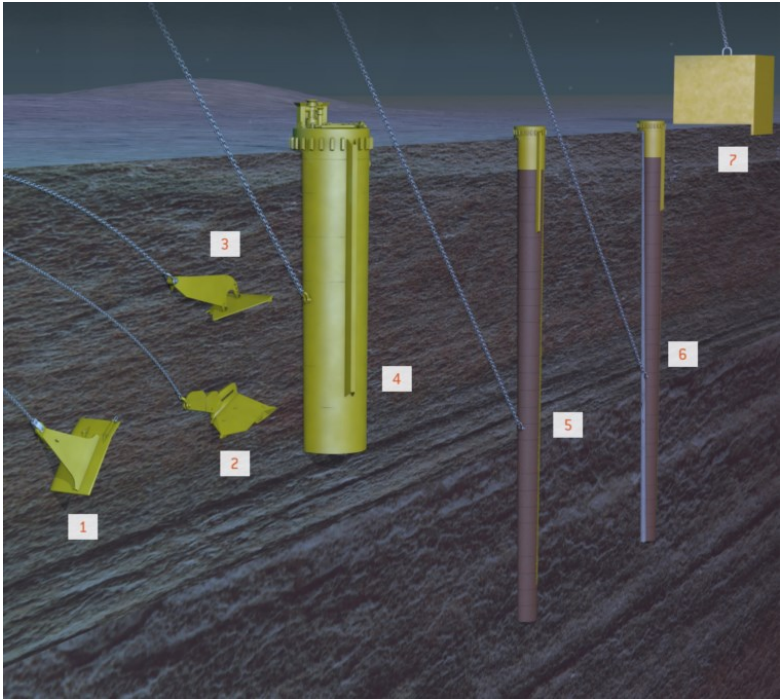
Figure 9. Anchor types (Acteon, 2021)

Different commercial anchor types are shown in Fig. 9, which goes as (1) suction embedded plate anchor (SEPLA), (2) drag vertical loaded anchor (VLA), (3) suction anchor, (4) driven anchor, (5 & 6) drilled & grouted anchor, (7) gravity anchor (Acteon, 2021; Weebly, n.d.). Performance characteristics of these anchor types in different soils have been summarized in Table 2 below, where the soil is divided into four categories as clay, sand, hard, and no sediment soil. VLC stands for the vertical load capacity of the anchor and precision stands for accuracy of the position. (Acteon, 2021)

Table 2. Comparison of the design concepts (Acteon, 2021)[1]

Anchor Type	Soil Type				VLC	Precision
	Clay	Sand	Hard	No Sediment		
SEPLA	***	*			***	***
Drag VLA	***				***	*
Drag Anchor	***	***	**			*
Suction Anchor	***	*			***	***
Driven Anchor	***	**	***		***	***
Drilled Anchor	*	*			***	***
Gravity Anchor	*	*	*	*	*	***

As stated in the earlier chapters, the surficial sediment texture of the Morro Bay Wind Energy Area is 80% mud and 20% mud & sand mixture. It can be concluded that the drag anchor is the best solution for the soil texture criterion, however, other criteria must also be considered to find the optimum solution with a good compromise between the cost and the performance.

In general spar and semi-submersible structures (taut or spread mooring) use suction or drag anchors, other types can also be used depending on the application. The TLP structures use driven piles. Deeply driven piles counteract high tension loads, mainly the vertical load components. TLP also uses gravity anchors depending on the application (Arany & Bhattacharya, 2018; Woellwarth, 2020).

Buoys and clump weights can also be important for the mooring. Buoys and clump weights can be utilized for mooring optimization. The research shows that they can significantly enhance the performance of the mooring system depending on the application (Neisi et al., 2022).

There are also other components that are generally used in the mooring application such as the connectors, swivels, shackles, sinkers, and fittings. These components cover general hardware

---

[1] Indicator (*) means fair performance, (**) means better performance, and (***) means the best performance.

that is used in the mooring systems. Connectors, swivels, and shackles are connecting elements. Sinkers and fittings, on the other hand, are typically used for positioning ships and offshore structures.

The following Fig. 10 summarizes the information given in this section.
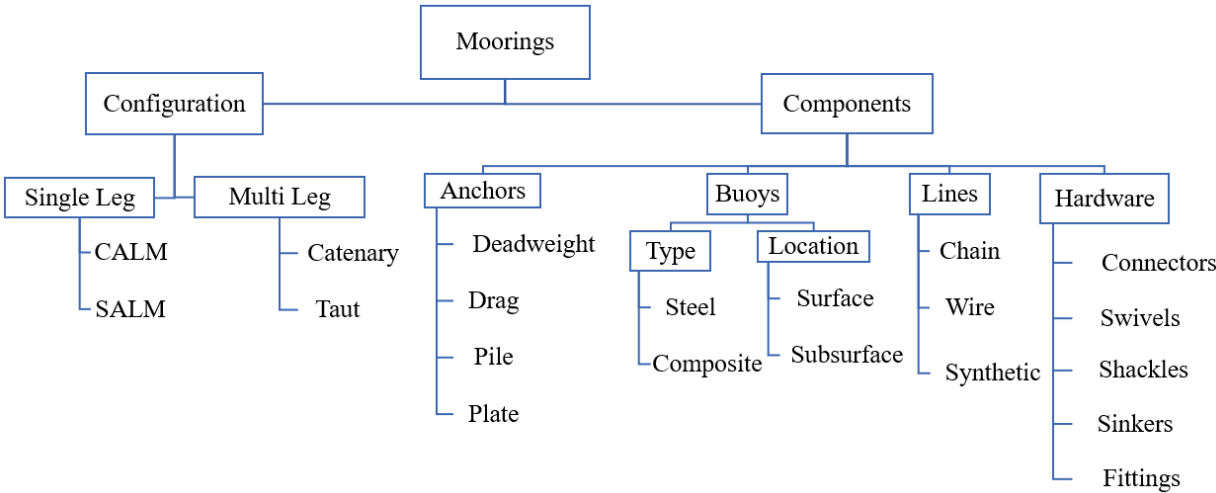
Figure 10. Mooring technology (Sound and Sea Technologies, 2009)

3.3 Selected FOWT Characteristics for the Analysis

Within the scope of this study, two different FOWT structures will be used. Firstly, a design application for a spar type FOWT was made for the NREL's 5 *MW* reference turbine (J. Jonkman et al., 2009) to demonstrate the basic design calculations, perform mooring analysis, and explain key design concepts that are important for the overall design and mooring system design processes. Ch. 5 explains this process in detail.

According to NREL's report for the Morro Bay Wind Energy Area, technology assumptions for the power of the turbines vary depending on the construction year of the project. The project is still in development and some details are not published at the time of this study, however, NREL's report suggests that 12 *MW* or 15 *MW* turbines will be used depending on the planned year of construction (Beiter et al., 2020).

Therefore, to follow the latest trend and have a state-of-the-art project, the International Energy Agency (IEA) 15 *MW* reference turbine (Gaertner et al., 2020) was found suitable for further analyses of this study (Ch. 6 to Ch. 9). Thus, a reference structure has been found for the semi-submersible type. This choice was based on the observation that semi-submersible substructures are the most common type, comprising 89% of all projects that have announced

their intended substructure type (Beiter et al., 2020), and around 75% of the projects that are being developed for the deep waters are designed as semi-submersible platforms (Hartman, 2021). The TLP type is disregarded in the study since the technology readiness level (TLR) is lower than the other types (Table 1).

3.3.1 Equinor Hywind 5 MW Spar Reference FOWT

In 2010, National Renewable Energy Laboratory (NREL) published a technical report which was prepared with the collaboration of the offshore company Statoil (now known as Equinor). In the study, a FOWT (Fig. 11) was modeled where the Spar substructure design of the Equinor named "Hywind" was merged with NREL's 5 *MW* reference wind turbine. This model has been selected for the study to demonstrate some basic calculations and to explain the concepts in further chapters. The model has a simple geometry and the simulation files as well as the technical reports, are public, thus, it is suitable for further explaining of some concepts, especially stability and hydrodynamics. (J. Jonkman, 2010)
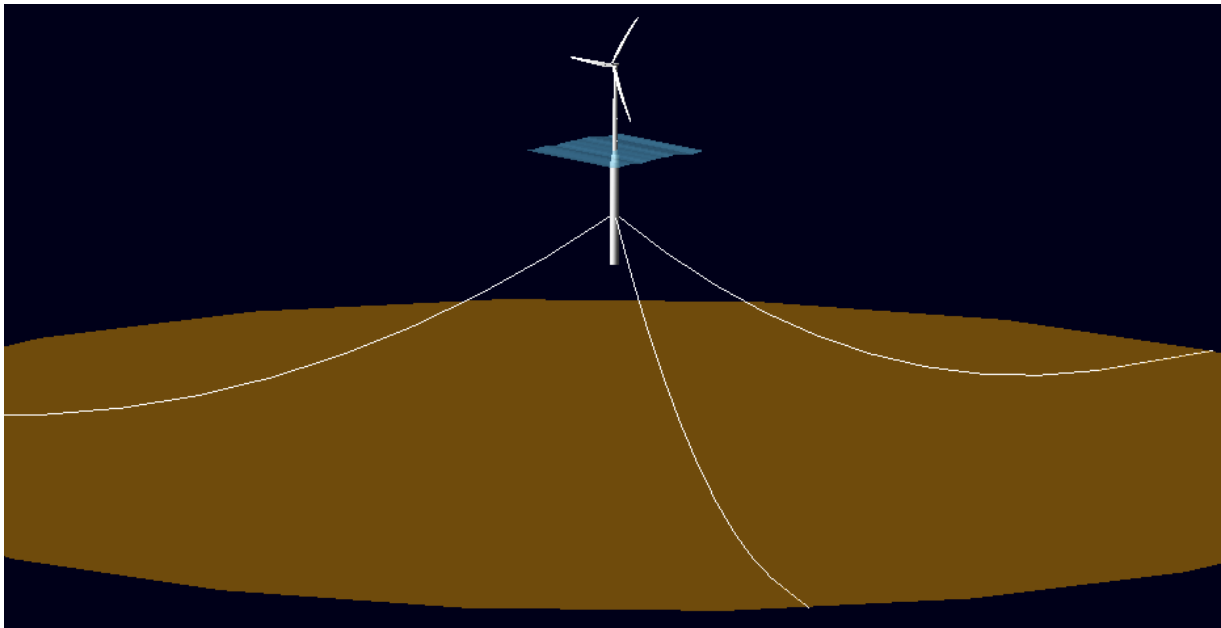
Figure 11. NREL 5-*MW* wind turbine on the OC3-Hywind spar (J. Jonkman, 2010)

3.3.2 UMaine VolturnUS-S IEA 15 MW Semi-submersible Reference FOWT

University of Maine Advanced Structures and Composites Center designed a platform named VolturnUS, and this platform was deployed by DeepCWind Consortium in the summer of 2013 as the first grid-connected offshore wind turbine in the United States. It was an innovative

14

design in terms of materials selection, construction, and deployment technologies that aimed to reduce the costs of offshore wind (Viselli et al., 2015).

In July 2020, NREL published a technical report of a semi-submersible FOWT which has the substructure design of the VolturnUS-S that is designed for the 15 *MW* Offshore Reference Wind Turbine design of the International Energy Agency (IEA). The following Fig. 12 represent the defined FOWT and the reference coordination system. (Allen et al., 2020)
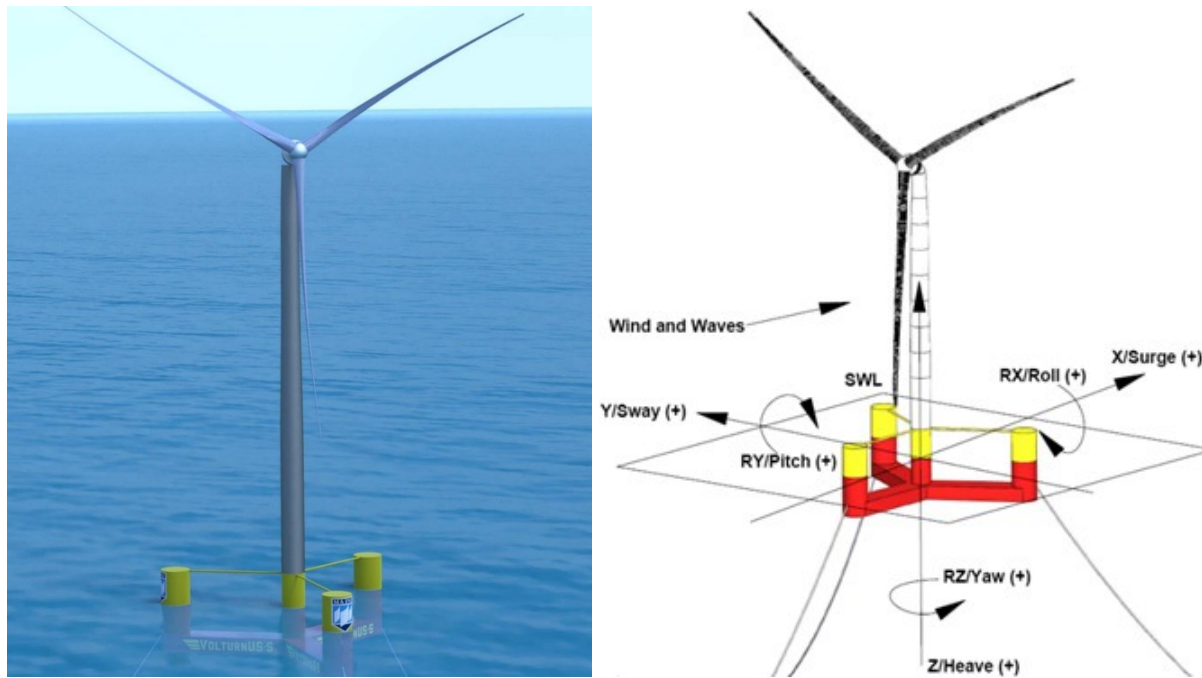
Figure 12. The UMaine VolturnUS-S 15 *MW* reference platform (Allen et al., 2020)

This platform is chosen for further analysis to develop a real case scenario for Morro Bay Wind Energy Area. In the further chapters, the mooring analyses and an optimization demonstration was explained with using different mooring parameters such as the fairlead angles, fairlead positions, anchor positions and line lengths. Simulation files and technical reports are also publicly available for this design which makes it suitable for verification. Detailed specifications will be provided in the further chapters.

4 MOORING ANALYSIS

Floating offshore wind turbines (FOWT) have remarkable operating and failure design conditions with combined effects from aerodynamic, hydrodynamic, and mooring-system dynamic effects. There are numerous ongoing projects for creating or developing an advanced methodology for coupled analysis of these effects (Matha et al., 2011). This chapter is dedicated to present brief information about the theory, methodology, and software for this study.

There are four main strategies for mooring analysis which are static, quasi-static, quasi-dynamic, and dynamic analysis. The main difference in the methodology comes from handling the wave frequency (WF) responses of the floating platform. The inertial and damping forces that are acting on the line are ignored in the quasi-static analysis. The shape of the mooring line and the tension distribution along the mooring line are functions of the top-end positions only. It is appropriate for calculating the mooring line response due to the mean offset and the low frequency (LF) motions. However, for the dynamic analysis, the time-varying fairlead motions are calculated. It becomes an input to the dynamic analysis of the mooring line, therefore, the time-varying effects due to added mass, damping, acceleration, and drag forces are intercepted adequately. Generally, the recommended practice is to perform dynamic analysis for mooring systems. The quasi-static analyses (Fig. 13) might be used for mooring systems if the WF impact is negligible. (Ma et al., 2019)
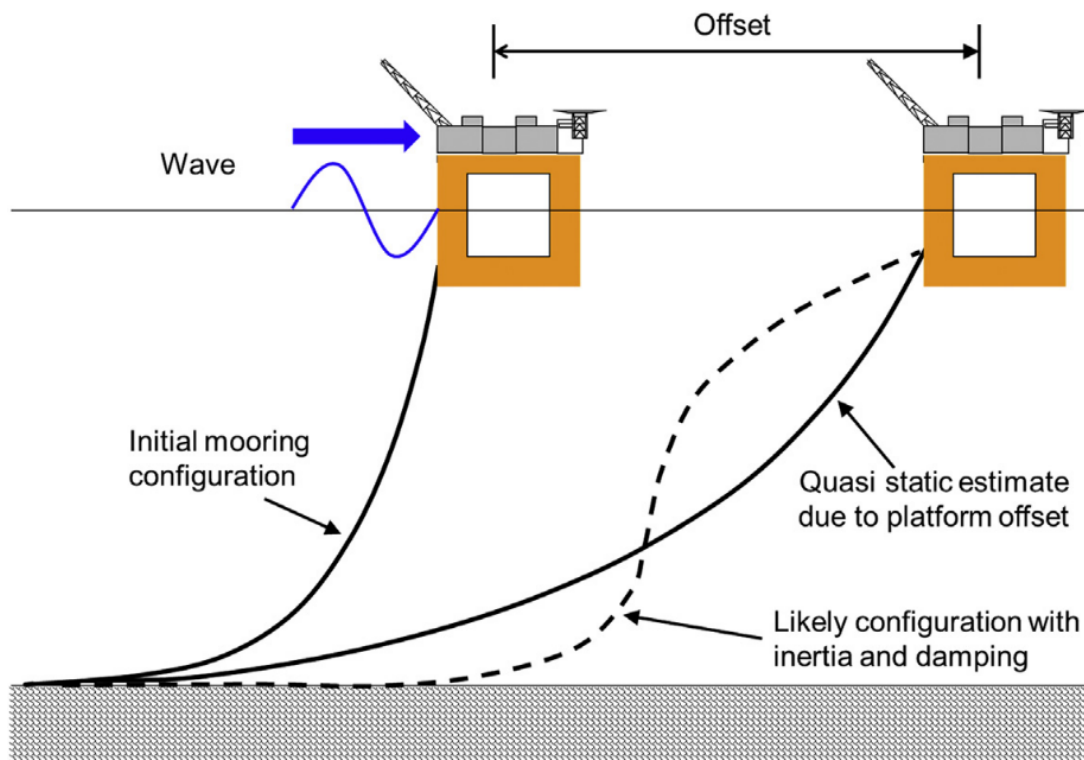
Figure 13. Difference between quasi-static and dynamic analysis (Ma et al., 2019)

4.1 Theoretical Background

It is important to understand the theory before selecting a tool for engineering analysis. Therefore, the following sub-sections are dedicated to giving brief information about the mathematical theory behind the mooring line analysis.

4.1.1 Governing Equations

To understand the configuration and tension mechanism of the mooring line, consider a small mooring line element in 2D (Fig. 14).
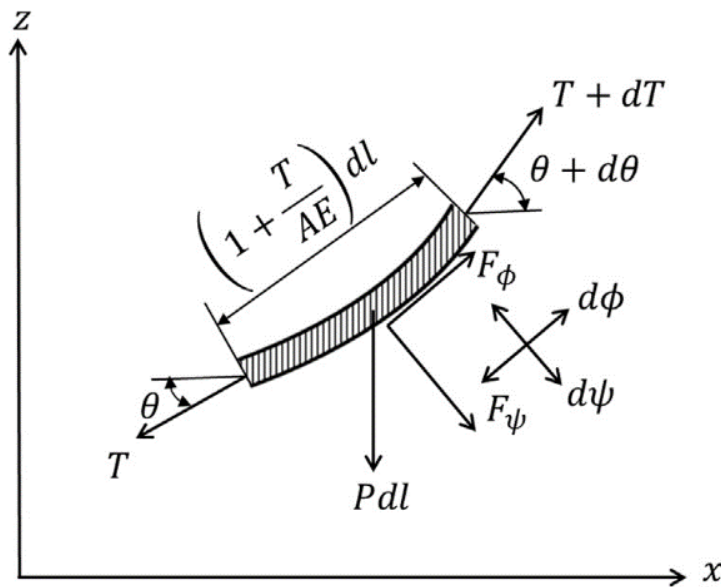
Figure 14. Force and displacement on an element of a mooring line (Ma et al., 2019)

Where T is the effective tension, P is the wet weight per unit length, *dl* is the length, and AE is the axial stiffness. Displacements are denoted as the *dϕ* for the direction tangential to the mooring line and *dψ(l)* for the direction normal to the mooring line. The torsional stiffness and the line bending terms are assumed to be negligible which is a proper assumption for line materials with a wide radius of curvature. (Ma et al., 2019)

Let F denote the hydrodynamic force acting on the mooring line element, where the mass is m, ψ and ϕ are the normal and the tangential components of the line, the following equations can be written:

$$-T + (T + dT) * cosd\theta + F_\phi * \left(1 + \frac{T}{AE}\right) dl = m\frac{d^2\phi(l)}{dt^2} \tag{1}$$

$$(T + dT) * dt - Pcosd\theta - F_\psi * \left(1 + \frac{T}{AE}\right) dl = m\frac{d^2\phi(l)}{dt^2} \tag{2}$$

Since the *dl* is an infinitesimal element, *cosdθ = 1*, *sindθ = 0*, and the *dTdθ = 0*. Therefore, the following equations can be written in the tangential and normal directions:

$$dT - Psin\theta dl + F_\phi * \left(1 + \frac{T}{AE}\right) dl = m\frac{d^2\phi(l)}{dt^2} \qquad (3)$$

$$Td\theta - Pcos\theta dl + F_\psi * \left(1 + \frac{T}{AE}\right) dl = m\frac{d^2\phi(l)}{dt^2} \qquad (4)$$

The hydrodynamic forces (F_ϕ *and* F_ψ) in equations (3) and (4) on a mooring element can be computed by various approaches e.g., solving the Navier-Stokes equations numerically by pressure integration for the determination of hydrodynamic forces or experimental methods can also be used. (Ma et al., 2019)

The common practice for the numerical tools in the industry is to use Morison Equations to calculate the hydrodynamic forces. In basic terms, they combine Morison equations for a fixed structure in moving waters and a moving structure in still water. (Ma et al., 2019)

Eqs. (3) and (4) are based on force dynamic balance. The (x, z) coordinate system has the following relationship with *(l,θ)*

$$dx = \left(1 + \frac{T}{AE}\right) cos\theta dl \qquad (5)$$

$$dz = \left(1 + \frac{T}{AE}\right) sin\theta dl \qquad (6)$$

From the change of coordinates, one can write:

$$d\psi = dz * cos\theta - dx * sin\theta \qquad (7)$$

$$d\phi = dx * cos\theta + dz * sin\theta \qquad (8)$$

Eqs. (5) to (8) are the governing differential equation for a mooring line along with the adequate boundary conditions, fairlead point, and seabed conditions. They cover both dynamics and elastics. These equations are nonlinear. Therefore, to solve them, numerical tools must be utilized, such as the finite element method (FEM). (Johansson, 1976)

4.1.2   Mooring Line Stiffness

A mooring line exerts a horizontal (T_H) and vertical (T_V) force respectively on the floating platform. If the offset of the platform (vessel drift) increases, then the mooring reaction (restoring) forces will increase as well. (Ma et al., 2019)

18
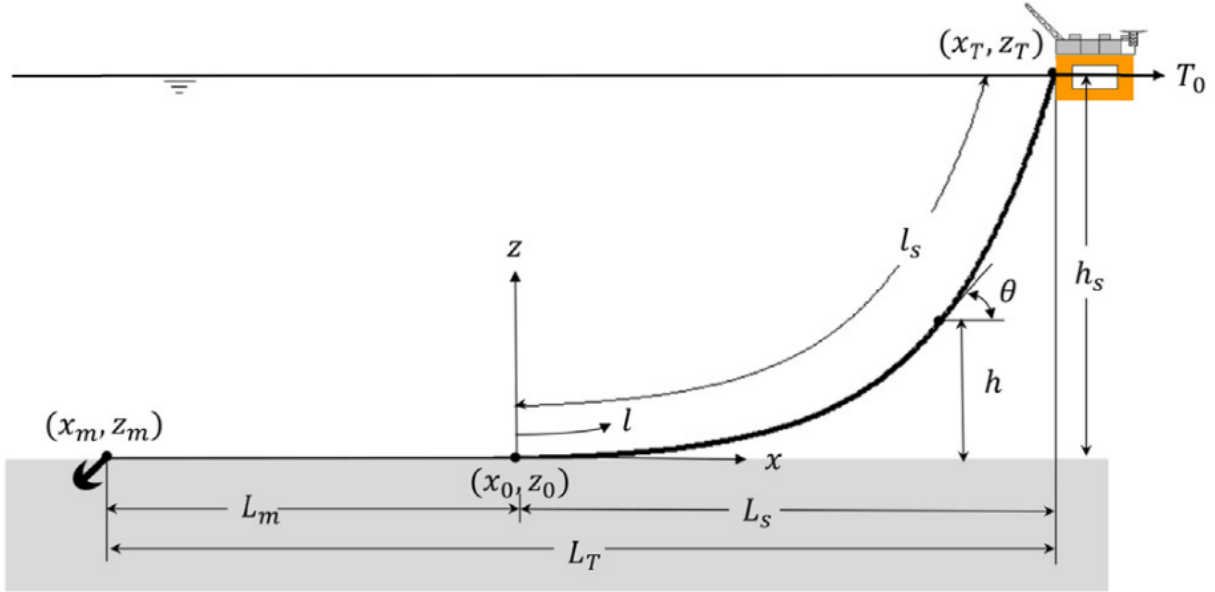
Figure 15. Catenary mooring geometry (Ma et al., 2019)

Mooring stiffness defines a proportionality between the displacement and the force. It is similar to a spring system. Tension increase at the line top will result in axial elongation and geometric deformation on the mooring line. Thus, mooring stiffness contains stiffness contribution from axial stiffness (AE) and geometric stiffness for quasi-static analysis. (Ma et al., 2019)
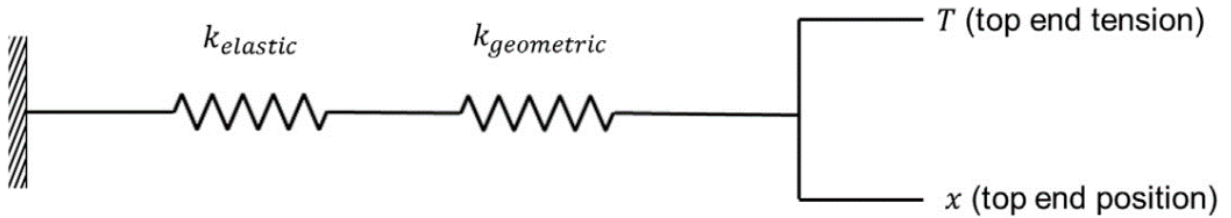
Figure 16. Quasi-static analysis of a catenary line (Ma et al., 2019)

The total stiffness of the catenary line can be expressed as,

$$\frac{1}{k_{Total}} = \frac{1}{k_{elastic}} + \frac{1}{k_{geometric}} \tag{9}$$

4.1.3   Mooring Line Dynamics

Mooring line tension caused by the wave frequency (WF) motion is described as:

$$M\frac{d^2r}{dt^2} + B\frac{dr}{dt} + K * r = F(r, t) \tag{10}$$

19

Where, M is mass (added mass included), B is damping, K is stiffness matrix, F is an external exciting force, and $r = (x,y,z)$ is displacement vector from the mean position. (Ma et al., 2019)
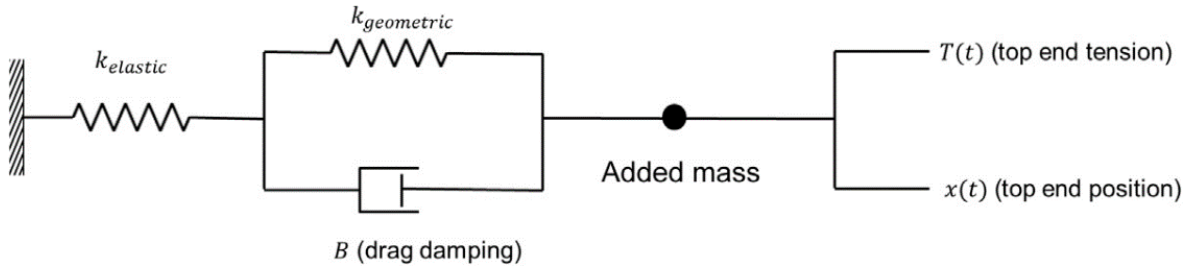
Figure 17. Dynamic analysis of a catenary line (Ma et al., 2019)

As mentioned, the FEM is a well-known method to solve mooring line dynamic equations.

4.1.4 Mooring Systems

If a mooring system with multiple lines connected to a floating offshore platform is considered, the motion of the platform in six degrees of freedom can be expressed as:

$$\sum_{j=1}^{6}\left[(M_{ij} + M_{aij})\frac{d^2\eta}{dt^2} + B_{Lij}\frac{d\eta}{dt} + B_{Qij}\left|\frac{d\eta}{dt}\right|\frac{d\eta}{dt} + K_{ij}\eta_j\right] = F_i \qquad (11)$$

Where "i" is the direction of the fluid force and "j" is the mode of motion. Surge, sway, heave, roll, pitch, and yaw motions of the platform are $i = 1,2,3,4,5,6$ respectively. B_L is the linear damping coefficient and B_Q is the quadratic damping coefficient. The right-hand side of Eq. 11 contains environmental forces (wind, wave, current, WF, and LF). On the other side, the added mass, damping, and stiffness from mooring lines should be considered. (Ma et al., 2019)

4.2 Software Selection

Various studies uncover that the mooring line dynamics significantly affect the tension of the mooring lines, fatigue, and extreme loads on the structure. Therefore, adequate simulation of the mooring system is crucial. (Azcona Armendáriz, 2015) Many commercial, open-source, and in-house software packages are available for mooring line analysis. For this study, more than 20 of these software packages had investigated.

Generally, software packages present similar specifications. Also, most of them are validated. Thus, it is reasonable that results for a target mooring analysis will be within the same range.

However, some of these software packages stand out from others. Therefore, a comparison was made within the available software.

Design standards are the major criteria for the comparison. In the standards, mooring lines are required to be analyzed using fully coupled analysis in the time domain, moreover, the software is required to be able to model the current and the wind in the vertical direction. Time-varying wind modeling is a requirement, however, for the current, it is only necessary to model a steady current velocity (Thomsen et al., 2017). Plenty of software packages can simulate hydrodynamics as well as the mooring models (Davidson & Ringwood, 2017).

4.3   Chosen Software

Of all the candidate software packages, AQWA (ANSYS, 2012), OrcaFlex (Orcina, n.d.), Lily Pad 2D CFD (Weymouth, 2015), and modeFRONTIER (ESTECO SpA, n.d.) have been found as the most suitable software packages for different parts of the study. AQWA was used for the basic design demonstration and explanation of some concepts. OrcaFlex and modeFRONTIER were used for the 15 *MW* semi-submersible FOWT mooring analysis and optimization. Lily Pad CFD software was used for study of the vortex-induced vibrations. Detailed explanation of these software will be provided in the following sub-chapters.

Some other software packages have been highlighted as well. The FLOW-3D® (Flow Science, 2019) and the OpenFAST (B. Jonkman et al., 2022) are also strong software for the desired coupled analyses.

4.3.1   *OrcaFlex*

OrcaFlex is a general-purpose software package suitable for a wide range of global dynamic analysis applications. For offshore wind applications, OrcaFlex can couple the hydrodynamics with a built-in aerodynamic turbine model, giving a fully-coupled-dynamic analysis tool suitable for both fixed and floating platform offshore wind turbines. Its analysis applications include mooring systems, platform motion, and power cable design. A fully coupled dynamic mooring analysis can be made for FOWT structures.

OrcaFlex offers various analysis methods such as frequency, quasi-dynamic time domain, and nonlinear finite element (FE) analysis in time domain. The software uses the Morison approach to calculate wave loads. The input is needed (RAOs and quadratic transfer functions (QTF)) for

radiation-diffraction loading. OrcaFlex solves tension, bending, and torsion using a discrete lumped mass approach which will be explained further. (Orcina, n.d.)

4.3.2 FEM and Lumped Mass Approach

As mentioned earlier, dynamic effects (inertia, added mass, hydrodynamic drag) are considered in the dynamic model of the mooring lines. In time-domain analysis, the dynamic equations of the system are numerically solved, and the mooring line is discretized by several elements. Therefore, various formulations have been developed to deal with the dynamics of the mooring line, like the FEM, finite difference method (FDM), or multi-body models. In typical FEM, mass is distributed along the entire element. A variation of the FEM is the lumped mass (LM) model, where the element's adjacent nodes have the concentrated mass, therefore, nodes are treated as springs and point masses. Despite the methodology, most models converge to similar results when adequate finite discretization is used. However, various studies show that lumped mass approach is computationally efficient for the mooring line analysis, therefore it is widely used in software packages. (Wendland & Schulz, 2005; Masciola et al., 2014; Hall & Goupee, 2015; Cevasco et al., 2018; Rodríguez Luis et al., 2020)

4.3.3 ANSYS AQWA

AQWA is an integrated system developed for hydrodynamics and mooring line analysis. It investigates the effects of wind, waves, and currents on marine structures. It can compute the second-order wave forces using full quadratic transfer function matrices; therefore, it can be used for a wide range of water depths. Additionally, it can be coupled with other ANSYS modules for detailed structural assessments. It can perform time-domain dynamic analysis for floating offshore wind turbines with a broad range of physical connections (mooring lines, fenders, weights, etc.). (ANSYS, 2012) This software will be used for the uncoupled analysis in the basic design demonstration.

Finally, it should also be noted that these software packages can be coupled with each other. One can use OpenFAST for aero-servo-elastics and couple it with OrcaFlex for hydrodynamics (Masciola et al., 2011; BSEE, 2015). Another example is from the study of Hasanvand & Edalat (2021), in the study, AQWA was used to find hydrodynamic response characteristics and the outputs were imported to the OrcaFlex for fatigue assessment.

4.3.4   Lily Pad CFD for Vortex-Induced Vibrations (VIV)

Vortex-Induced Motions (VIM) are the rigid body motions in moored structures such as TLP, Spar, or Semi-submersibles which have large oscillation periods. Vortex-Induced Vibrations (VIV) are for slender bodies such as cables and pipelines. VIM (Fig. 18) and VIV are important topics for offshore structures. The main reason behind VIM and VIV is the occurrence of vortex shedding. For the offshore structures, when the ocean flow current interacts with the body, vortex shedding may occur; irregular crossflow forces occur on a body. Lock-on issues may occur if the vortex shedding, and natural frequencies of the body motions approximate each other. It means that the vortex shedding and the oscillations of the body in the transverse direction synchronize, which results in motions with large amplitudes. Therefore, VIM and VIV must be assessed for the fatigue life calculation of the mooring lines. (Williamson & Govardhan, 2004; da Silveira et al., 2007; Fujarra et al., 2012; BSEE, 2015)

This study focuses on the mooring line analysis; however, a 2D CFD assessment will be carried out for the mooring system.
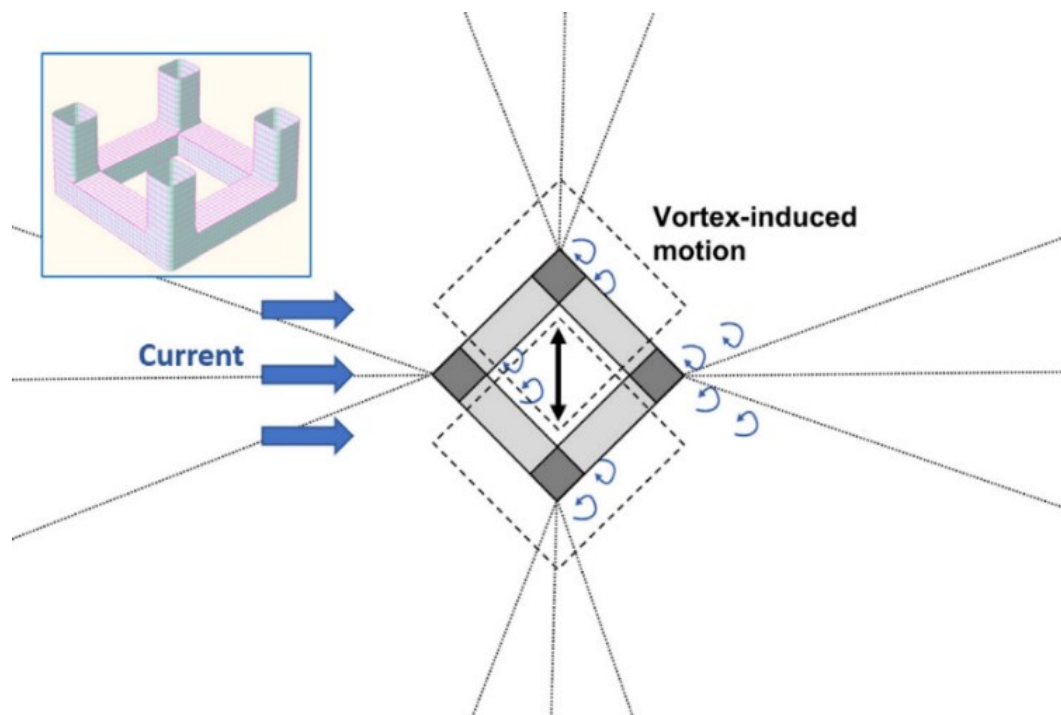
Figure 18. Semi-submersible experiencing VIM caused by a current (Ma et al., 2019)

Lily Pad is an open-source Implicit Large Eddy Simulation (ILES) 2D CFD software that was written in Java language in the Processing (Foundation Processing, 2001) Development Environment (PDE) for the unification of pre-processing, testing, and utilization into a stand-alone platform.

The software adopted the Boundary Data Immersion Method (BDIM) for coupling the fluid and solid equations with the main goal of presenting vigorous, rapid software. A 3D version of the Lily Pad is in development under the name of Lotus CFD which aims to deal with the limitations of the 2D software while maintaining robustness. (Weymouth, 2015)
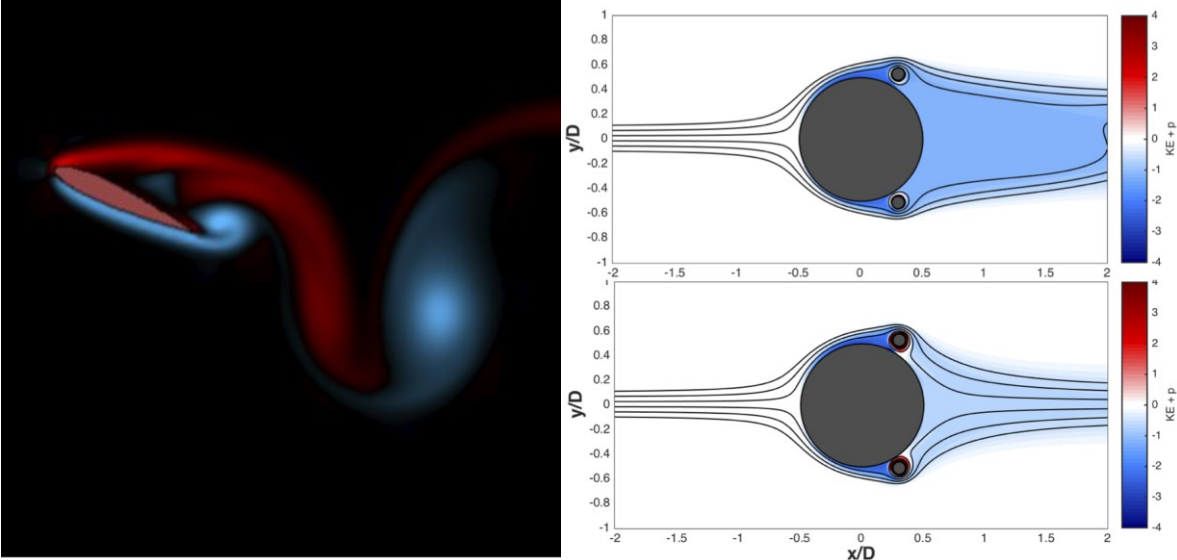
Figure 19. Lily Pad example applications (Weymouth, 2015)

Lily Pad software and BDIM methods were utilized and verified in numerous research (Weymouth & Yue, 2011; Maertens & Weymouth, 2015; Audot et al., 2019). Some verified example applications have been presented in Fig. 19 from Lily Pad.

4.3.5   modeFRONTIER for Mooring Optimization

The software is developed by ESTECO SpA to provide a platform for process automation and multidisciplinary optimization (ESTECO SpA, n.d.). The software capabilities include enhancing computing performance by monitoring the computer power usage, integrating, and handling automation, optimization, inputs, outputs, and coupling different software and simulation tools with each other. It is also capable of visualizing quality data outputs.

5 BASIC DESIGN DEMONSTRATION FOR THE SPAR TYPE

This chapter is dedicated to the demonstration of a basic design process and mooring analysis for the Hywind 5 *MW* Spar type FOWT. Spar type is chosen for its simple geometry. First, preliminary calculations for the stability, mooring lines, and power cable will be made. Moreover, geometry modeling will be done in Ansys Workbench. After the modeling phase, hydrodynamic diffraction and hydrodynamic response analysis will be made on AQWA. Parameters and outputs in the software will be used to explain key concepts. The AQWA tutorial (Castello, 2021) prepared by Dr. Xavier Castello was followed under his guidance for both the preliminary calculations and simulations. This tutorial is publicly available.

5.1 Preliminary Calculations

For the calculations, the first step is to prepare a sketch that shows the different parts of the structure. For simplicity, the structure is represented by cylinders except for the nacelle and the rotor. The following Fig. 20 is the sketch of the structure.
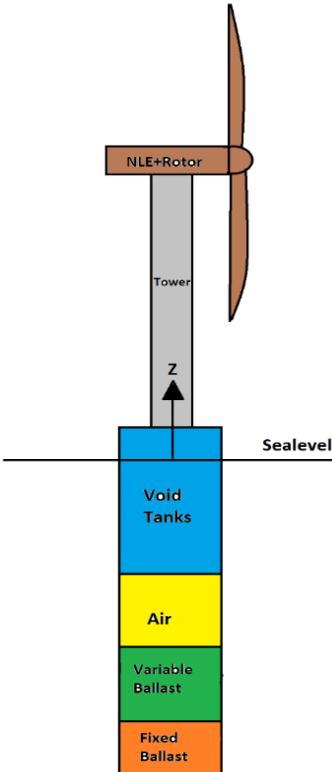
Figure 20. Sketch of the spar turbine

The structure is divided into 6 sections. From bottom to top respectively, fixed ballast, variable ballast, air, void tanks, tower, nacelle & rotor.

5.1.1 *Static Stability Equilibrium & Inertia Calculations*

For the stability calculations, the first task is to estimate the weight and find the correct draft for the structure. To achieve this, hull external diameter, length, porosity, and densities are needed, the area can be found using the simple cylinder area formulation. Porosity is the loss due to shell thickness and other structural losses. To find the equivalent diameter after losses, the external diameter is multiplied by the porosity. For each of the sections, mass, center of gravity, and inertia around the sea level axis must be found for the hydrodynamic diffraction and response analysis. The global axis is on the sea level because it is the default in AQWA, if it is not respected, it can cause errors. After finding the masses and center of gravities of the sections, the correct draft will be found with the balance of the mass and displacement.

Table 3. Spar hull size (Equinor, 2022)

Do	15.00	m
Area,o	176.71	m^2
Length	100.00	m
Freeboard	15.00	m
Draft	85.00	m
Porosity	0.98	
Di (eqv)	14.70	m
Area,i	169.72	m^2
∇	15020.74	m^3
Δ	1.54E+07	kg
CoB	-42.50	m

In Table 3, dimensions are taken from the brochure, and the areas are calculated using the simple circle area formula ($A = \pi D^2/4$), porosity is taken as 0.98 with the assumption of 2% shell loss. Displacement (Δ) is calculated with volume ($\nabla = Area\ x\ Draft$) and seawater density ($\rho = 1025\ kg/m^3$). For cylinders, the center of buoyancy is located at a half distance from the draft. In the beginning, an initial draft value is given, this draft changes according to the static equilibrium calculation. The global center of gravity is needed for static equilibrium calculation. All the masses and centers of gravities must be assessed to find the global center of gravity. Therefore, the masses of the 6 sections are calculated on the spreadsheet that is provided in the APPENDIX A1. A mass summary is made in Table 4.

Table 4. Mass summary for the spar

Part	Mass, kg	CoG, m	Moment, kg*m
Hull	2.40E+06	-35.00	-8.40E+07
Variable Ballast	5.31E+06	-61.74	-3.28E+08
Fixed Ballast	6.79E+06	-81.00	-5.50E+08
Nacelle & Rotor	2.30E+05	100.00	2.30E+07
Tower	6.70E+05	56.50	3.79E+07
Total	1.54E+07		-9.01E+08

For the fixed ballast weight calculation, magnetite is considered as the material and the density of the magnetite (5000 kg/m^3) is used. For the variable ballast, seawater is used. For the calculation of the hull mass, a linear mass, bulkhead mass (for 5 bulkheads), and secondary equipment mass are considered. Since the detailed information for these masses is not publicly available, these masses are just assumptions from the available information on the brochure and the website.

Tower and substructure (nacelle and rotor) masses are taken from the brochure. After calculating all the masses, the balance of weight and displacement is imposed with Excel's goal seek tool, therefore the real draft is found, it is 85 m above the bottom of the structure, therefore the center of buoyancy is 42.5 m below the waterline and the global center of gravity is at 58.5 m below the waterline. Thus,

$$CoB - CoG = -42.5 - (-58.5) = 16\ m \tag{12}$$

Therefore, the structure is in good standing for static stability. For the inertia calculations, simple formulation for the cylinders,

$$I_z = mr^2\ ;\ I_x = I_y = \frac{1}{12}m(3r^2 + h^2) \tag{13}$$

have been used for cylindrical parts, and it is calculated around the waterline as it is the requested format of input for the AQWA. For the inertia of the nacelle, the shape is simplified like a brick, for the hub and blades inertias are taken as estimated values because of the complex geometry, but their masses are small therefore the error will be small as well.

In this part of the study, a few assumptions were made regarding the weights and shape since some of the information is not publicly available. However, for this chapter, the aim is to carry out a basic design demonstration and explain some important concepts both for the inputs and

outputs for the hydrodynamic diffraction and hydrodynamic response analysis, rather than the accuracy of the results.

Real model and technical data will be used for the 15 *MW* semi-submersible to cancel the errors from the assumptions in the next chapter. Thus, the aim will be to find results that are close to the real-life scenario with fully coupled analyses.

5.1.2 *Mooring Lines and Power Cable*

Mooring line and power cable selection is a rather simple process. Another spreadsheet is needed for the mooring line calculations. A depth of 1000 *m* is considered for this study with 3 mooring lines, and a fairlead depth of 34 *m* (40% of the hull draft). The angle at the fairlead is considered 45° for a taut leg configuration. Therefore, the line length is found as,

$$\frac{(1000 - 34)}{\cos(45°)} = 1366.13 \; m \tag{14}$$

Thus, the radius of the lines can be calculated as,

$$1366.13 * \cos(45°) = 966 \; m \tag{15}$$

As mentioned in the earlier chapters, the lines consist of chains at the top and bottom connections (50 *m* for the length of chain for each section) and polyester for the connection in between since that is the adequate arrangement for the deep-water moorings. The polyester material is less stiff than the chain, it is light and elastic. Therefore, it adds elasticity to mooring while reducing the total weight.

For the power cable, it is assumed that it will be connected from the bottom of the hull (85 *m* below the waterline), and it will be laying on the seabed. Therefore, the line depth is extended by 85 *m* to ensure the laying, and the angle to the vertical line is also taken as 45°. Thus, the length of the power cable can be found as,

$$\frac{1000 + 85}{\cos(45°)} = 1534.42 \; m \tag{16}$$

At this stage, some values that depend on the material are needed. Therefore, the line selection guide of the InterMoor© (InterMoor, n.d.) is used to find some properties of the cables. The top tension is assumed to be 15% of the line-breaking strength, normally it is defined at the installation of the platform. The breaking loads and axial stiffnesses are required to estimate the

top tension and line stretching. Internal diameters, dry masses, and maximum breaking loads are taken from the product brochure.

The polyester line will have the same equivalent breaking load as the chain. The diameters of the materials are 202 *mm* for the polyester line, and 120 *mm* for the chain, these values are chosen from the brochures, and the power cable diameter was assumed to be 100 *mm* for the demonstration.

The chain nominal diameter is around half of the chain equivalent diameter. The polyester lines are under pressure; thus, the equivalent diameter is less than the nominal diameter. Therefore, it was assumed that the equivalent diameter is 75% of the original diameter. The reason behind this is to counterbalance the buoyancy of the mooring lines which the AQWA will calculate.

After defining the material parameters, the axial deformation of the polyester line can be found. Since the deformed line will be longer after the tension is applied, compensation is needed in the AQWA model, therefore, the stretched length is deducted from the total length of the line. Finally, it was found that the stretched length of the line is around 16 *m*, for the polyester line has around 1.3 *km* of total length.

The defined parameters for the power cable are just to have an initial calculation that was used in the model parameters. The power cable needs to be adjusted manually on AQWA since the touchpoint and seabed laying needs corrections.

As mentioned, the weight of the lines was not considered in the initial weight estimation. Therefore, net vertical forces on the mooring equipment are calculated separately (Table 5).

Table 5. Top tensions and vertical forces

Type	# Lines	Total Top Tension, N	Vert Force, kg
Mooring	3	5.93E+06	6.05E+05
Cable	1	7.50E+05	7.65E+04
Total		6.68E+06	6.81E+05

To increase the accuracy of the calculations, these vertical forces can be included in the mass summary for an accurate draft calculation for the platform in the dynamic time-domain simulations.

A coordinate table is prepared for the mooring equipment fairlead points, cable connection points, and anchor points. The calculation is simple, the projections of the lines in the (x,y) directions are found, and provided in the following Table 6.

Finally, all the initial mooring equipment parameters for the simulation are defined. The complete calculation spreadsheet is provided in the APPENDIX A2.

Table 6. Mooring equipment coordinates

Angle	X	Y	Z	
	R	7.5	m	
0	7.5	0	-34	
120	-3.75	6.5	-34	Fairleads
240	-3.75	-6.5	-34	
0	973.5	0	-1000	
120	-483	836.58	-1000	Anchors
240	-483	-836.58	-1000	

It was mentioned earlier that there is no available information for some of the parameters, therefore, it should be noted that a few assumptions were made for these parameters. Dr. Castello's online tutorials (Castello, 2021), and his direct guidance have been followed for this chapter. The aim is to introduce the basics. However, for the mooring analysis 15 *MW* reference platform, high accuracy will be aimed.

5.2   Geometry Modelling

The Ansys Workbench SpaceClaim is used for geometry modeling (Fig. 21). It is important to highlight the face normal check for accurate volume calculations for the software. Before exporting the model, the "share geometry tool" must be used to ensure that the nodes in between two faces from different parts are shared.

Figure 21. Ansys spar FOWT 3D model

It should be noted that the AQWA is only interested in the hull structure that is interacting with the water. The hull part can be modeled, and the upper structural elements can be added by their weights and inertia contributions, which will decrease the amount of mesh for the simulations, however, the complete structure is modeled for the visualization.

5.3 AQWA Simulations

After preparing the geometry, hydrodynamic diffraction analysis can be made with AQWA. To analyze the complex motions and responses, some primary hydrodynamic parameters must be obtained.

The hydrodynamic diffraction solver presents an integrated environment for these parameters to be found. This tool can also be used in structural analysis with generating pressure and inertial loading; therefore, it is used for the design processes.

Moreover, the solver results can be exported within the software for an FE model for a detailed structural assessment (ANSYS, 2012). Domain size can be arranged in the details section.

In the hydrodynamic diffraction analysis, the first step is to define the center of gravities and the inertias. The weights of the structures are included as point masses and their inertias are added manually. These parameters were calculated in the spreadsheet in the earlier sections. AQWA combines the masses and inertias for the global characteristics since the structure is a rigid body.

The bottom of the structure is flat; thus, a large hydrodynamic drag is present in the vertical direction. The additional heave motion damping from the fluid viscous drag must be considered. Therefore, a drag disk is added for the analysis. To include the hydrodynamic drag coefficient the flat circular disk normal to the fluid flow was placed at -85.1 *m*, this is a high number because the flow is laminar for the demonstration. (Newman, 2017)

Afterward, mooring equipment coordinates (Table 6) and parameters that are calculated on the excel spreadsheet are included by adding connection points on the structure and fixed points on the seabed. A power cable is attached to the bottom of the structure.
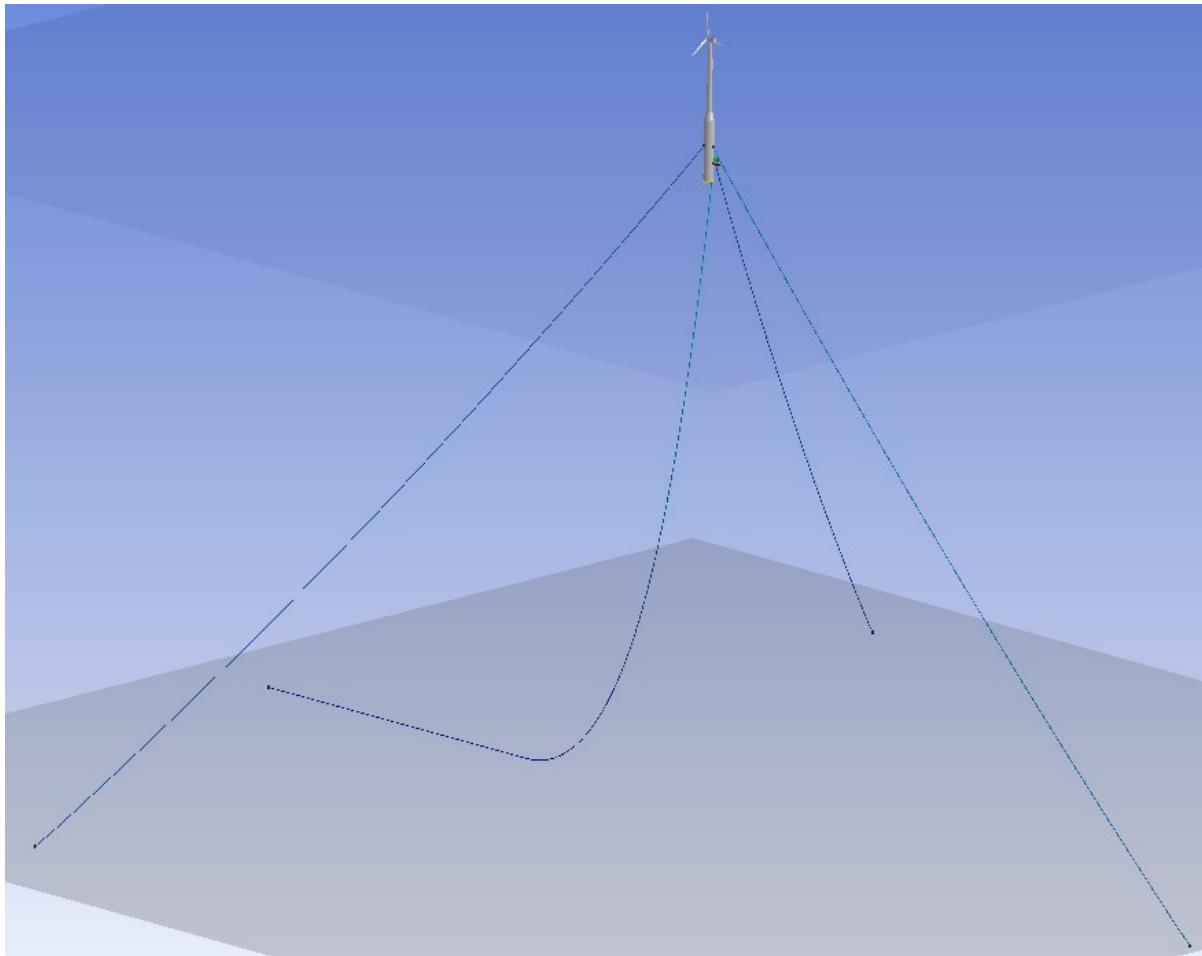
Figure 22. Mooring configuration for the spar type FOWT

Taut leg configuration is used in the model (Fig. Figure 122), therefore there is no seabed contact for the mooring lines and they are pre-tensioned along the length. However, the power cable is hanging freely, and an adjustment will be needed. As explained earlier, for the taut leg system, the anchors need to resist vertical forces as well as horizontal forces (Ch. 3.2.2).

The positive dZ range is set to 20 *m,* dZ range is needed for the cables that are attached between a connection point on the structure to the fixed point on the seabed. This range determines the possible endpoints while accounting for the slackness and maximum tension positions that also includes possible effects from the seabed slope.

The mesh is especially important for the hull (water interaction area); thus, fine mesh is needed for the hull. A simplification in the model was needed at this stage since the student version of the software was used and therefore the number of mesh was significantly limited (2000 mesh limit). However, the upper parts are only for visualization, and they do not contribute to results in AQWA. Therefore, the geometry was remodeled with simpler parts to run the simulations with the allowed amount of mesh, the hull geometry was not changed. The wind and current

can be added as coefficients, AQWA cannot perform a coupled analysis for wind turbines with the turbine dynamics along with time-varying wind and current.
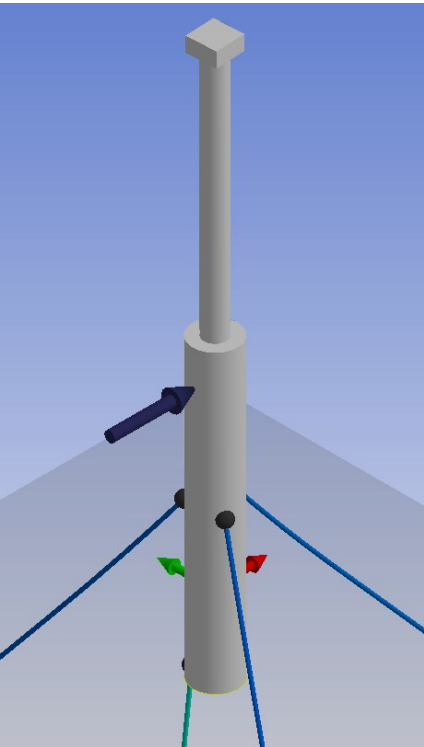
Figure 23. Simplified model

The model is simplified (Fig. 23) by removing the blades and conical sections. This simplification does not affect the analysis results since only the hull shape is considered by AQWA, other element geometries that do not interact with water are not important since their mass and inertia are already introduced to the software. In the tutorial, the mesh number was around 40000, however, the AQWA student version has a limit of 2000 mesh. This can still cause problems such as miscalculations in hydrostatics.

In the analysis settings, the number of CPUs can be defined to solve the model. For the simulation, the full QTF (Quadratic Transfer Function) matrix is left on default. The full QTF matrix is important for the precision of the results since it includes second-order terms such as the slow drift forces over a broad range of water depths (ANSYS, 2012). Another error needs to be addressed at this stage. AQWA student version has an error that can be solved by introducing a simple Python script to the software. This script must be included under analysis settings, and some empty files must be created within the file directory.

For complete post-processing, additional output options may be needed. The "structure selection" option is a functional tool when there are multiple floating bodies present in the model such as semi-submersible structures.

The next step is to include wave parameters, the number of wave directions can be set to a number bigger than three. The number of wave directions was set to 4 unique directions for reduced computational effort, higher numbers can be used for enhanced analysis.

Dynamic response analysis is crucial for the floating structures, therefore adequate prediction of the response due to nonlinear wave and resonance is required. Two approaches are present for the dynamic response analysis, Morison's equation application, and the linear potential theory. Morison's equation takes the viscosity effect into account by nonlinear hydrodynamic drag force representation, while the linear potential theory assumes zero viscosity of the fluid. (Ishihara et al., 2007)

AQWA uses linear potential theory to analyze hydrodynamics, thus it is based on non-viscous flows, meaning that the viscous drift force calculation is not available in frequency-domain analysis. Therefore, the viscous drift correction can be added to the results from the diffraction/radiation analysis. The viscous drift force can be estimated in the time-domain analysis by utilization of the "Morison model", which consists of Morison elements that form the hull (only tube-shaped Morison elements are available in AQWA). These elements must be modeled with precise freeboard clearance from the waterline to capture wave elevations accurately. (Journée & Massie, 2001)

For the results section, hydrostatics results, pressure, and motion results are added. It is possible to visualize the results in the AQWA. To see the animation, the result type can be set as "phase angle", thus, an animation of a complete wave period can be presented.

At this point, it is adequate to introduce the Response Amplitude Operators (RAOs) by adding RAOs (for heave and pitch motions) to the solver, RAOs can be modified later.

The response of a floating structure to waves depends on numerous parameters, a number of these parameters are both direction and frequency dependent. These parameters are utilized to form the transfer functions (RAOs) between the directional wave spectra and the motion spectra of the floating vessel. (Skandali et al., 2020) The legitimacy of the operator is based on the linearity assumption between the floating system response and the wave excitation. Thus, RAOs are calculated in a regular seaway for different wave directions and frequencies via numerical simulations. Therefore, the floating structure motion response for the 6 degrees of freedom can be represented. (Ibinabo & Tamunodukobipi, 2019)

The next step is to run the simulation solver. An adjustment for the wave frequency range might be needed to avoid errors. By limiting the range, possible errors can be avoided. Therefore, two sets of ranges are defined in the simulation. The first range was set between the 60 s to 30 s periods, this range is far from the interest area since it does not result in a significant structure

response. A second range is included, which is between 30 *s* to 5 *s* periods, this range is important since it results in a major response for the structure. Lower than 5 s periods were not considered since those waves are quite small, therefore the influence on the structure is insignificant. One can get 1 *s* period time steps by modifying the interval, this is an adequate value to avoid the solver error.

Once the solver run is complete, hydrostatics results are checked for the center of gravity, the center of buoyancy, and volumetric displacements. The results were the same as the spreadsheet calculations.

Moreover, RAOs are examined for the heave (Fig. 24) and pitch (Fig. 25) motion. It was found that the heave peak response occurs around 0.05 *Hz* with a period of 20 *s* and the pitch response occurs around 0.04167 *Hz* with a period of 24 *s*.
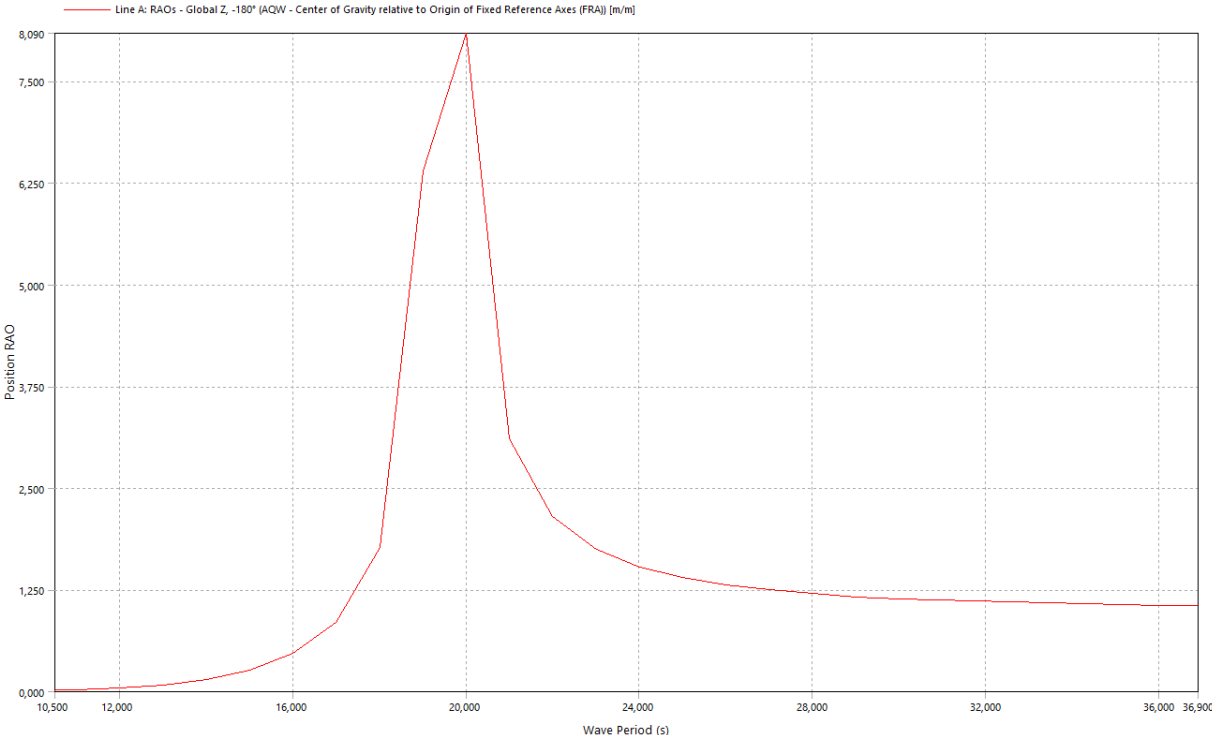
Figure 24. Heave motion RAO

It can be observed that the largest response occurs at the 20 *s* for the heave motion (unit is m/m). This means that the structure is in resonance at this frequency. Resonance occurs when the oscillation frequency matches the natural frequency of the structure. This results in a structural response with significant amplitude. The motions can lead to total failure for the structure, which explains the importance of the RAOs for different motions. The structure is symmetrical, thus the pitch and roll motions have the same resonance characteristics for this case. Therefore, it is proper to include two RAOs, one for the heave motion and one for the pitch motion.
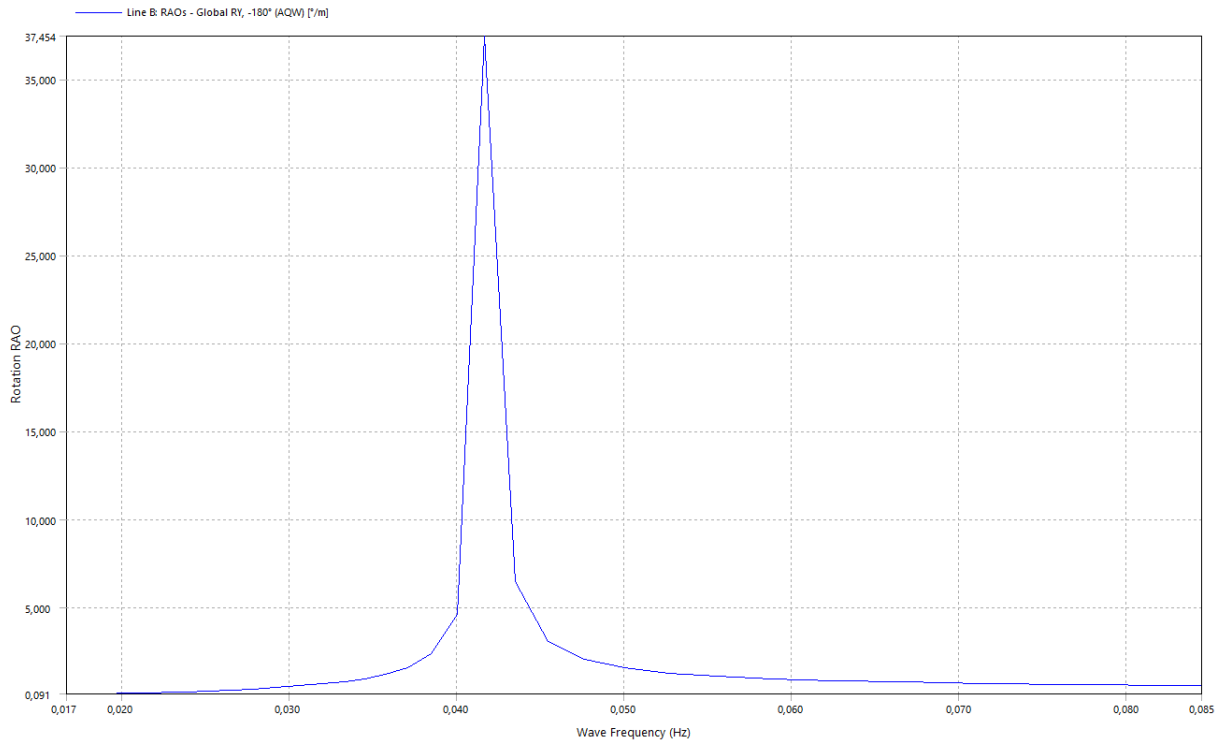
Figure 25. Pitch motion RAO

Lastly, for the pitch motion, the largest response occurs at the 24 *s* period (unit is °/*m*).

After finding these periods, the response of the structure can be observed by monitoring the pressure and motion results with these periods. The diffraction/radiation problem is divided into two separate problems as a solution strategy.

First, the floating structure is fixed, end it takes forces due to incident waves into account (diffraction), while the second problem focuses on the wave radiation forces which is the condition without the incident waves, thus the surface is calm at the beginning, and then the floating body oscillates (radiation).

The linear wave diffraction can be visualized in the results section, and it was seen that the structure response is significant for the resonance period. However, this solution does not include the viscous drag and mooring lines which will dampen the motion, since it is only a linear solution. Additionally, the obtained resonance periods are unlikely to match with that of storm wave conditions periods for most of the locations since the obtained values are high.

Generally, structures are designed in a way that a match with the wave frequency is avoided since it is the condition that damages the structure the most and can cause a total failure.

For the visualization of the results, the "contour type" can be changed to the "wave surface elevation" which makes it easier to represent the diffracted and incident waves on the structure.

The smallest period (5 *s*) is selected for better visualization of the wave diffraction. One can also choose wave components according to which one is needed for monitoring.

For example, if the incident wave is deactivated in the settings, one can observe the radiated waves from the hull motion and diffracted waves from the hull structure (Fig. 26).
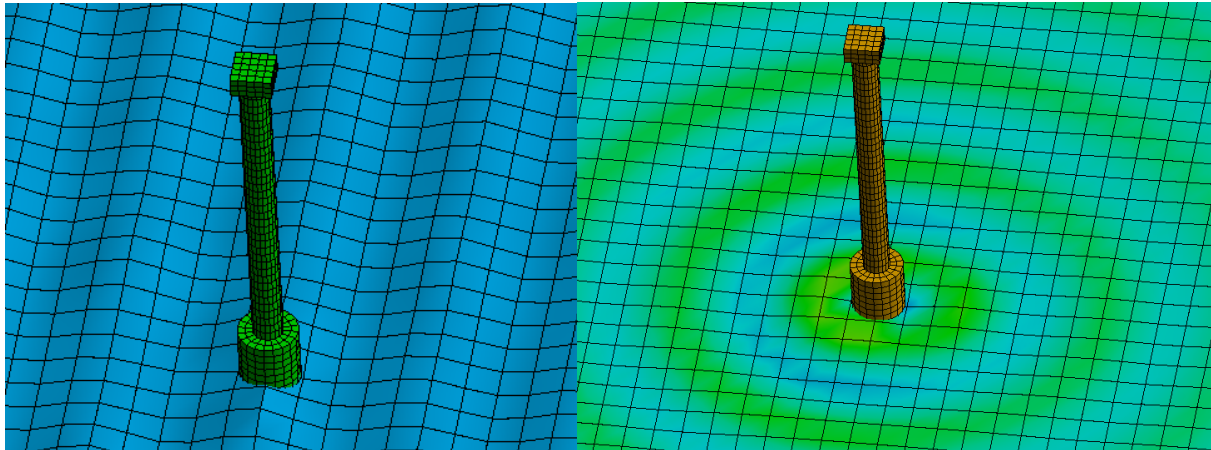
Figure 26. Diffraction/radiation visualization

After obtaining these results from the solver, another simulation was run for the time domain response. The hydrodynamic time response tool performs dynamic analysis for floating structure performance. At this stage, a broad range of connection elements can be included such as mooring lines, power cables, fenders, and articulations that limit the motions of a floating body. Moreover, seakeeping, slow-drift effects, and extreme-wave conditions can be monitored as well as the damage conditions. (ANSYS, 2012)

To perform this analysis, the static stability of the system must be calculated to survey the structure conditions, as mentioned earlier, the weight of the mooring system was not introduced in the weight calculations, and compensation must be made.

Default settings are used for the analysis. For the simulation, at least one wave should be introduced with wave parameters. In real life, waves are not regular, the natural seaway is irregular. In basic terms, many regular sine waves are superposed to form irregular waves. This simplification leads to the ocean wave spectrum, which represents the wave energy distribution of different characteristic waves. Therefore, an irregular wave in JONSWAP (Joint North Sea Wave Observation Project) wave spectrum was introduced. Since the static equilibrium check is required, a small wave was introduced to avoid a possible disturbance in the sea. Generally, the sea spectrum choice for the simulations must be based on the target location.

Structure position and animation for the structure response were added for the solver results. After the solver run, it was observed that the structure sank more, this is due to the mooring

system forces. It was also observed that the structure tends to move downwards and to the side. Two possibilities have been considered that can cause this motion; the defined wave might not be as small as desired, thus causing a drift on the hull, or there is an inaccuracy in the arrangement of the power cable which disturbs the system.

To find the exact problem, the total mooring force (mooring sum) was added to the analysis of the results. Thus, total vertical forces from the mooring system on the hull have been found.

It was observed that the force decreases while the platform sinkage increases along with the iteration steps. A comparison for the vertical force between the spreadsheet and the AQWA results has been made, and it was seen that the software results are lower than the spreadsheet estimation.

The difference comes from the power cable, which was improperly calculated at the initial estimation, which assumed that the power cable was also arranged as the taut leg configuration, however, it is hanging freely at the bottom of the structure.

To compensate for this difference in the vertical force, hydrostatic stiffness of the hull and the sinking distance can be. The solution is to decrease the mass of the variable ballast and make a correction in the draft. After the correction, the platform became stable.

Afterward, another time-domain response analysis was made by dragging the new analysis to the solution of the last one. This time, an irregular wave response for a duration of 5 *mins* was targeted in the storm wave conditions. At this stage, a lot of analysis options are present such as the mooring forces, winch actions, and failure. JONSWAP irregular wave was added, and parameters were controlled manually for simplicity. The wave range was modified from frequency to period. For the storm wave modeling, the peak period was chosen as 16 *s*, peak enhancement factor (gamma factor) was set to 2, as it was suggested in the tutorial (Castello, 2021) prepared by Dr. Castello. Then, it was observed that the wave spectra create the maximum energy at the selected peak period.

Afterward, wave surface elevation results, animation, and statistics for the structural position for the pitch angle of inclination and the heave vertical motion were added to the solution. Then, force results (Fig. 27) can be found for the structure along with the mooring system forces and other attachments if any of those are present. The aim is to check if the selected mooring system can survive this storm or not. Therefore, whole cable forces results were added to the solution. After running the hydrodynamic system solution, wave amplitude was examined to confirm that the wave conditions are matching the desired conditions. The wave amplitude for the wave was found as 6 *m* for the 5 *mins* simulation duration. AQWA cannot visualize the incident

waves in the time domain it can only be visualized using third-party software packages, however, animations were checked to see the motion of the structure.

Statistics for the mean and standard deviation for the pitch and heave motions can also be included for detailed surveying of the mooring system and hull design. Graphic results for the desired motion result were also added. It was found that the pitch motion is around ±1.5° which is within acceptable limits. It can be concluded that for the desired simulation duration of 5 *mins*, with waves of 6 *m* height and 16 *s* period, the structure behaves adequately.
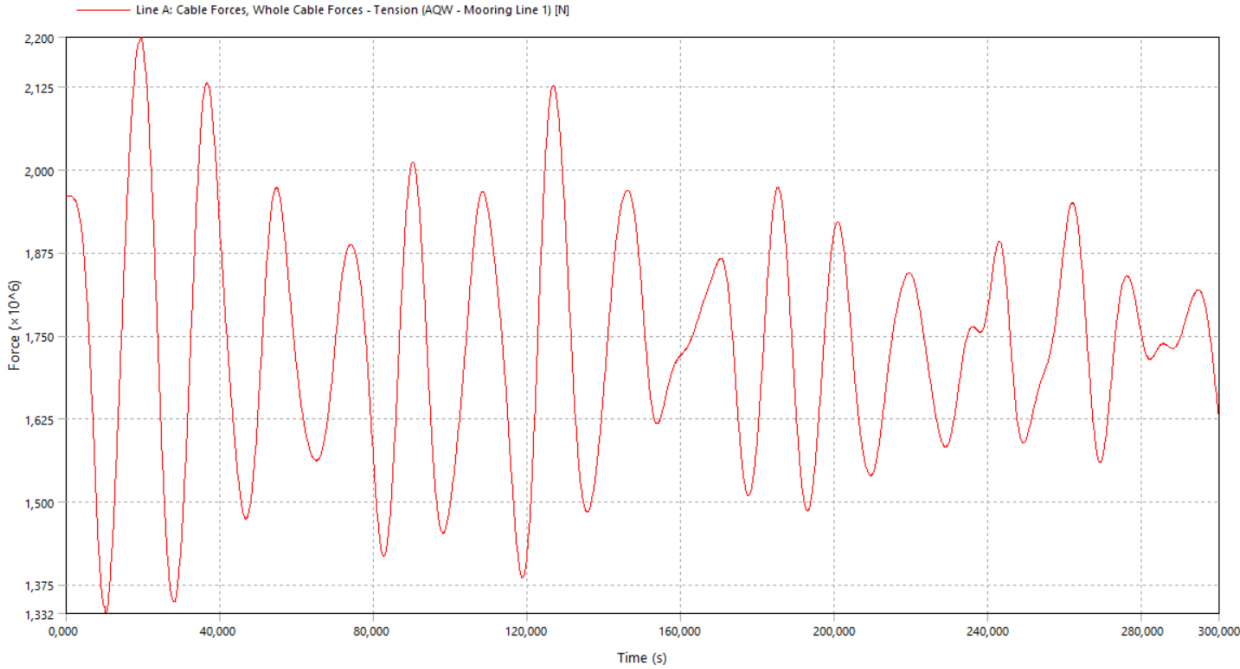
Figure 27. Mooring line results for irregular wave conditions

Another simulation was implemented at this stage to increase the energy of the storm and it was arranged to occur at the resonance frequency of the structure. Earlier it was found in the hydrodynamic diffraction analysis that the resonance occurs around 19 *s* in heave and 24 *s* for the pitch. Thus, a wave period of 24 *s* was the input, and the wave height was increased to 10 *m* for the new simulation. It was expected that the response of the structure will be extreme.

It was observed that the wave height was much bigger than the previous simulation and one wave with around 10 *m* amplitude occurred around 240 *s* of the simulation. It was also observed that the structure is in resonance as expected. The structure motion was found bigger than the wave amplitude with about 20 *m* of total heave motion amplitude and the inclination of the pitch was found around ±17° which also occurs around 240 *s* of the simulation.

More results are added to the solution such as statistics and mooring cable forces. It was found that the mooring line top tension was around 2000 *kN* at the beginning of the simulation,

however, it suffered more in the dynamic condition with a top value of 2694 *kN* occurring around the 140 *s* of the simulation (Fig. 28).
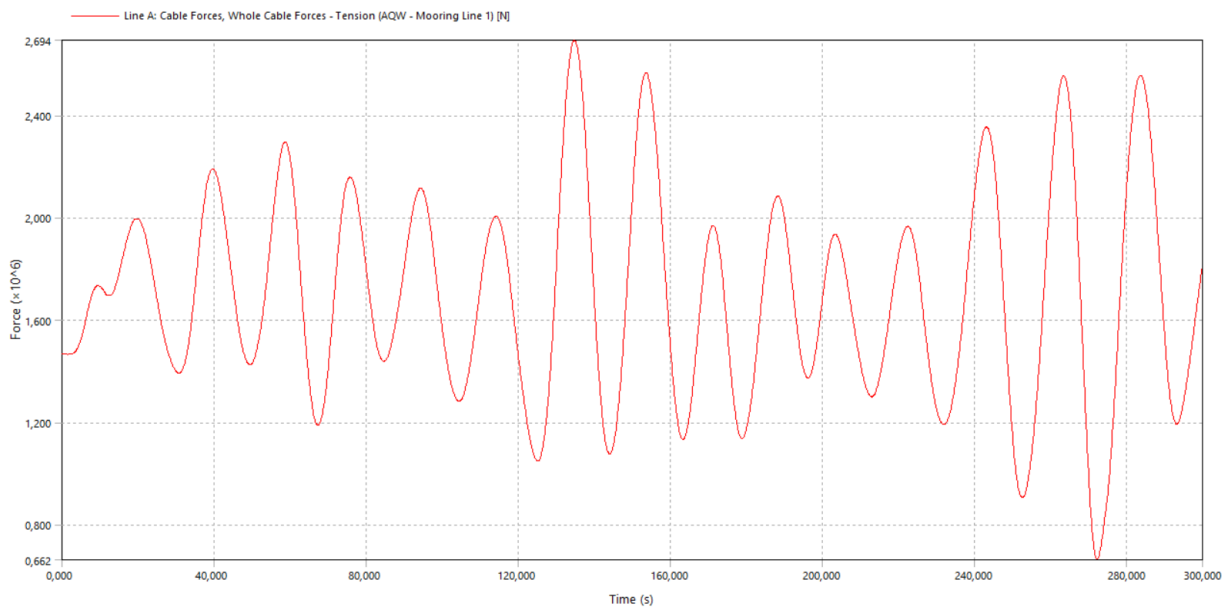
Figure 28. Mooring line results for irregular wave (resonance)

In conclusion, this chapter provides design basics for a Spar-type structure. The process started with the sketch and spreadsheet calculations. Realistic assumptions were made by using the real-life product guides provided by offshore wind-related companies. The Spar hull has a simple geometry, therefore these calculations are basic, however, for the semi-submersibles, inertia, and stability calculations are more complicated but the general principles are the same. The hull size, static stability, mooring lines, and power cable properties are calculated for the preliminary design.

Afterward, these calculated parameters are used for the 3D model of the FOWT, and the hydrodynamic diffraction simulation is performed while solving errors and making corrections in the initial parameters.

Lastly, time-domain simulations with severe wave storm conditions are performed and an additional simulation for observing the resonance of the structure was made. Some important hydrodynamics concepts for the mooring line simulations such as RAOs and wave spectra are briefly explained to cover the basics of the mooring line analysis.

6 SIMULATION SETUP AND EXECUTION FOR 15 *MW* SEMI-SUBMERSIBLE FOWT

As stated earlier, VolturnUS-S IEA 15 *MW* semi-submersible wind turbine model (Fig. 29) is used for the simulations. To carry out the mooring analyses, environmental load combinations should be introduced to the software as well as the topology of the environment. These load combinations are determined by the International Electrotechnical Commission (IEC, 2005) standards and ABS guidelines (ABS, 2020) for offshore wind turbines.
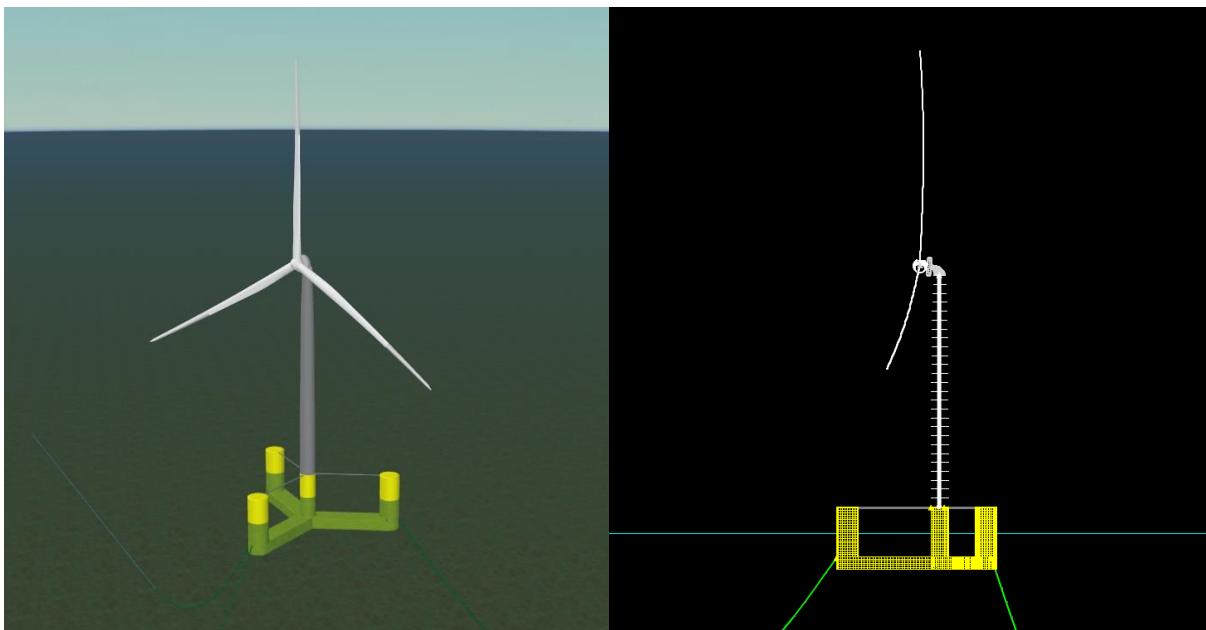
Figure 29. OrcaFlex reference model of the VolturnUS-S 15 *MW* FOWT (Orcina, 2022)

Generally, the FOWT design process includes a detailed examination of the strength characteristics of the structure and its main components regarding both ultimate and fatigue loads. Ultimate loadings are one of the major limiting factors for various components of the structure. They may arise from extreme situations or unfavorable load combinations on the structure. Therefore, load combinations that are determined by the standards must be investigated for an adequate design for the FOWT and the components. (P. Madsen et al., 1999) Fatigue loads are due to operation under cyclic loads. Generally, they occur in long term due to crack formation and propagation.

Ultimate load and fatigue life calculation processes have been explained in further chapters. The following sub-chapter covers the design load cases for the floating offshore wind turbine structures in detail.

6.1 Design Load Cases

According to the *Guide for Building and Classing Floating Offshore Wind Turbines* (ABS, 2020), design load cases are determined by the IEC 61400-1 standard (2005). Therefore, the load cases can be analyzed under 10 conditions.

1. Power production (1.2 to 1.6)
2. Power production plus the occurrence of a fault (2.1 to 2.6)
3. Start-up (3.1 to 3.3)
4. Normal shutdown (4.1 to 4.3)
5. Emergency stop (5.1)
6. Parked (standing still or idling, 6.1 to 6.4)
7. Parked and fault conditions (7.1 and 7.2)
8. Temporary (Load-out, transportation, installation, maintenance, and repair, 8.1 to 8.4)
9. Power Production (Accidental, 9.1 to 9.3)
10. Parked (Accidental, 10.1 to 10.3)

Design load cases include the main combinations of environmental conditions. They are generally used to determine the limit states of the FOWT structures (ULS, SLS, ALS, and FLS). Additionally, ABS has one more category of load cases which is named "Survival Load Cases" and they include loads with 500-year return period for the determination of the "Survival Limit State (SurLS)" of the structure.

ABS guideline also states that all these design load cases must be assessed in the design stage with a simulation length of 3-hours (1-hour simulations can be used in some cases with adequate sensitivity studies). The simulations must be fully coupled time-domain simulations. However, 10-minute simulations can be used for the initial design stages.

For this study, a local OrcaFlex license was granted by Orcina Ltd. to the University of California, Los Angeles (UCLA). A workstation was appointed by the C&EE department. This workstation had 128 GB of total physical memory (RAM) and two processors (Intel® Xeon® 2.60 GHz, 8 Core(s), 16 logical processors) which allows 32 simulations to be run on the OrcaFlex at the same time in the Batch Processing Mode. On average, every 32 simulations take between 1-2 hours and 1.5 to 2.5 GB of memory. For example, for the fatigue load case under normal power production conditions (DLC 1.2) 648 simulations (x2 for different water depths) must be carried out. It took around 2-3 days and around 2.5 TB of memory space just for one DLC.

Initially, the number of finite elements was decreased at the tower and upper structure to decrease the computational effort. Also, frequency domain simulations (linearizing the problem) were considered, however, OrcaFlex uses external software for the blade and aerodynamic effects which makes it impossible to run the simulations in the frequency domain. Therefore, one needs to remove the external function and the blades in order to run the model in the frequency domain which results in over-simplification.

At this stage, advice given by Prof. Mario de Vicente (UPM, 2022, personal communication) was followed. He stated that from his experience, design load cases under normal power production (DLC 1.2, 1.3, and 1.6) and parked conditions (extreme loading, DLC 6.1) are the critical load cases for the mooring system design. Therefore, this study focuses on these load cases with 10-min fully-coupled-time-domain simulations. It should also be noted that these DLCs cover the largest percentage of the design lifetime of the FOWT structure and various studies have been found that are also focused on the same DLCs (P. Madsen et al., 1999; J. M. Jonkman, 2007; F. J. Madsen et al., 2019; Pillai et al., 2022). For the semi-submersible FOWT structures, 99% of all fatigue load of for the components comes from DLC 1.2 (Pan et al., 2021), therefore it was found adequate to follow this load case for the fatigue calculations.

Additionally, a unique set of DLCs have been created for this study that accounts for the directionality of the environmental loads of the target location.

It should be noted that for an acceptable and finalized design, all the described load cases must be assessed in a fully coupled time domain and with 3-hours of simulation time with adequate hardware.

After the selection of the critical DLCs, "*Design Load Basis for Offshore Wind Turbines*" by DTU (Natarajan et al., 2016) was followed for the simulation setup along with the Lifes50+ (2015) and COREWIND project reports (COREWIND, 2019).

DTU design basis provides a detailed explanation of the selection of the simulation parameters for the design load cases that are described in the IEC-61400 (2005).

Lifes50+ (2015) design reports give information about the methodology for a complete floating offshore wind turbine design along with the main components. COREWIND reports (2019), on the other hand, are early reports and assumptions that include possible design considerations for the FOWT project for the Morro Bay Area along with the other two areas, however, some important information is missing in this report because some of the data were not available at the time of the project (e.g., current speed). Both projects are EU-funded projects. Therefore, some information and guidelines from these reports were also considered along with the ABS guidelines. There is still not enough information about the current speed data, however, the

maximum average current speed data (20-year period) was found from the MarineCadastre reports which is 1.26 m/s. Since there are no other information that is publicly available at the time, this value has been used for the simulations.

The DLC 1.3 represents the power production in extreme turbulence (extreme-normal event). This DLC is for fault-free power production simulations. Yaw errors are set to ±10° and six seeds per wind speed and yaw errors are used with the extreme turbulence model. Wind speed is ranging between 4 to 26 *m/s* in steps of 2 *m/s* and the vertical shear exponent was set to 0.14. Three wave seeds are recommended for each wind speed therefore 18 seeds for each joint pair of wind and wave conditions have been used.

The DLC 1.6 represents the power production under a severe sea state (extreme-normal event). The conditions are similar to the DLC 1.3 but this time severe sea state conditions with a return period of 50 years of wind speed and waves should be considered.

The DLC 6.1 represents the parked turbine with an idling rotor and yaw error (±8°) at a turbulence intensity of 11% and a wind of 50-year-return period. The simulations must be repeated for 3 water depths that are specified in the design guidelines and six seeds per wind must be used. Extreme sea state must be modeled for the simulations.

The last load case (DLC 10.3) was made for the mooring loss event. Environmental conditions are set with the extreme wind model, extreme sea state, and extreme current model. The mooring line that has the highest average tension (upwind mooring line) must be set to snap, and the other mooring lines were checked.

In addition to the DLCs provided in Table 7, one more load case was created. It was named as the directional load case, which is a customized load case for the site-specific directionality characteristics of the environmental forces in the Morro Bay area.

These load cases are simulated for evaluating the maximum tensions (ultimate limit state) for the mooring lines.

On the other hand, DLC 1.2 is the fatigue load case under normal conditions. It represents the biggest percentage of the total life of the structure. The entire operational range of the wind turbine must be covered. Two different water depths must be considered. At least three different wave seeds must be used in three different directions and six seeds per wind speed and yaw errors are to be used.

After evaluating the analyses, required safety factors have been included in the calculations for evaluating the limit state for the mooring lines.

Table 7. Summary of the critical design load cases (ABS, 2020)

Turbine Condition	DLC	Wind Condition	Waves	Wind and Wave Directionality	Sea Currents	Water Level	Analysis Type	SF
1) Power Production	1.2	NTM $V_{in} \leq V_{hub} \leq V_{out}$	NSS Joint prob. dist of H_S, T_P, V_{hub}	MIS, MUL	NCM	NWLR or $\geq$ MSL	F	FDF
	1.3	ETM $V_{in} \leq V_{hub} \leq V_{out}$	NSS $H_S = E[H_S|V_{hub}]$	MIS, MUL	NCM	MSL	S	N
	1.6	NTM $V_{in} \leq V_{hub} \leq V_{out}$	SSS $H_S = H_{S, SSS}$	MIS, MUL	NCM	NWLR	S	N
6) Parked	6.1	EWM $V_{hub} = V_{10\,min,\,50\text{-}yr}$	ESS $H_s = H_{s,\,50\,\text{-}\,yr}$	MIS, MUL	ECM 50-yr Currents	EWLR 50-yr	S	N
10) Parked (ALS)	10.3	EWM $V_{hub} = V_{10\,min,\,1\text{-}yr}$	ESS $H_s = H_{s,\,1\,\text{-}\,yr}$	MIS, MUL	ECM 1-yr Currents	EWLR 50-yr	S	A

Table 7 summarizes the chosen critical DLCs for the mooring analyses. The directional load case was created from DLC 1.2 with specified directional angles from the wind, wave, and current roses. For this load case, normal power production conditions with realistic directions have been targeted. Over 1000 simulations were conducted to evaluate these combinations.

The methodology that was described as the design basis of the Lifes50+ (2015) project is used for the fatigue calculation which assumes that the wind and wave directions are aligned for the structure. For the fatigue calculations, joint probability distributions for the combined environmental loads must be utilized.

The COREWIND (2019) project includes some details about the Morro Bay Wind Energy area such as the scatter diagrams, significant wave heights, and wind speeds with different return periods and water levels.

This data was combined with the new data that was shared with the public by BOEM & NOAA to carry out the simulations and the calculation of the fatigue life of the mooring lines.

6.2 Geometry Definitions

In the earlier chapters, brief information was given about the VolturnUS-S IEA 15 *MW* reference wind turbine. This chapter is dedicated to presenting detailed information about the design and the base model that includes the initial mooring system design. The reference FOWT that is used in this study is a steel semi-submersible FOWT structure that consists of 4 columns. The following Table 8 presents the properties of the platform. (Allen et al., 2020)

Table 8. Semi-submersible platform properties (Allen et al., 2020)

Parameter	Unit	Value
Hull Displacement	m^3	20,206
Hull Steel Mass	t	3,914
Tower Interface Mass	t	100
Ballast Mass (Fixed / Fluid)	t	2,540 / 11,300
Draft	m	20
Freeboard	m	15
Vertical CoG from SWL	m	-14.94
Vertical CoB from SWL	m	-13.63

The hull arrangement (Fig. 30) includes three buoyant columns that have a diameter of 12.5 *m*. The columns are spaced 51.75 *m* from the tower's vertical axis.
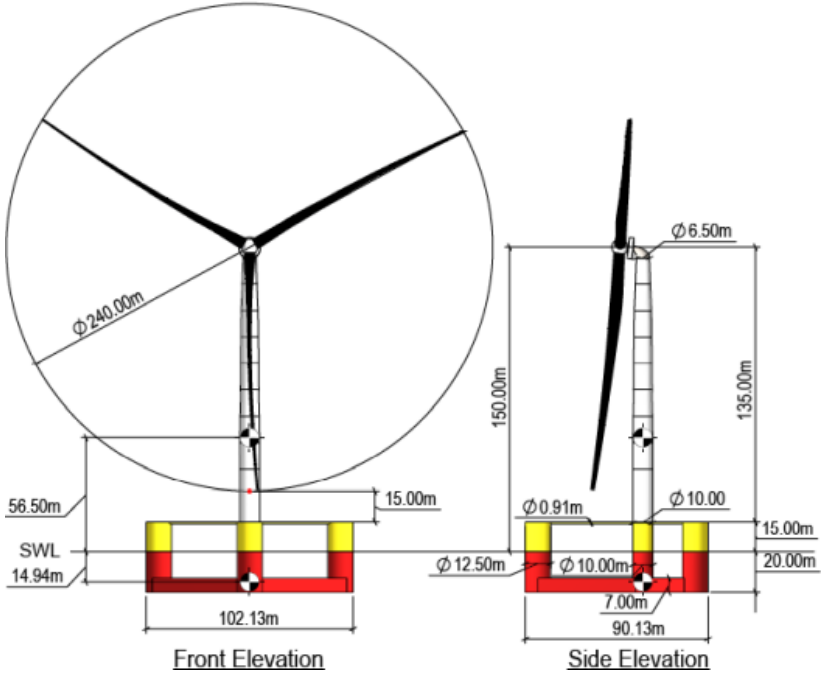
Figure 30. General arrangement of the FOWT (Allen et al., 2020)

6.3 Simulation Setup

This chapter is devoted to the simulation setup for the OrcaFlex software that is used for the coupled simulations. Thus, the provided information in the documentation of the OrcaFlex has been used which is publicly available online.

6.3.1 General Data

OrcaFlex simulation setup starts with general data settings which apply to the whole model. Main simulation parameters are set at this stage such as the analysis type, simulation length, time step, tolerances, intervals, and user-defined parameters. For analysis, the simulation period can be divided into several consecutive stages which define the whole period. Different stages can be specified in the data that is used for simulation control. For the mooring analyses, a build-up stage was set for the simulation which starts from -75 s and ends at 0 s which covers stage 0. This is a general application that diminishes the transient effects which is a result of the change from the static position to the motion in the full dynamics. A smooth ramping-up for the structure must be ensured. Any additional stages (if needed) can be introduced in the general data. Simulations have two stages, the first stage (stage 0) has been set to -75 s to 0 s which covers the build-up (transit) period of the simulation, and this stage is not included in the post-processing of the results. The second period is set from 0 s to 600 s to simulate a 10-minute of desired load combination on the structure.

Static analysis is required to perform dynamic simulations which aim to find the accurate orientations and positions for all the elements in a model such that the moments and forces are in equilibrium. One cannot perform a dynamic simulation for a model that does not have a static equilibrium. In general, models are nonlinear, therefore the statics calculation requires an iterative approach using the multi-dimensional form of Newton's method.

1. DoFs of all objects except the lines are fixed.
2. Line statics are calculated to find the equilibrium configuration for all the lines. The goal of the line statics is to supply an adequate initial position for the whole system statics of the overall statics calculation. All lines are included and coupled system solve has been set for the line statics calculations.
3. All the DoFs are released and a whole system static analysis has been performed using Newton's method where the previous two stages give the initial guess.

For the simulations, coupled system solver has been selected. By default, the maximum number of iterations is 400 (calculation stops if the convergence has not been achieved after the defined number of iterations) and the tolerance is set to 1e-6 (solution accuracy) for the whole system statics analysis. Minimum and maximum damping are the last parameters to set at this stage, sometimes it is necessary to reduce (damping down) the step taken at each stage to control the process of convergence. The software has an automatic damping system that selects an adequate factor of damping for the iteration, however, one can set a min and max factor to limit the damping. In general, default values are adequate for the simulations, however, in some cases, the damping limits have been increased. It should be noted that an increase in the damping values results in a slower convergence, therefore the selected values must be as small as possible.

For the dynamics setup, the solution method for the dynamic response of the system can either be in the frequency domain or the time domain.

The frequency domain dynamic analysis is linear; therefore, it involves a linearization process that approximates nonlinearities to linearities. To map the underlying stochastic environment, this solver utilizes the static analysis results as the configuration of the system to produce linear transfer functions. In each frequency of interest, these LTFs are used to calculate the response of the system. The frequency domain system is not applicable for the time-varying operation analyses because the system is defined by the static state. It is faster than the time-domain methods, however, the applicability is limited because of the linearization and invariance of time.

Time domain dynamic analysis, on the other hand, is nonlinear. There are two different time domain integration schemes which are named "implicit" and "explicit" time domain on the OrcaFlex software.

In practice, the implicit integration is unconditionally stable (generalized-α integration scheme) with the option of variable or constant time steps. The explicit integration is conditionally stable (semi-implicit Euler) therefore the time step must be small compared to the natural nodal period which may result in higher computational effort.

For the study, implicit time domain integration was used for the ultimate and fatigue load analyses with guidance from Mr. Paul Jacob (Orcina, personal communication).

External algorithms can be included in the user-defined results section under the general data for different purposes. The base model includes an external function for the generator power calculation for the wind turbine. As mentioned earlier, a third-party software (Bladed) gives the data for aerodynamics.

6.3.2   Environment Data

Environment data includes the sea, seabed, wave, current, and wind data. Sea surface is defined as the 0 *m* position for the coordinate system which helps to model other parameters such as the depth and mooring line coordinates.

In the sea data section, temperature data that is varying with the depth which was found on the BOEM website has been introduced to the software as well as the sea density data. As mentioned in the earlier chapters, the mean depth of the Morro Bay area is 1046 *meters*. Therefore, 22 levels of depth have been introduced to the software. For the vertical density variation (Fig. 31), the interval values are calculated by the software with interpolation.
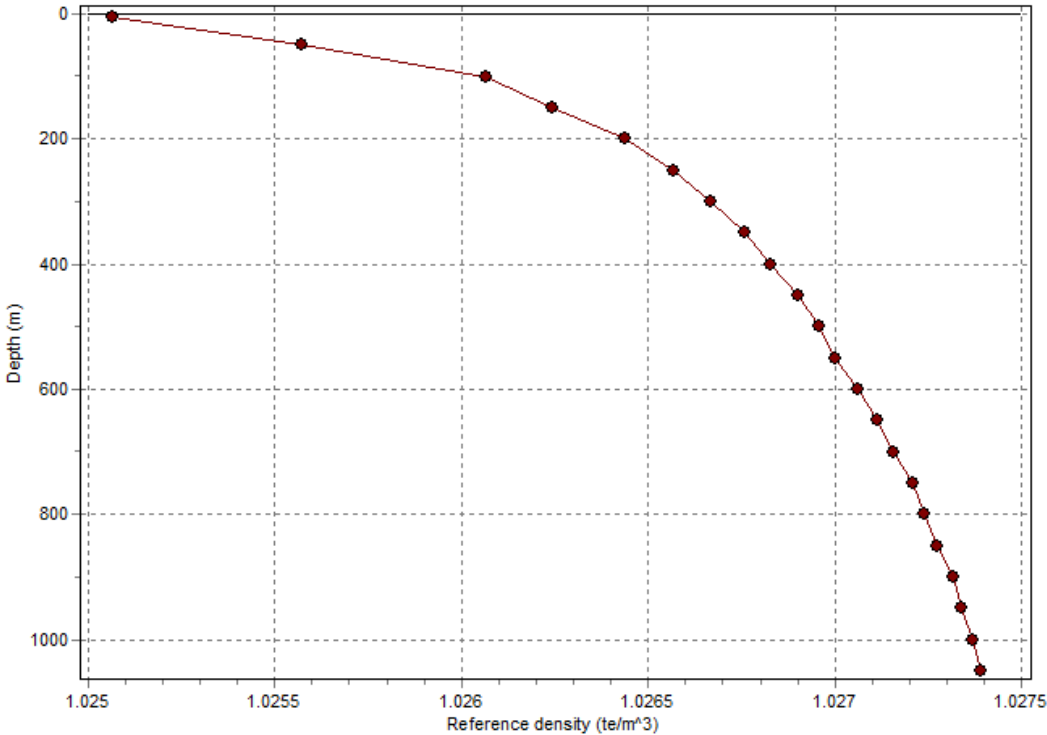
Figure 31. Density variation with respect to depth

Seabed data is then introduced to the software with the mean depth (-1046 *m*) and mean seabed slope (1°). It is possible to model different kinds of seabed types which goes as flat, profiled, or 3D. A flat seabed with an elastic seabed model was chosen for simplicity. The elastic model means that the seabed behavior is like an elastic spring in the normal direction, since the data about the seabed is limited, the default values of seabed stiffness have been used. However, it is possible to model a complex nonlinear seabed in OrcaFlex which is useful in detailed anchor studies.

One of the most important data is wave data. In the wave panel, it is possible to set the direction, height, period, wave type, wave seed, and spectral parameters.

For the wave type, ABS (2016) guidelines were followed and ISSC (also known as Bretschneider or modified Pierson-Moskovitz) spectrum was used as recommended for the open ocean conditions. In general, it is possible to introduce a user-defined spectrum for the site-specific conditions in OrcaFlex, and the NOAA provides historical buoy records, and it can be downloaded from their database for a detailed wave spectra analysis for the Morro Bay Wind Energy Area, however, several third-party software for raw data processing is required.

It is also possible to set several wave trains with different characteristics to simulate different events.

For the frequency spectrum discretization method, equal energy was used. The wave calculation method is instantaneous position (exact) with the wave kinematics cutoff depth of infinity, wave search method of height or stiffness. These are the default recommended parameters in the software.

The sea current profile data is limited for the Morro Bay Area; therefore, the default power law has been set for the current profile in the software.

For the wind, NPD (Norwegian Petroleum Directorate) spectrum has been used, which is recommended by the classification societies, and it is the most common practice in the offshore industry (Shu et al., 2018; Ma et al., 2019).

Specific attention should be paid to the reference wind speed and wind elevation parameters to ensure the accuracy of the wind speed at the hub. A wind seed number can also be set in the panel.

In practice, a seed is the start point of a simulation, if one does not change any input parameters in a simulation, by using the same seed number, the simulation will give the same results as the one before which is not the case in real life, therefore one can use the seeds like an ID number for creating the same simulations, but to ensure reliable output for the simulations, different random seed numbers must be used. Thus, random seeds have been introduced to the software while creating the batch files in Excel.

6.3.3 All Objects Data

All objects data panel presents general information about the structure and the connections. The created base model consists of 3 mooring lines, a semi-submersible floating platform with four columns, a tower, a nacelle, a hub, and 3 blades.

As can be seen from Fig. 32 the tower and mooring lines are modeled as line type objects in the software.

50
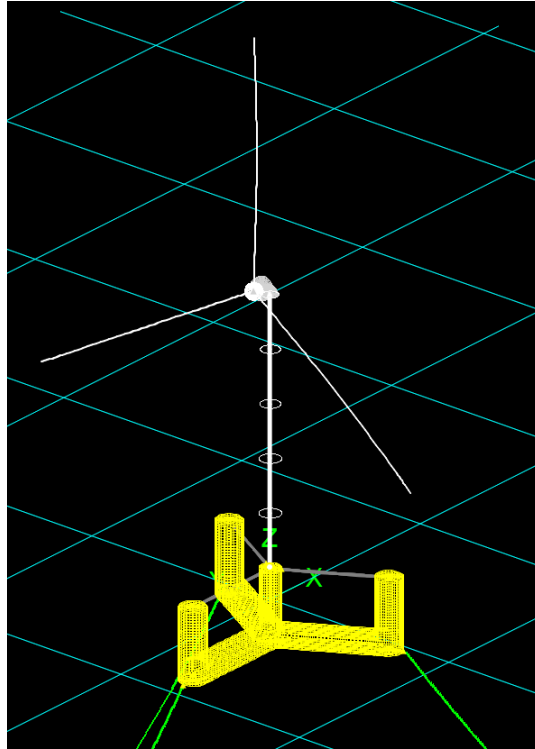
Figure 32. OrcaFlex Base Model (All Objects Data)

Mooring lines consist of three sections with two different materials (chain and polyester). These materials and their material properties are included in the OrcaFlex library (line type wizard). One can also add custom materials if needed.

The line type objects are shown in finite element representation. The number of FE for the tower has been decreased to reduce the computational effort. For the mooring lines, a target segment length of 1 *m* is used, longer segments are not allowed by ABS (2022) guidelines. In general, one can determine the target length by sensitivity studies.

For the configuration of the taut mooring arrangement, OrcaFlex has a tool that is named "line setup wizard", some parameters should be set in the wizard e.g., declination angle. This tool can be used for calculating anchor positions or lengths of the mooring lines. A base case has been created for the structure with the initial mooring configuration. This initial configuration was made by following the recommendations provided in the *Mooring System Engineering for Offshore Structures* (Ma et al., 2019), it is stated that an anchor distance of 1.4 times the water depth is considered an adequate starting point for the design of the taut mooring arrangement which corresponds around 45° fairlead angle for the fairlead point located at the bottom of the semi-submersible columns. Details of the mooring lines of the base model have been provided at the following Table 9. It should be noted that a power cable needs to be included in a real design as well, however it was discarded for this study to reduce the computational effort.

Table 9. Base Model mooring line dimensions

Component	Composition	Upper Ch. Length (m)	Polyester Length (m)	Bottom Ch. Length (m)	Total Length (m)
Upwind Line	Ch – Py – Ch	100	1300	100	1500
Downwind Line 1	Ch – Py – Ch	100	1200	100	1400
Downwind Line 2	Ch – Py – Ch	100	1200	100	1400

The material properties for the chain and polyester have been set from the line type wizard. For the chain, an initial bar diameter of 0.1 *m* (studless R4) has been selected and the polyester line with a nominal diameter of 0.2 *m* was selected (8-stranded multiplait). These initial values have been selected after analyzing the oil and gas rigs' mooring parameters that are built for similar depth ranges.

Finally, the parameters for the base model were set. The model is created with recommended parameters for the initial mooring analyses. In general, the purpose of this model is to give a starting point for the limit state calculations. Fig. 33 represents the base model that was created for the OrcaFlex simulations.
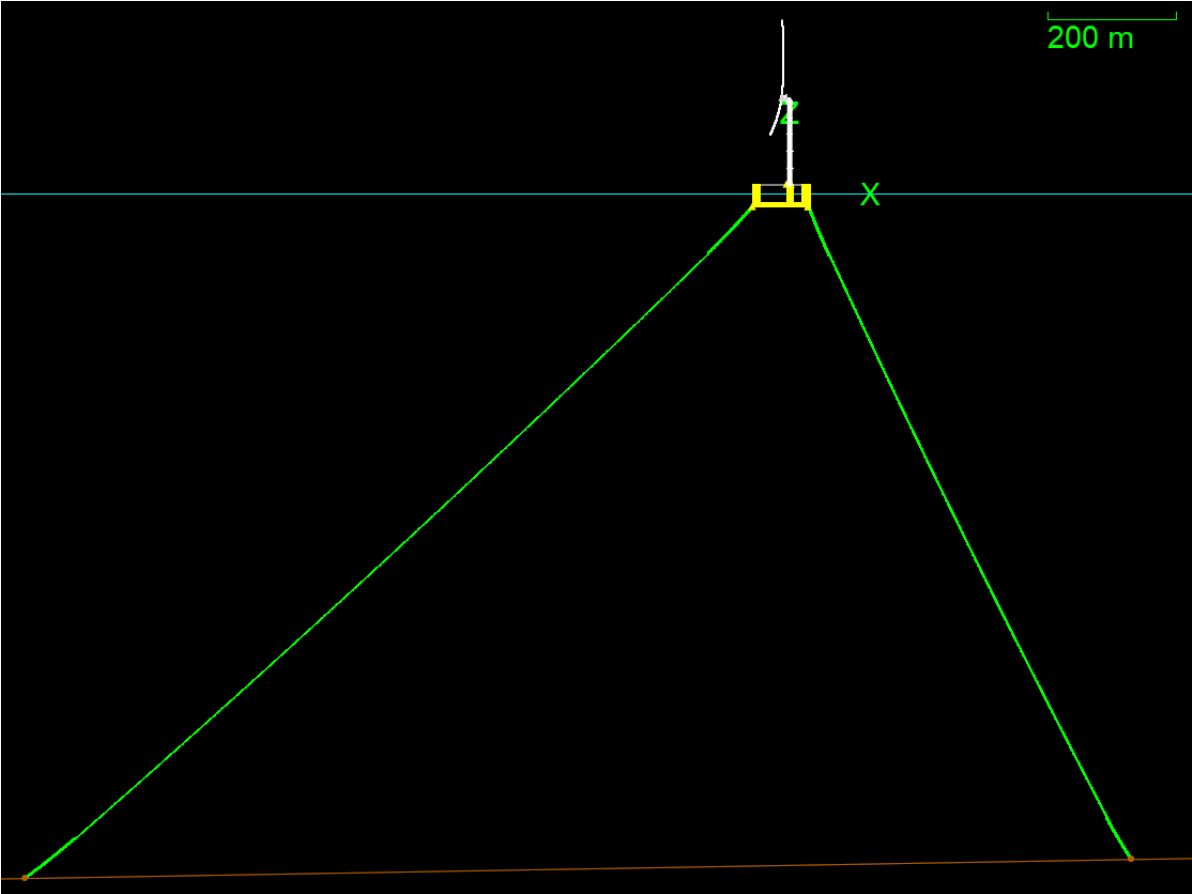
Figure 33. Base Model for the mooring analyses

6.3.4 Automation of the Simulations

It was mentioned in the earlier stages that several load cases that contain many load combinations correspond to hundreds of simulations. Thus, an automation process is needed for both the pre-processing and post-processing of the simulations. One of the most convenient methods is to create Excel tables for the desired load combinations. These tables are feasible in terms of the control of the environmental parameters that are required to change for each simulation. A base model data file is needed which will be updated for each load case. There is an OrcaFlex Excel add-in tool that aids the user with processing the data from the created tables to batch files that can be fed to the solver in the batch processing mode. As mentioned, 32 simulations can run in parallel with the available hardware for this study. There are several ways for automation, for example, if a specific result is needed from a simulation (e.g., max Von mises stress), one can add a Python code to the post calculation options that automatically saves the desired result to an Excel file.

Table 10. Example Excel table for OrcaFlex Excel tool

Script table	DLC Script.txt			
// Case	LoadData	Select Environment WindSpeed =	Select Environment WindDirection =	SaveData
1	"BaseCase.dat"	5	-10.00	Case01.dat
2		10	-5	Case02.dat
3		15	5	Case03.dat
4		20	10	Case04.dat
5		25	15	Case05.dat
6		30	20	Case06.dat
7		35	25	Case07.dat

The above Table 10 is an example of the Excel sheets that OrcaFlex tool can read. After a base design data was set, the tool can load the data and create new data files from the base data. It can be saved in OrcaFlex data files or text data files (.txt,. yml) for batch processing. This table can create data files with different wind speeds and different wind directions from the base model file.

7 SIMULATION RESULTS

To evaluate the simulation results, a Python script was used. First, the path should be defined for the folder directory that contains the simulation (.sim) files, then the models should be called to the OrcaFlex programming interface (OrcFxAPI). Then the commands defined in the OrcFxAPI library are used for loading the simulations and saving the effective tension results over the line length for the 10 minutes simulation period. A list of maximum effective tension results has been created by using for loop and append commands as can be seen below:

```
directory = 'D:\BaseModel'
maxEffList1 = []
for files in os.listdir(directory):
    if files.endswith('.sim') & files.startswith('DLC'):
        path = os.path.join(directory,files)
        model1 = OrcFxAPI.Model(path)
        model1.LoadSimulation
        line1 = model1['Mooring1']
        Results1 = line1.TimeHistory('Effective Tension',
OrcFxAPI.SpecifiedPeriod(0,600), OrcFxAPI.oeArcLength(1500))
        maxEffTen1 = max(Results1)
        maxEffList1.append(maxEffTen1)
```

This code finds the simulation files in the target directory and takes the time history results for maximum effective tension at the mooring lines between the desired period of simulation which is 10 *min* (600 *s*). The arc length was set to the whole length of the cable (1500 m for the upwind line), and finally, the list was made that holds the maximum effective tension results which is used in the limit state calculations.

7.1 Evaluation of the Maximum Mooring Line Tensions

The maximum tension results for the mooring lines have been summarized in Table 11. The "M1" stands for the mooring line in the upwind direction, "M2" and "M3" stands for the mooring lines in the downwind direction. DLCs 1.3, 1.6, and 6.1 are used for the ultimate limit state (ULS) calculation, along with DLC 10.3 which defines the accidental limit state (ALS). The directional load case has been evaluated as well.

Table 11. Maximum tension results

DLC	M1 Max. Ten. [kN]	M2 Max. Ten. [kN]	M3 Max Ten. [kN]
1.3	2525.60	1776.64	1781.16
1.6	2467.63	1816.78	1816.78
6.1	2355.73	1720.55	1756.53
10.3	-	1790.64	1860.7
Directional	2557.19	1849.034	1825.48

Afterward, factors of safety that have been provided by the ABS (*Guide for Position Mooring Systems*, 2022) and API RP 2SK (Shu et al., 2018) have been applied. The factor of safety for the DLCs 1.3, 1.6, and 6.1 is 1.67. For the DLC 10.3 (ALS) it is 1.25. Thus, the LS results are following:

Table 12. Limit state check for the Base Model

	MBS [kN]	M1 Max [kN]	M2 Max [kN]	M3 Max [kN]	LS Check
Chain	9864	4217.75	3034.02	3034.02	PASS
Polyester	6818.67	4217.75	3034.02	3034.02	PASS

In conclusion, the base model has passed the limit state check for the selected load cases, however, the results show that the selected cross-section diameters are over conservative, therefore, optimization is needed for the material cost reduction.

It should also be highlighted that the transient condition for the loss of the upwind mooring line could not be done in OrcaFlex because of the modeling system of the software. The software only allows for a smooth release of the mooring line, which results in neglecting the instantaneous loads that are due to the snapping of the line. Basically, a smooth release and drifting in the structure can be simulated in the software. This is adequate for the evaluation of the tensions for the downwind mooring lines for the accidental limit state as requested in DLC 10.3, however, it is not adequate for DLC 10.1 which is analyzing the transient condition.

For the directional load case, the same safety coefficient (1.67) cannot be utilized, since the results are a little higher than the highest tension of the required DLCs, this will result in an over-conservative design, a lower safety factor must be defined for this load case.

7.2 Evaluation of the Fatigue Life

The OrcaFlex software is equipped with different methods for fatigue calculations. For the mooring line fatigue calculations, the damage from the effective tension ranges for DLC 1.2

has been utilized with T-N curves. Thus, the first step is to simulate all the load conditions defined under DLC 1.2 (Power Production). Afterward, the wave scatter table for the desired area must be utilized to define several wave classes that the structure will experience. Upon the calculation of the damage, one of the three analysis methods must be chosen which goes as deterministic regular wave fatigue analysis, deterministic irregular wave fatigue analysis using the rain flow cycle counting method, or stochastic irregular wave fatigue analysis using spectral methods.

The rain flow method has the highest accuracy; however, it is also the most exhaustive in terms of computation effort and storage. It is based on the simulation load cases random wave collection. Each random wave load case is to be separated into a series of half-cycles with the utilization of a cycle-counting technique. The damage summation for each half-cycle is done with the Palmgren-Miner rule. In general, the damage accumulation can be written as:

$$D = \sum \frac{n_i}{N_i} \tag{17}$$

Where, n_i is the number of cycles of a tension range and N_i is the number of cycles to failure under a constant tension range. Thus, the damage value for the load case is obtained and then scaled with the exposure time that was set for the load case. Afterward, the summation of all the damage from all the load cases has been to calculate the total damage. Generally, the T-N curves can be represented by:

$$NR^m = K \tag{18}$$

Where the m is the slope of a T-N curve and K is the intercept parameter.

While setting the fatigue analysis, the simulation file name, (mooring line) name, simulation period, and the exposure time must be set (under load case data) to perform a rain flow fatigue analysis. The exposure time was determined from the scatter diagrams for the Morro Bay area, which was included in the COREWIND (2019) project design basis reports.

Other required data are the analysis and T-N curves data. At the analysis data, critical damage, and the number of arc lengths for the desired mooring line must be set. The critical damage is set to 0.1 since it is common practice to use a fatigue factor of safety of 10 for critical components hence a critical damage level of 0.1 is set which is the default value of the OrcaFlex. Arc lengths are set according to the sections of the mooring lines (chain-polyester-chain) and the T-N curves must be specified for each section. For the T-N curves data, three parameters must be set which are the reference breaking strength of the material (kN), and m and K

parameters (Table 13). RBS can be found in the OrcaFlex library, the reference values for the other parameters are from API RP 2SK (Shu et al., 2018) standard. (Xue & Chen, 2017).

Table 13. Fatigue analysis parameters for the Base Model mooring lines (ABS, 2022)

Component	m	K	RBS (kN)	Diameter (m)
Studless Mooring Chain (R4)	3	316	9864	0.1
Polyester (8-strand multiplait)	5.2	25000	6818.67	0.2

Finally, mooring fatigue analysis have been made for the base model. The results are presented at the Table 14 below. Fatigue analyses have been repeated two times to ensure the accuracy of the results.

Table 14. Initial fatigue results for the Base Model

Component	Fatigue Life (years)	Arc Length (m)
Mooring Line 1 (Upwind)	17 - 18	100.5
Mooring Line 2 (Downwind)	300 - 400	1300.5
Mooring Line 3 (Downwind)	300 - 400	1300.5

It can be seen from the results that, the mooring line in the up-wind direction has a fatigue life of 17 to 18 years which is less than the desired design life and for the mooring lines in the down wind direction has a design life of 300 to 400 years which is over conservative for the desired design conditions.

The upwind mooring line fatigue occurs around the top connection of the mooring chain and the polyester line, the downwind mooring line fatigue on the other hand, occurs around the bottom connection of the mooring line chain and the polyester. The selected polyester diameter has been found over conservative as well.

It was expected that in the beginning that the upwind mooring line will experience the highest tensions, the results were in line with this expectation.

Upon obtaining these results, a correction was necessary for an acceptable fatigue life for the mooring lines. Thus, another model was created where shorter chain length has been used for the mooring lines. The chain length of the upwind line was decreased from 100 m to 75 m.

Additionally, diameters have been changed for the materials. The chain diameter has been increased by 20% for the upwind line while the chain diameter of the downwind lines has been decreased by 20%, the polyester line diameter has been decreased by 20% as well. In the beginning, all three lines were modeled with same material and diameters, this time the approach have been changed.

Table 15. New mooring characteristics for improved fatigue life

Component	RBS (kN)	Diameter (m)
Studless Mooring Chain for Upwind (R4)	13570	0.12
Studless Mooring Chain for Downwind (R4)	6593.54	0.08
Polyester (8-strand multiplait)	4363.95	0.16

After changing the parameters (Table 15), the same steps have been followed for the fatigue analysis. The load combinations under DLC 1.2 have been simulated against the structure again, and the simulation files are then fed to the solver. After repeating the fatigue analysis procedure, the following results (Table 16) have been found.

Table 16. Evaluation of the fatigue life for the new model

Component	Fatigue Life (years)	Arc Length (m)
Mooring Line 1 (Upwind)	~ 42	74.5
Mooring Line 2 (Downwind)	180 - 220	1300.5
Mooring Line 3 (Downwind)	180 - 220	1300.5

It can be observed that the fatigue design life of the upwind mooring line has been improved. And it satisfies the minimum design life criteria (30 years for FOWT).

Additionally, the downwind lines became less conservative.

The fatigue occurs at the same locations as the previous model, which are close to the connection point between the top chain and the polyester for the upwind line and the bottom chain and polyester for the downwind lines.

After the changes, the design life has been improved to be safer and more acceptable for DLC 1.2. However, it is still not the optimum design.

The safety factor for the fatigue life has been determined as 3 by ABS (2022) and API RP 2SK (Shu et al., 2018), therefore the design life should be set to 90 years for all components.

Thus, a detailed optimization study is needed that accounts for the fatigue life and the cost of the mooring system. Such optimization must consider the mooring and anchoring parameters such as the locations, angles, and materials along with the platform drifts.

A small optimization study was conducted for this study which is explained in Ch. 9 in detail.

Another issue that can affect the fatigue life is the vortex-induced vibrations characteristics of the design, the next chapter has been dedicated to a 2D CFD application that evaluates the flow and vorticity characteristics of the polyester cable.

8   VORTEX-INDUCED VIBRATIONS STUDY

As explained earlier, VIV/VIM phenomenon is a contributor to the overall fatigue damage of the mooring lines. Generally, the long-term distribution of the current conditions is utilized to calculate the fatigue damage from the VIV/VIM motions, and the results are summed with the wind/wave combined fatigue damage (Shu et al., 2018).

OrcaFlex software can be coupled with third-party software (e.g., SHEAR7, VIVA) to assess the VIV/VIM characteristics of a structure, however, the mentioned software is not publicly available at the time of this study. Therefore, a 2D study in Lily Pad open source CFD software was made to check the flow around the cross-section of the mooring line that was modeled in the earlier stages. For this study, guidance was provided by Dr. Leixin Ma (MIT, UCLA) who is an expert in vortex-induced vibrations.

In general, there are some difficulties that are permanent in CFD software (e.g., time integration of the finite-scale nonlinear momentum equations, and inversion of a Poisson equation for the pressure). The fluid equations themselves are not the main reason for the CFD software complication. The real problem comes from coupling the equation to the irregular data at domain boundaries. This coupling is accomplished by boundary-fitted mesh adaptation which increases the complexity of the numerical algorithmic method along with the computing effort. The main goal of the Lily Pad is to handle these problems to present rapid and vigorous software. (Weymouth, 2015)

The Boundary Data Immersion Method (BDIM) was adopted for solid and fluid equation coupling in Lily Pad. In Lily Pad, the BDIM method was utilized for altering the motion equations for solid-fluid interactions to solve them in a uniform Cartesian grid. Therefore, the analytic governing equations have been adjusted to provide a basic and efficient numerical method instead of concealing the numerical complexity or embracing physical simplifications. In the software, the fluid and solid governing mechanical equations are utilized in non-dimensional form.

The uniform flow velocity and the grid size are the main scaling factors for this non-dimensionalization of the software since the parameter dimensions such as size or time are customized by the user and cannot be geared into the governing equations. Therefore, robustness is ensured for the grid-based parameters, however, scaling is needed for the engineering coefficients such as the length, time-step, and viscosity of the fluid.(Weymouth & Yue, 2011)

A script has been developed in Lily Pad at the Processing 3.5.4 development environment. Lily Pad provides classes that can be implemented for users to solve the desired CFD system. There are four main classes: Field, VectorField, Body, and BDIM. The cross-section of the mooring line was assumed to be fixed, and since the fairlead angle is 45°, the cross-section of the line that is perpendicular has an elliptical geometry.

```
AncientSwimmer mooring;        // For Pressure Results
BDIM flow;                     //Initialize Flow
FloodPlot plot;                // Visualize
CirculationFinder cf;          // Find the circulation behind the body
PrintWriter output;            // Initialize results output
int n=(int)pow(2,8);           // Define the nb. of grid points
float L = n/8.;                // Define the length in terms of grid points
float St = 0;                  // Strouhal (St) number (not applicable)
float Re = 246886;             // Real Reynolds (Re) number
float ReG = Re/L;              // Grid-based Reynolds number
float t = 0;                   // Initialize time
```

This part of the code defines the setup of the simulation. The AncientSwimmer is a class provided by the Lily Pad software which helps to get pressure results for two bodies in a flow. The default AncientSwimmer class was adjusted for the application. Normally, it has two bodies (one NACA profile and one circle body), however, the NACA profile was replaced with the ellipse body for the mooring line, and the circle body was defined with a very small diameter and is located outside the domain boundary, therefore it does not influence the calculations. The modified AncientSwimmer class has been provided at the APPENDIX B. The BDIM class defines the flow. The FloodPlot is for visualization and the CirculationFinder finds the circulation behind an object in a defined flow.

The number of grid points must be set as "*a large power of two to allow sub-division in the multi-grid solver.*" Increasing the grid points results in an increase in resolution and accuracy for the simulations but the computational time increases as well. The ellipse length is given as n/8 grid cells, in the software, all distances must be given as unit grid spacing for the non-dimensionalization as mentioned earlier. This means that all dimensions are defined with respect to resolution. (Weymouth, 2015)

Strouhal number is applicable for objects with motion, and it is required by the AncientSwimmer class, however, the mooring line has been assumed to be fixed, and therefore the St number has been set to zero. The real Re number was calculated with the formula:

$$Re = \frac{\rho * U * L}{\mu} \tag{19}$$

Where ρ is the density of the fluid, U is the flow (current) speed, L is the chord length and μ is the dynamic viscosity of the fluid. The average temperature of the Morro Bay area has been found as 6.7°C, and this value was used for finding the density and viscosity parameters.

$$Re = \frac{999.87 * 1.26 * 0.2828}{0.0014431} \cong 246886 \tag{20}$$

Re number is non-dimensional, however, it must be adapted to the software in terms of grid points therefore it is divided by the grid-based length.

```
void setup(){
  size(1000,500);                                      // Window size
  Window view = new Window(n,n/2);                     // View coordinates
  mooring = new AncientSwimmer(4*L,n/4,L,3000*L,0,St,view);  // Geometry
  flow = new BDIM(n,n,0,mooring,1/ReG,true);           // Flow definition
  plot = new FloodPlot( view );                        // Plotting
  plot.setLegend("Vorticity",-0.95,0.95);              // Legend
  output = createWriter("mooring/out.csv");            // Result output
  cf = new CirculationFinder(flow,mooring,view);       // Circulation
  cf.setAnnotate(true,1.0/L); }
```

This part of the code initializes the view, geometry, flow, plot, and output of results.

```
void draw(){
  t += flow.dt;                                        // Update the time
  flow.update(mooring); flow.update2();                // 2-step fluid update
  cf.update();
  plot.display(flow.u.curl());                         // Vorticity display
  mooring.display();                                   // Geometry display
  cf.display();
  // saveFrame("mooring2/frame-####.tga");             // Image output
  PVector[] forces = mooring.pressForces(flow.p);      //Pressure force calculation
```

This part is for time update, display, and visual outputs. Moreover, the last part calculates the pressure forces over the body. The simulations were set to 10 cycles.

In general, the number of grid points and the number of cycles can be set in by a sensitivity study, however, since the task is simple, these values were set manually by trying different values. As can be seen, the simulations were set with a few lines of code. This script gives a base to the simulations, one can add more lines for different purposes such as calculating the lift and drag forces with integrating the pressure vector. For this study, the software was used to highlight the flow separation phenomenon which is the main reason for the vortex-induced vibrations and cannot be disregarded for the desired project with significant mooring length.
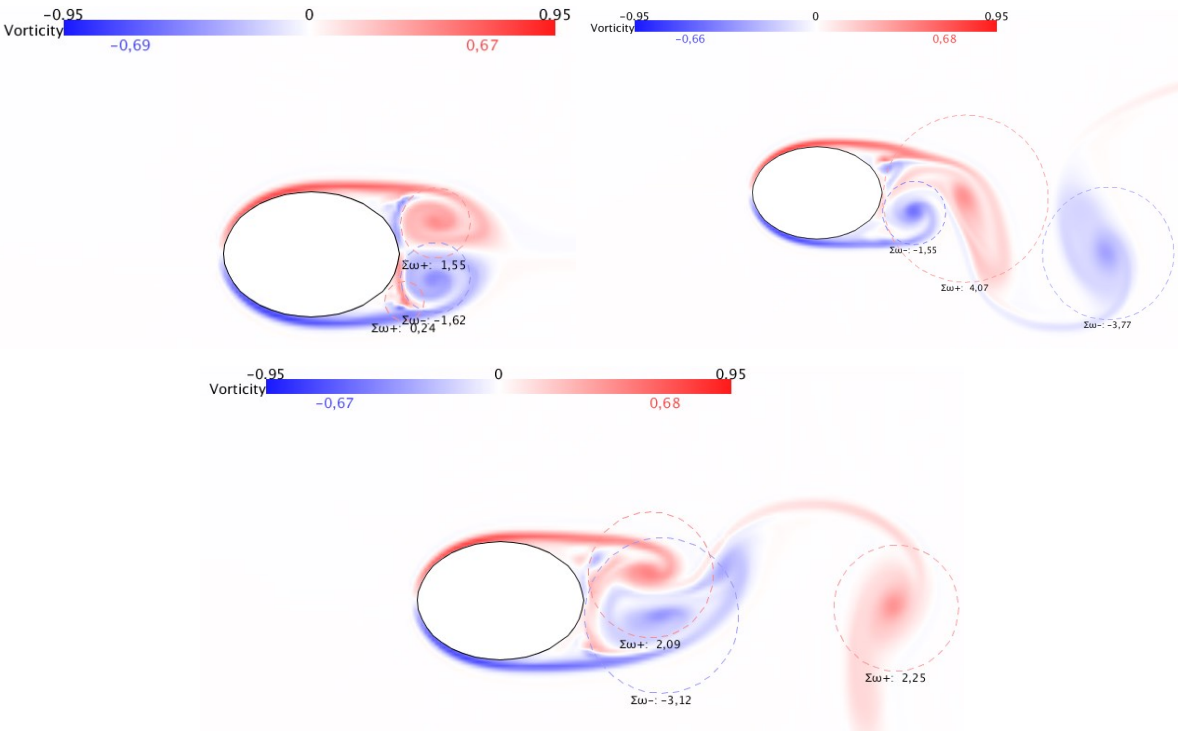
Figure 34. Flow around the cross-section of the mooring line

It was observed that flow separation occurs behind the cross-section of the mooring line with significant vorticity (Fig. 34). The only publicly available current speed data for the Morro Bay area is the 20-year maximum speed data which is 1.26 *(m/s)* and it was used in all calculations. This value is higher than average ocean current data which is 0.05 to 0.5 *(m/s)* according to Britannica (n.d.). The current speed is relatively high; therefore, it can be concluded that vortex-induced vibrations must be evaluated along with the vortex-induced motions with more complete data and advanced 3D CFD simulations (e.g., OpenFOAM)

9   FATIGUE LIFE OPTIMIZATION

It was stated in the earlier chapters that further optimization is required for a complete design cycle of the mooring system. This chapter is aimed to demonstrate a multi-objective optimization by coupling the OrcaFlex with modeFRONTIER via Python scripts for the optimization of the fatigue life of the upwind mooring line. The methodology, sequence, and results have been explained in further chapters.

9.1   Optimization Setup and Run

As mentioned, Python scripts were utilized for coupling the two software. These scripts were divided into three categories. Pre-processing, processing, and post-processing.

The base data files were already present from the previous fatigue study. These data files were copied to a new folder, and they were named "OPT" files with different numbers, 505 files were present for the fatigue load case.

```
# <fmiModelDescription fmiVersion="2.1" modelName="orcapy-preprocess2" guid="">
#    <ModelVariables>
#       <Variable name="UPP_L" valueReference="0" causality="parameter">
#          <Real/>
#       </Variable>
#       <Variable name="UPC1_L" valueReference="1" causality="parameter">
#          <Real/>
#       </Variable>
#       <Variable name="UPC2_L" valueReference="2" causality="parameter">
#          <Real/>
#       </Variable>
#       <Variable name="AZEnd1" valueReference="3" causality="parameter">
#          <Real/>
#       </Variable>
#       <Variable name="BXEnd1" valueReference="4" causality="parameter">
#          <Real/>
#       </Variable>
#       <Variable name="ADec1" valueReference="5" causality="parameter">
#          <Real/>
```

```
#       </Variable>
#       <Variable name="BDec1" valueReference="6" causality="parameter">
#          <Real/>
#       </Variable>
#    </ModelVariables>
# </fmiModelDescription>
```

For this study, the variables were defined as the line segment lengths for the upper chain, polyester line, lower chain lengths, the fairlead and anchor connection points, and angles for the upwind mooring lines. These are the seven optimization variables for the optimization sequence. The names are used by the modeFRONTIER software to define new inputs. This part needs to be kept as commented in the script at the top.

```
directory = os.getcwd()                            // Find the folder
for files in os.listdir(directory):                // Start Loop
    if files.endswith('.dat') & files.startswith('OPT'):   // Find data files in the folder
    path = os.path.join(directory,files)           // Define the path
    model = OrcFxAPI.Model()                        // Connect to OrcFxAPI model
    model.LoadData(path)                            // Load the model data
    line = model['Mooring1']                        // Line data
    line.NumberOfSections = 3                       // Divide the line to 3 segments
    line.Length[0] = UPC1_L                         // Define first segment length
    line.Length[1] = UPP_L                          // Define second segment length
    line.Length[2] = UPC2_L                         // Define third segment length
    line.EndAZ = AZEnd1                             // Define upper end of the line
    line.EndBX = BXEnd1                             // Define lower end of the line
    line.EndADeclination = ADec1                    // Define upper line angle
    line.EndBDeclination = BDec1                    // Define lower line angle
    model.SaveData(path)                            // Save the new data
  else:
    continue
```

The code defines the path of the folder and finds the data files that contain the model data information. These files contain all the data for the simulations, however, for the optimization, some of them are required as optimization variables.

Lastly, the data is saved and processed by starting the simulation sequence. This part is straightforward.

> *model.LoadData()*
>
> *model.CalculateStatics()*
>
> *model.RunSimulation()*
>
> *model.SaveSimulation(self.changedExtensionFileName('sim'))*

Firstly, the new data files are loaded, then the statics calculation was done before running dynamics, then the simulation files were saved with the ".sim" extension.

Afterward, post-processing of the results has been required.

meanEffListA = np.zeros(505)

meanEffListB = np.zeros(505)

hours = np.array([hours data that was calculated from scatter diagram])

gen = (files for files in (os.listdir(directory)) if files.endswith('.sim') & files.startswith('OPT'))

i=0

for files in gen:

  try:

    path = os.path.join(directory,files)

    model = OrcFxAPI.Model(path)

    model.LoadSimulation

    line1 = model['Mooring1']

    ResultsEndA=line1.TimeHistory('Effective Tension', OrcFxAPI.SpecifiedPeriod(0.0,600.0), OrcFxAPI.oeEndA)

    meanEffTenA = np.mean(ResultsEndA)

    meanEffListA[i] = meanEffTenA

    ResultsEndB=line1.TimeHistory('Effective Tension', OrcFxAPI.SpecifiedPeriod(0.0,600.0), OrcFxAPI.oeEndB)

    meanEffTenB = np.mean(ResultsEndB)

    meanEffListB[i] = meanEffTenB

    i=i+1

  except:

    print(files)

First, empty arrays with a length of 505 were created for appending the effective tension results, and an array was created that contains the hours per year data that was calculated from the wave scatter diagram from the Lifes50+ project report for the Morro Bay area.

Afterward, the simulation files were found and the effective tension results from both ends were taken to save to the list of mean effective tension arrays that was created earlier.

Finally, this array was multiplied by the "hours" array with respect to the correct order of hours that were added manually. Then, the results were summed by the following script.

opt1 = sum(meanEffListA*hours)

opt2 = sum(meanEffListB*hours)

The "opt1" contains the summed effective tension times hours results at the upper end of the line (fairlead) and the "opt2" contains the summed results for the anchor connection. These two results will be minimized for the optimization of the upwind mooring line. Therefore, the coupling was made.
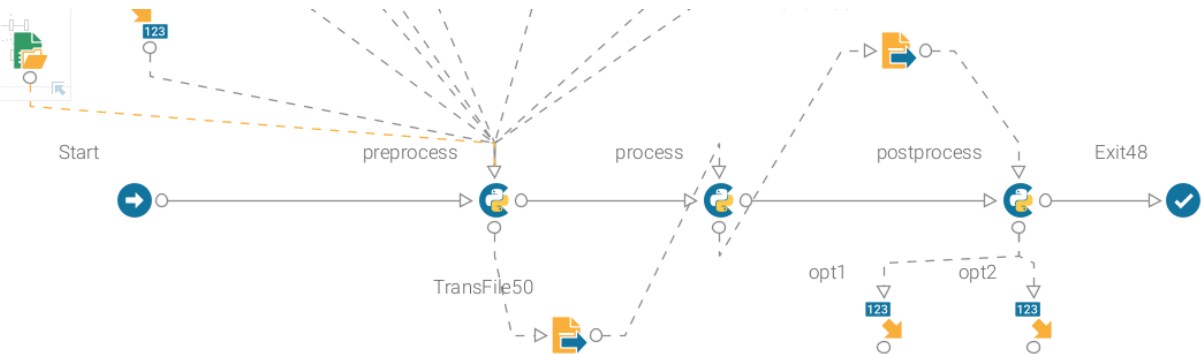
Figure 35. First workflow for modeFRONTIER

As can be seen from Fig. 35, the first workflow was made with the three pieces of the scripts. However, this was not the most efficient way in terms of computational effort.

Mr. Adarsh Elango (ESTECO SpA Application Engineer, personal communication) suggested that the program will run more efficiently if these three codes were merged into one. This is quite simple.

However, there was another issue that is more complex which is the multiprocessing setup. As mentioned in the earlier chapters, OrcaFlex has a batch processing mode that allows the user to run parallel simulations simultaneously. The number of parallel simulations was dependent on the hardware (cores) of the workstation and 32 parallel simulations were doable in the batch processing mode. Normally, it is easy to select the data files by hand and run the simulations in

batch mode for analysis, it was not possible to connect to the batch mode of the software. Another solution was found for Python with the guidance and support of the Orcina engineering team by utilizing the multiprocessing library of Python.

Finally, the merged code was integrated into multiprocessing functions to set the parallel processing. The final code (APPENDIX C) can parallelize not only the simulations but also the pre- and post-processing stages, one can also set the number of cores to use.
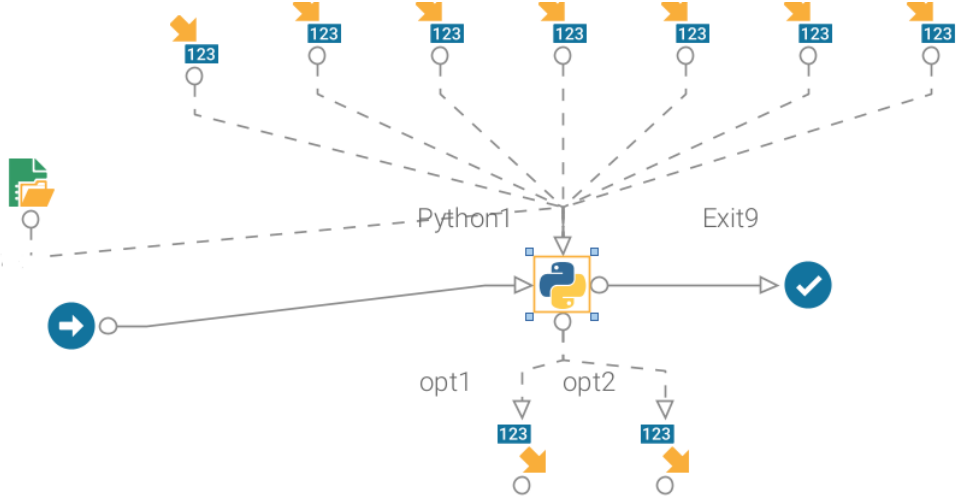
Figure 36. Final workflow for modeFRONTIER

As can be seen from Fig. 36 that the workflow was improved by needing fewer transfer files. The next step is to set up the initial design of experiments (DOE) run with the defined input parameters. In the modeFRONTIER software, one needs to define the default values and bounds (lower and upper) for the input parameters.

Generally, an optimization sequence is a part of the design cycle that targets to find the best design solution from a few feasible solutions for a target criterion or several criteria. Thus, an initial design (the base model) is present that lays the foundation of the process, and it is open for improvement within reason.

This improvement is directly affected by several assets such as the time, resources, data, experience, and expertise to formulate the optimization problem at hand. In optimization studies, numerous factors or parameters that need to be balanced with respect to each other to reach a certain goal while maintaining important characteristics for the final design. One can reach an optimum design in terms of a single goal that was set, but the design might end up being impractical. Therefore, the problem formulation must be adequately carried out and the design objectives (multi-objective optimization) must be set accordingly. In modeFRONTIER, after a multi-objective design optimization run, the software presents several feasible optimum designs for the user to evaluate. (ESTECO SpA, 2022)

In real life, it is well known that one cannot reach a perfect optimization solution for structural optimization. The aim is to find several solutions with a good compromise between the objectives. This leads to the concepts of Pareto optimality and dominance (Pareto et al., 1971). When a series of optimum solutions cannot be improved without violating each other (non-dominated) it is named a Pareto front (Pareto optimal set). Thus, to gain an improvement for one objective (or objectives), there is always sacrifice for another objective (or objectives). As mentioned earlier, the software presents several feasible designs after an optimization run, these are the Pareto optimal points in a Pareto front. The end product decision is a bargain that is based on objective and practicality. (ESTECO SpA, 2022)

The Pareto front can be astronomical (or even boundless) for real-life many multi-objective optimization problems. Therefore, it is unwise to try to determine it as a whole (or impossible) in terms of computational effort. Thus, to catch the whole Pareto spectrum that presents the bargains to the decision-making process, one needs to aim for *"a subset of the Pareto design which is as uniformly distributed and diverse as possible",* this leads to dominance criteria for the Pareto. The criteria state that the feasible and non-dominated feasible designs are chosen over the unfeasible and dominated feasible designs. Also, when a comparison cannot be made between a couple (i.e., two non-dominated feasible designs), one of them is randomly selected. Lastly, unfeasible designs that have a lower violation of constraint are chosen over the ones that have a higher violation. (ESTECO SpA, 2022)

In general, the DOE is the first step of the optimization sequence. The DOE is utilized for the determination of a suitable initial population for the optimization algorithm to work on. In other words, it is the initial investigation of the design space. The software provides two kinds of algorithms, space filler DOE or optimal designs. The optimal designs require an existing knowledge/database that contains previous optimum designs. (ESTECO SpA, 2022)

In each input space, space filler DOE targets the finest coverage for this space. In general, the space filler designs (SFD) approach has an initial exploring phase. At this stage, the information about the design or the numerical model is limited, or there are various objectives present for the design. (Damblin, Couplet, and Iooss, 2013)

The DOE size differs depending on the selected optimization algorithm. However, for genetic algorithms, the DOE quality has a small impact. (ESTECO SpA, 2022)

The DOE is a testing sequence. As mentioned earlier, the initial DOE run, which analyzes the relationships between all the variables (input and output) along with the initial boundaries is important for the initial screening of the design space. Therefore, one can observe the relationships between the parameters, and check the initial boundaries, objectives, and

constraints. This helps to rearrange the boundaries and define a better domain according to the desired goal, for this study, the aim is to minimize the length and the tension of the upwind mooring line. (*ESTECO Resource Library*, n.d.)

The general empirical formula for the DOE can be expressed as follows (ESTECO SpA, 2022):

$$DOE\ Size = 2 * n_{input} * n_{objectives} \qquad (21)$$

Initial input parameters are the three segment lengths for the mooring line, upper and lower connection points, and connection angles. Therefore, there are 7 input parameters. The output parameters are the summation of effective tensions times the hours,

$$DOE\ Size = 2 * 7 * 2 = 28 \qquad (22)$$

Mr. Adarsh Elango (ESTECO SpA Application Engineer, personal communication) suggested to use the size 30 on his experience. Therefore, 30 different design setups were created with random input parameters. Various methods that are present in the software for the production of these random input parameters. Uniform Latin Hypercube (ULH) DOE is one of the methods which is evolved from the Monte Carlo technique (ESTECO SpA, 2022).

The Monte Carlo sampling is a long-established technique for the extraction of random numbers concerning the statistical distribution that was chosen. The extraction is completely random in this sampling method; thus, the drawn value can be in any location at the defined distribution range. Constraining the Monte Carlo sampling technique forms the Latin Hypercube. The constraint *"refers to the way each variable is sampled"*. Stratified sampling is the foundation of the LH technique. In stratified sampling, the statistical distribution is divided into several non-overlapping groups (strata) that have the same probability. Then, from each stratum (sub-group), a random sample is selected concerning the density function. Therefore, distribution over the range of the density function is relatively uniform since each stratum holds one sample. Thus, enhanced precision is ensured when compared to the Monte Carlo method. This is useful in terms of decreasing the number of required runs to reach a satisfactory uniform random sampling. (Iman & Conover, 1982)

The ULH DOE (or advanced Monte Carlo sapling) is a stochastic algorithm of space-filler (SF) DOE. The ULH utilizes the uniform distribution, in the case of mooring line parameters, the input parameters have the same probability, and no constraints were defined for this. Therefore, the uniform distribution is suitable for the application. The ULH aims to maximize the distance between the products and minimize the correspondence between input parameters over the

variable range to achieve a uniform distribution. It is a convenient method for GA optimizations. (McKay et al., 1979)

The ULH can create uniform distribution over the discrete and continuous input parameters, while the LH is limited to the continuous ones, this is the main difference between the ULH and LH sampling. (McKay et al., 1979)

The DOE size was set to 30, which means that 505 simulations will run 30 times for the initial sampling, which results in 15150 simulations. It can be observed that the computational effort is intense for these simulations. Dynamic analysis in the time domain requires time and memory. Some simplifications in the model were necessary to reduce the computational burden. A few simplifications have been made in favor of this burden under the guidance and support of Dr. Matthew Hall (NREL Research Engineer, personal communication). Dr. Hall suggested that, for the mooring optimization, common practice is to simplify the FOWT model by removing the upper structure and adding the mass and inertia characteristics as point masses. Therefore, the blades were removed from the FOWT model while the masses and inertias are maintained, and the number of FE elements on the upper structure have been reduced. This reduces the complexity of the model significantly. It was mentioned in the earlier chapters that the aerodynamics data comes from an external software (BLADED) for the model. After removing the blades, it was possible to utilize the frequency domain simulations. As explained earlier, frequency domain simulations are much faster than time domain simulations since the problem is linearized.

Additionally, a sensitivity analysis was performed for the target segment length of the finite elements. As mentioned in the earlier chapters, ABS rules require that the target segment length cannot be higher than 1 *meter* for finite element applications. Since the hardware has a limiting effect on the study, only upwind mooring line tensions were set for the optimization. Therefore, the decrease in the number of finite elements is not important for this part of the study. Also, the sensitivity analysis for the end tension results of the upwind mooring line shows that the results don't change significantly (<1%) until 20 *meters* of segment length.

After the initial DOE is finished, the optimization sequence was set. Generally, there are two classes of optimization algorithms which are gradient-based and gradient-free methods. Since the requirement of the information about the derivative is not present for the gradient-free methods, they are simpler for implementation. The genetic algorithm (GA) is an example of a gradient-free method. (Li et al., 2019)

GAs are popular types of evolutionary algorithms (EAs) which are stochastic optimization techniques that are based on the natural evolutionary processes. GAs stand out from other

70

common optimization techniques in a few ways. They utilize the coding of the set of solutions instead of the solution itself. They scout a solution population instead of one solution. They utilize the fitness functions instead of the derivatives and they utilize the probabilistic transition rules instead of the deterministic ones. (Shafieefar & Rezvani, 2007)

They present some degree of randomization for the process of searching. Thus, the slow convergence in the search process due to error in modeling is decreased, the progress has enhanced speed and the local optimums are avoided to ensure the global optimum convergence. (Andre et al., 2001)

GAs are heuristic algorithms, which means the algorithm finds an optimum by improving a target solution iteratively with a certain amount of quality. Heuristic algorithms make little to no assumptions on the optimization problem and can search wide solution spaces to find the optimum solutions with a fair computational effort. (F.-S. Wang & Chen, 2013)

The GA formulation is based on Darwin's (1859) evolution. According to the approach, the strongest individuals (good adaptation) will transfer their genes to the next generation while the weak individuals (bad adaptation) cannot transfer theirs. For the GA, discrete characteristics (for example parameters of design) in the domain of solutions are named the "phenotype", in general, these are coded in a "genotype" (chromosome), and all discrete characteristics in a genotype are named as "gene". The GA iterative process permits the members of the population to evolve at every step. (Felix-Gonzalez & Mercier, 2016)

A basic example loop of the GA algorithm (Fig. 37) and the steps are following:

1. A random initial population is spawned.
2. Selection of the parents (via fitness function) for transferring the genes
3. The operators (crossover and mutation). The crossover unites the genes for the selected parents to produce a new generation (offspring). This is an iterative approach. It is based on the aim that the best genes in subsequent populations will more frequently emerge over each crossover iteration, therefore the convergence will be reached over time. The mutation operation alters a parent's genes randomly, thus, the algorithm avoids the local optimum solutions.
4. The offspring population replaces the old population.
5. The last step is to finish the process either by reaching the defined tolerance or the defined number of maximum offspring reproduction.
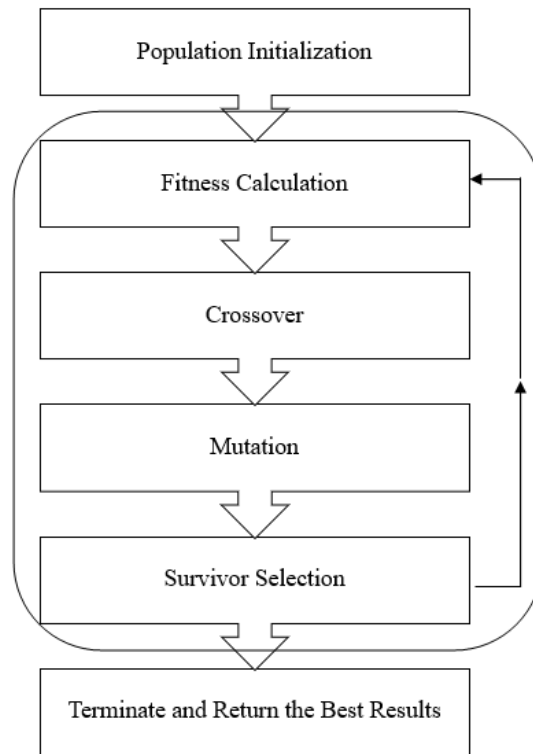
Figure 37. Basic GA algorithm (Ja'e et al., 2022)

Important benefits of the GAs are the robustness (in exchange for a lower rate of convergence for highly sensitive cases), befitting to multi-objective or many multi-objective optimizations (with complex objectives), and befitting to the problem of any dimension. Also, it provides a proficient exploration process for the design space. (Johnson & Rahmat-samii, 1994)

The gradient-based algorithms, on the other hand, are deterministic techniques that find the next points by utilizing the derivatives (via approximated finite differences). In general, these methods have better convergence characteristics compared to the GAs in terms of the required number of iterations (time), but they cannot utilize a random search like GAs. Thus, the exploration process of the design space is not broad, which can lead to a convergence in the local optimum points. The gradient-based methods are beneficial for their accuracy and convergence rates. They can also address problems of any dimension; however, it may lead to high demands in terms of computation. (Christensen & Klarbring, 2009)

Sequential quadratic programming (SQP) is a powerful iterative method for nonlinear (and non-quadratic) constrained optimization problems of general purpose:

$$P_k \begin{cases} Minimize\ f(x) \\ subject\ to\ g_j(x_k) \leq 0\ (j = 1, \dots, m) \end{cases} \tag{23}$$

Under the assumption that the problem is not too big, the functions and gradients can be evaluated with sufficiently high precision, the problem is smooth and well-scaled. The process

72

starts with the selection of an initial point (x_0), at each iteration (k), the method utilizes second-order Taylor expansion to replace the classical Lagrange function by its quadratic approximation at around the iterate "x_k", and the functions of constraint (g_j) by their first order Taylor expansion at the same point, solve the problem to get the next point "x_{k+1}" and continue the iteration. The SQP includes derivatives, thus the computational burden increases with the number of constraints and variables. (Christensen & Klarbring, 2009)

The HYBRID algorithm is composed of a steady-state GA and SQP (AFilterSQP adapted to multi-objective) algorithm. This combination algorithm in the software aims to boost the classical GA via parallelization, elitism, and metamodels, thus, enhancing the strength of computation and information gathering. (Turco, 2011a)

The DOE defines the initial population of the optimization algorithm. A design from the GA parent population (random and non-dominated) is selected for initialization of the SQP algorithm, thus, the efficiency of the search procedure is boosted. The method can deal with discrete and continuous variables. (Turco, 2011b) This algorithm was found suitable for the multi-objective optimization of the upwind mooring line.

After the selection of the optimization algorithm, one needs to define the number of evaluations depending on the availability of computer hardware. For the study, this number was set to 100 (+30 from the initial DOE run), and the selection was made under the guidance of Mr. Adarsh Elango (ESTECO Application Engineer, personal communication) after a survey of the available workstation hardware and computation time.

In general, mooring optimization involves many inputs such as the line materials, diameters, lengths, and constraints. The initial optimization study was conducted for the upwind mooring line. Initially, 7 input parameters and 2 output parameters were set for the optimization, a full-scale optimization was not possible because of the hardware limitations.

Table 17. Optimization input parameters

Name	Default Value	Lower bound	Upper bound
Anchor Angle (°)	45	30	75
Anchor Position (m)	-1191	-1475	-78
Fairlead Position (m)	-20	-20	15
Fairlead Angle (°)	135	120	180
Upper Chain Length	100	10	100
Polyester Length	1300	880	2060
Bottom Chain Length	100	10	100

Thus, only the upwind mooring line which has the highest tension results were studied. As mentioned, the input parameters were the 3 section lengths, anchor location and the angle at the seabed, fairlead location and angle at the platform, upper and lower bounds were defined (Table 17) for the input parameters.

The output parameters were set according to the fatigue calculation method of the OrcaFlex software. The two main parameters of the fatigue calculation are the tension results and the duration of each load case. Thus, the outputs were set as a sum of the mean effective tension of the end multiplied by the hours (per year) for both ends of the line. The initial aim was to minimize these two outputs. The initial DOE run presented that these two outputs have close magnitudes. Thus, the first objective function was defined to minimize the sum of these two outputs, since their magnitude is close, they were not normalized. A second objective was for minimizing the line length (sum of the 3 sections), to reduce the material usage.

9.2   Optimization Results

After the initial optimization run, Fig. 38 (scatter chart) and Fig. 39 (parallelized coordinates chart) have been obtained. The following Fig. 38 represents the design space. "MinTension" (vertical axis) represents the first objective (sum of the end tensions multiplied by the duration) which is maximizing the fatigue life and "MinLength" (horizontal axis) represents the second objective which is to minimize the total length.
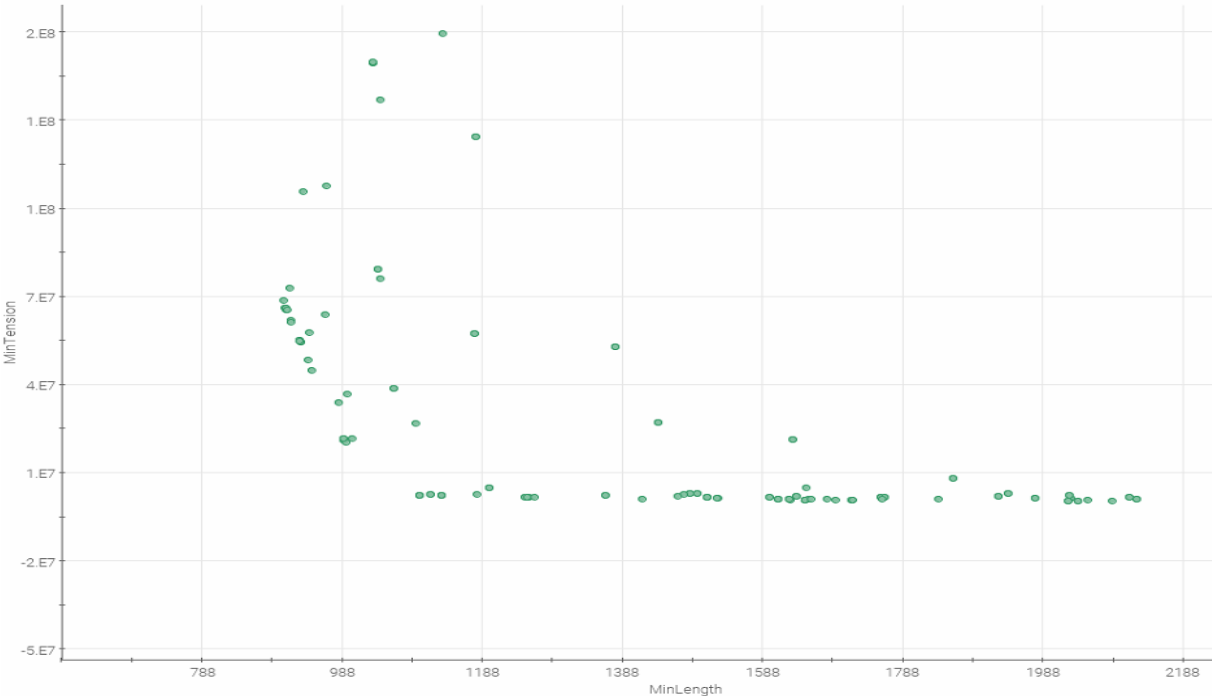
Figure 38. Initial optimization scatter chart (modeFRONTIER)

74

It can be observed that a compromise is required for the selection of the optimum design. Length minimization of the mooring line can lead to an increase in the tension results, a compromise needs to be made. Additionally, the design variables should be controlled to check the physical feasibility of the design.

It was mentioned earlier that the primary target of this optimization study is to maximize the fatigue life of the upwind mooring line. Thus, the parallelized coordinates chart has been utilized for optimum design evaluation.

The parallelized coordinates chart (Fig. 39) presents the relationships between the input variables and output objectives. Each line represents an evaluated design. Additionally, one can modify the lower and upper bounds of any parameter on the chart. This modification eliminates the designs that are not suitable for the new boundaries.
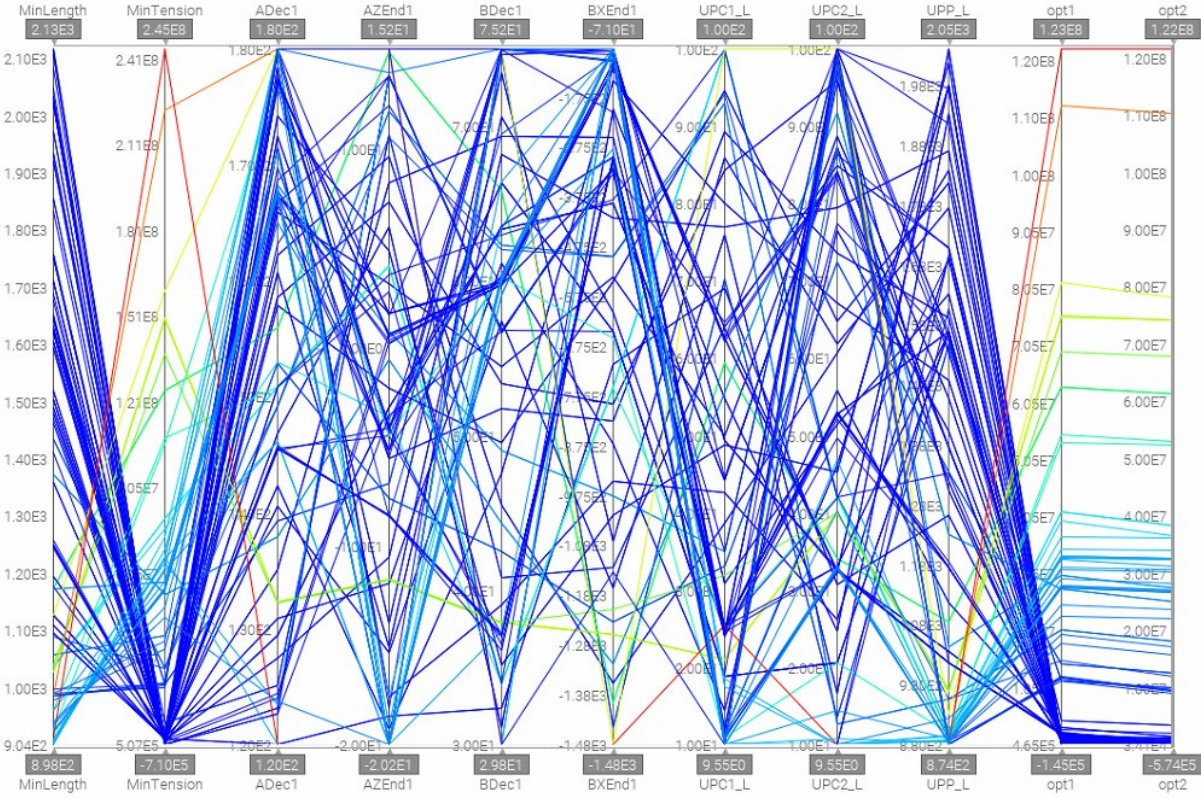
Figure 39. Parallelized coordinates chart for initial optimization (modeFRONTIER)

This chart was utilized for finding the best 10 optimum Pareto solutions by modifying the upper bound of the "opt1" and "opt2", which are the sum of the end tensions and duration for the upper and lower ends of the mooring line and the lengths "UPC1_L, UPP_L, UPC2_L". By decreasing their upper bounds until 10 Pareto designs are left from 130 evaluated designs.

The following Table 18 contains the characteristics of the first 10 Pareto solutions for the described optimization problem. These are based on the OrcaFlex simulations; therefore, the coordinate system and units are coming from the OrcaFlex software.

Table 18. Initial optimization results (modeFRONTIER)

<ID>	Connection Angle (°)		Position (m)		OBJ2	OBJ1	Offset (m)
	Fairlead	Anchor	Z-axis	X-axis			
119	122.63	56.70	-3.42	-317.43	2023.17	507130.93	1048.47
93	177.19	63.55	-4.05	-296.24	1647.96	810516.74	1050.66
74	145.51	37.12	-4.47	-300.46	1647.42	811850.16	1048.48
110	180.00	75.00	15.00	-78.00	1626.97	952679.29	1073.95
116	166.49	74.91	-5.19	-83.70	1624.60	1132438.82	1072.57
111	124.01	59.74	0.24	-320.99	1415.17	1242860.41	782.71
103	145.31	36.47	-4.05	-296.24	1262.04	1692243.48	588.75
123	145.51	36.12	-8.46	-296.45	1248.63	1727853.44	572.04
115	177.23	59.92	0.62	-78.22	1098.71	2437636.63	520.02
117	177.47	59.98	0.47	-78.22	1098.26	2440519.57	519.36

These design solutions (optimization results) were checked in the OrcaFlex software for assessing the feasibility of the optimization results. The last column of Table 18 presents the platform offset under average normal wind speed. This value was obtained after monitoring the design results at the OrcaFlex software to have an average overview of the offset value.

The OrcaFlex can create time history charts for platform offset after a dynamic analysis run. The offset results show that the platform offset is quite high for all 10 designs, ranging between 520 to 1050 *m*. The following Fig. 40 is the offset result of the design ID 111, it presents an example for the time history charts.
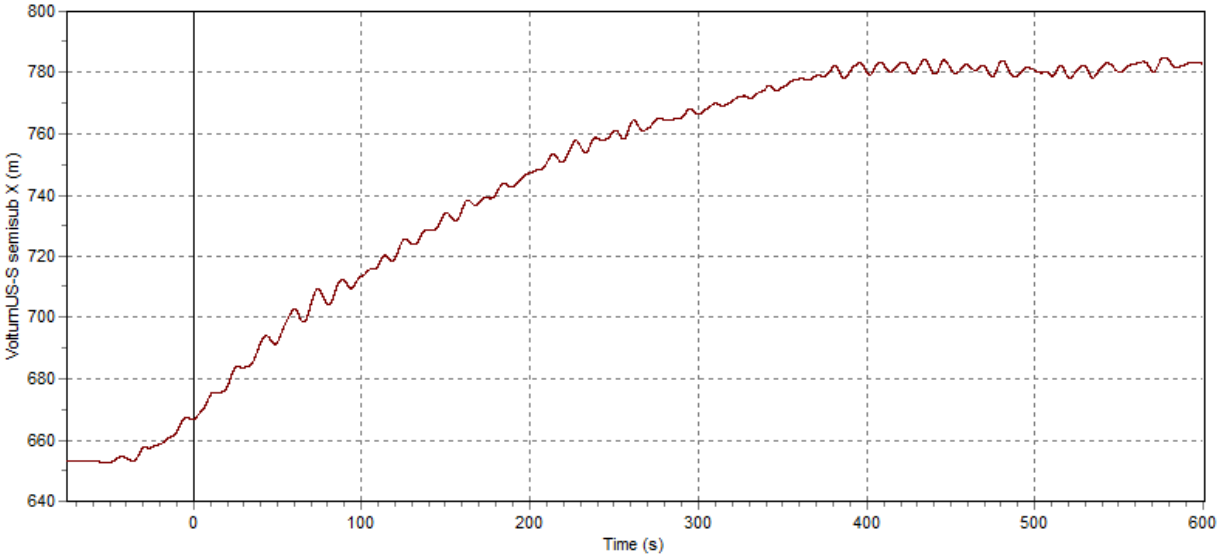
Figure 40. Example platform offset time history results

The following Fig. 41 was also obtained from OrcaFlex, it presents the final arrangement of the design ID 119, which gives the minimum tension results.
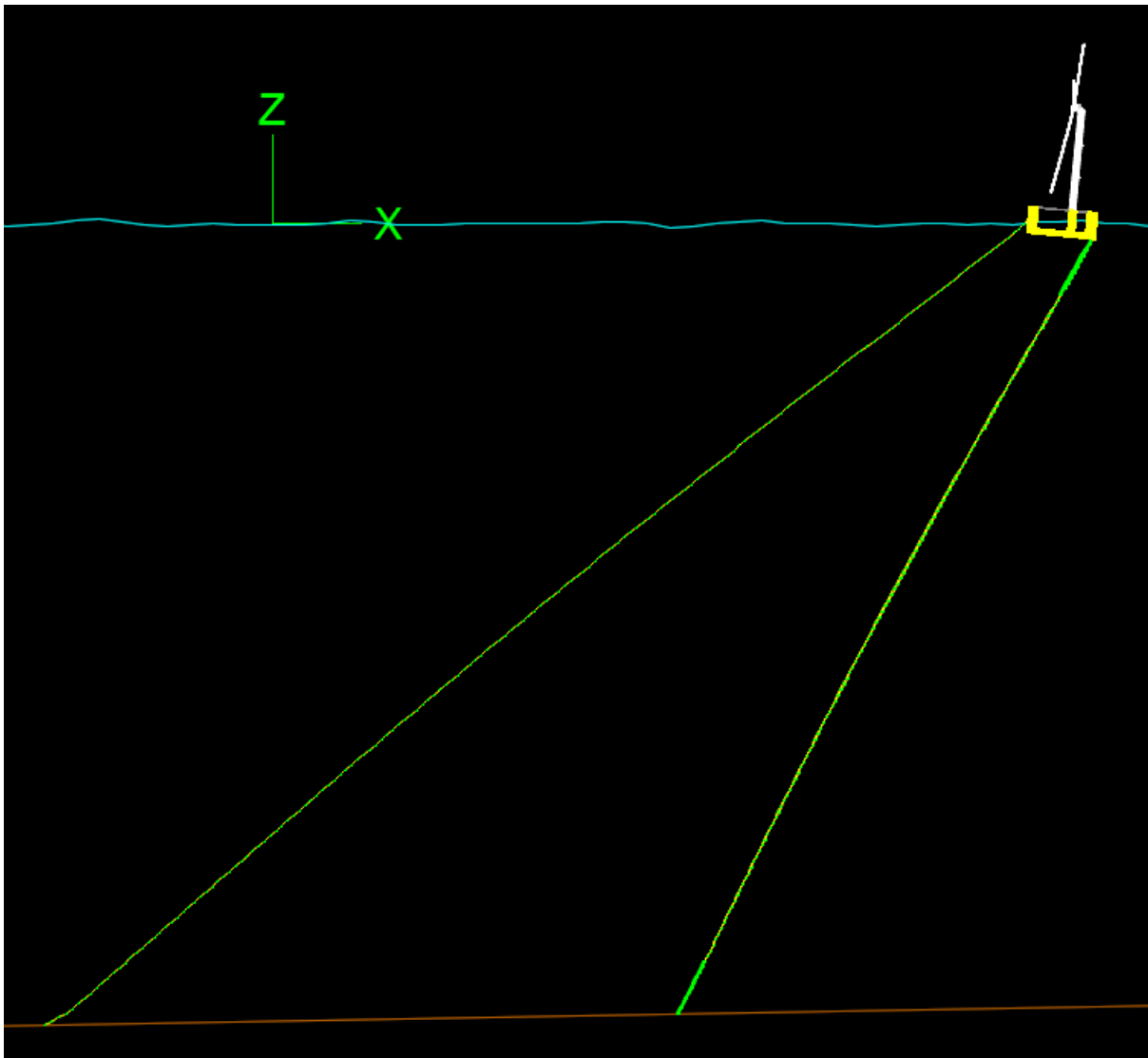
Figure 41. Minimum tension vessel offset (OrcaFlex)

It was observed that in the Pareto designs, the upwind mooring line position and length were arranged in such slackness that after a simulation runs, the platforms drift significantly towards the downwind mooring lines that the load is transferred to these two mooring lines.

The initial position of the floating offshore wind turbine structure was set at the origin of the Z-X axis. It can be observed from Fig. 41 that the structure has drifted significantly. One can also observe that the upwind line is slacker, while the downwind lines are tensioned.
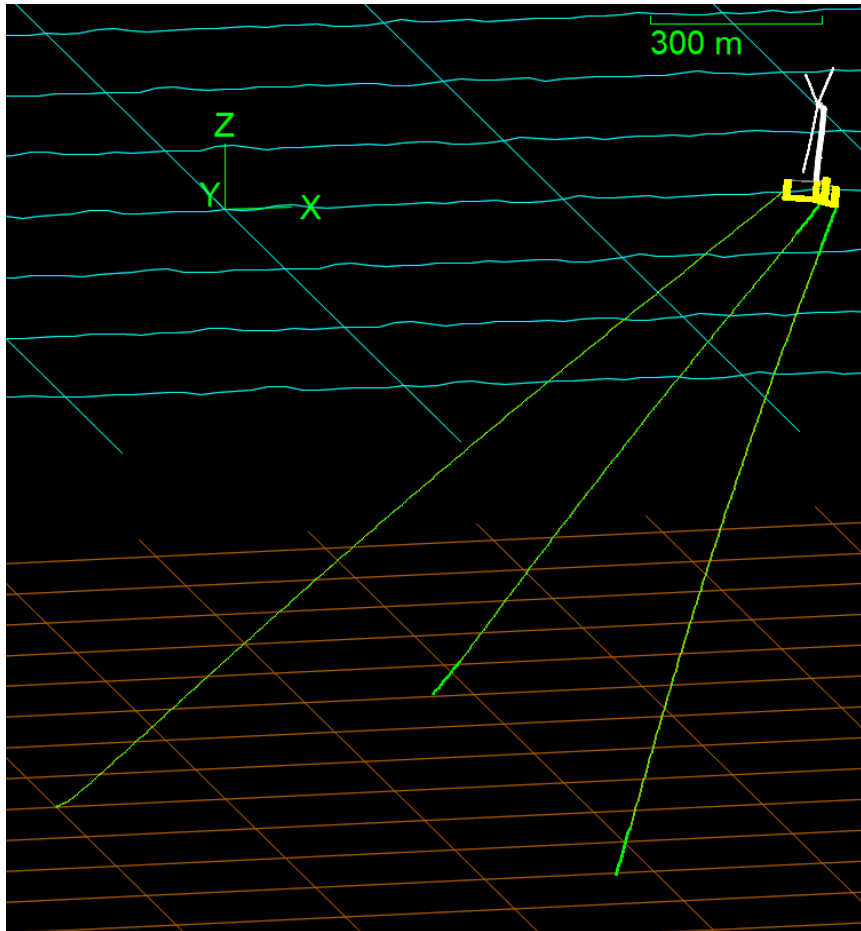
Figure 42. Minimum tension vessel offset (perspective view - OrcaFlex)

The following Fig. 42 has also been obtained from the software, it presents the perspective view. The final arrangements of the mooring lines and the structure can be observed clearer from this view.

According to the API RP 2SK (Shu et al., 2018), the offset limits for the floating structures are to be determined by the operator or the owner. In general, the positioning of the offshore wind turbines in offshore wind farms is made with respect to their turbine diameters.

According to Prof. Rodrigo Pérez (UPM, personal communication), as a rule of thumb, the turbine spacing is 5 to 8 times the diameter of the wind turbine. Thus, the platform offset of 2 times the diameter was set as the offset limit for the study.

$$Offset\ Limit = 2 * D = 2 * 240 = 480\ m \tag{24}$$

The Pareto designs that were obtained from the initial optimization study have high vessel offset results that are exceeding the offset limit (480 m). High offset is not safe, and it is not feasible in terms of power production. Additionally, the downwind mooring lines are bearing higher tensions, thus, their fatigue life decreases.

A secondary optimization run was required. In the initial setup, the outputs were set for the tension results of the upwind mooring line. Two more outputs were added to the script for the second run which accounts for the end tensions for one of the two downwind mooring lines. These end tensions were multiplied by the hours per year and their sum was taken for the objective function.

A simple modification was made to the original script. The outputs for the downwind mooring lines were set in the same way as the upwind mooring line. For computational efficiency, only one of the downwind mooring lines was added since their arrangement is symmetric. Finally, a third objective was set for minimizing the new outputs (for both ends of the downwind line).
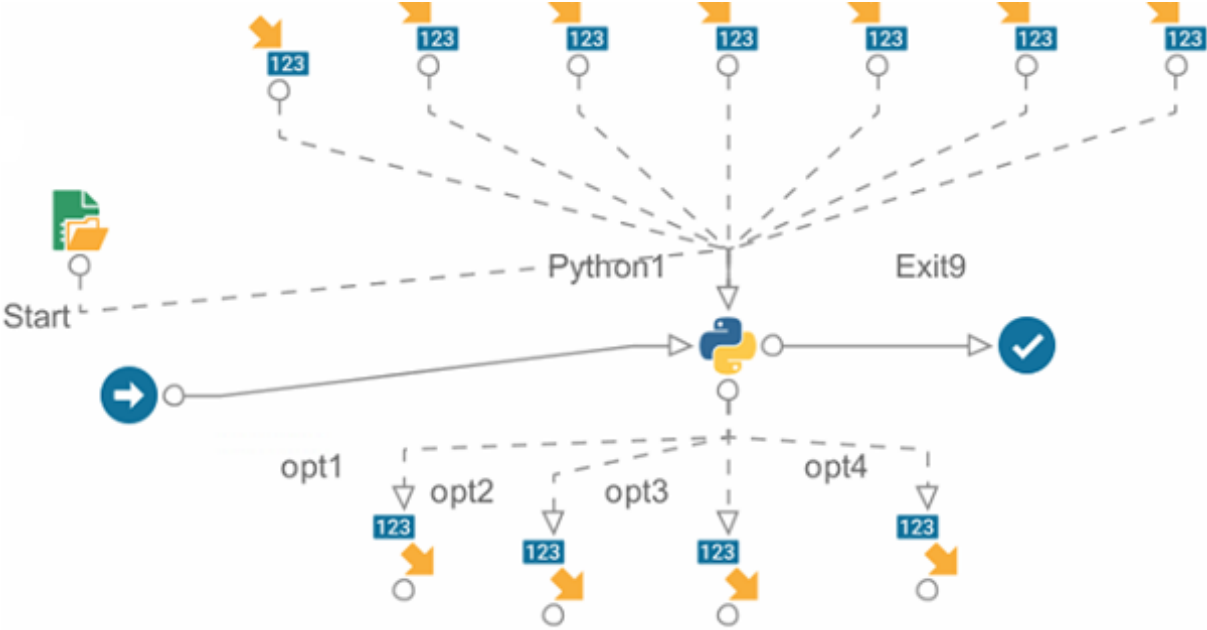
Figure 43. Workflow for second optimization run (modeFRONTIER)

Afterward, the same procedure was followed with the modeFRONTIER software for the optimization run. The following results (Fig. 44 and Table 19) were obtained.

In the 3D scatter chart (Fig. 44), the green dots represent the feasible designs, and the white dots represent the unfeasible designs that were evaluated by the software. The X, Y, and Z axis presents the 3 design objectives that are minimizing the length and tension of the upwind mooring line and downwind mooring line respectively.
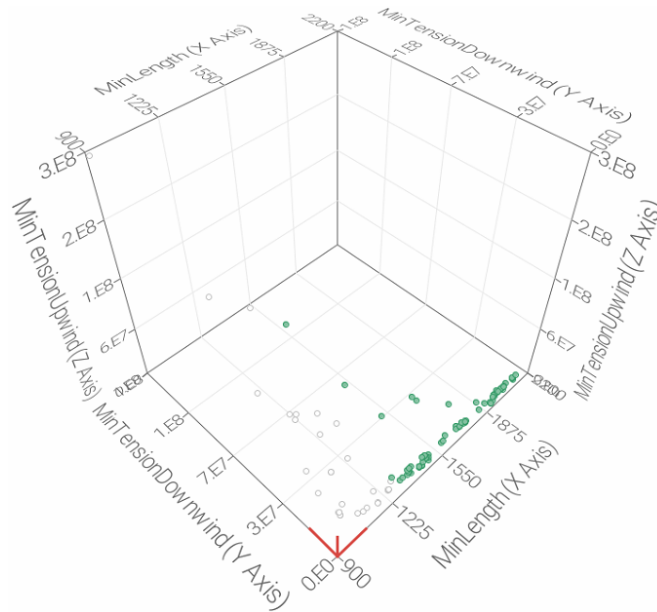
Figure 44. Optimization results 3D scatter chart

The Pareto Table (Table 19) presents the 10 feasible designs for the three objectives, and they are the best 10 designs among all the feasible designs for the tension minimization of the upwind mooring line. The first 8 solutions are still exceeding the vessel offset limit that was set earlier. Only design ID #31 and #114 are below the offset limit.

Table 19. Second optimization results

	Connection Angle (°)		Position (m)			
<ID>	Fairlead	Anchor	Z-axis	X-axis	Upwind Line Length (m)	Offset (m)
124	139.30	59.99	-17.89	-250.48	1488.03	959.66
107	180.00	75.00	-20.00	-78.00	1495.29	1062.27
126	180.00	72.62	-20.00	-78.00	1495.29	1026.27
59	130.83	61.15	1.22	-193.54	1494.30	920.20
113	120.00	30.00	-20.00	-407.03	1486.78	809.79
83	120.31	75.00	-20.00	-196.97	1109.99	457.25
89	120.00	74.83	-19.96	-78.02	1180.37	689.65
48	145.51	53.29	-8.46	-290.66	1485.29	905.13
31	120.00	32.33	-18.55	-711.73	1363.29	336.76
114	127.91	53.90	-10.50	-790.31	1457.97	378.77

In general, the results have been improved in terms of line length and offset for the upwind mooring line, however, this time design results in slack arrangements that are closer to the catenary arrangement. Since no objective or constraint was defined for the material costs or for the offset limit itself, this result is logical although it is not likely to be the most economical solution.

To further investigate design ID #31, the fatigue load case was created again following the same procedure as Ch. 7.2 that describes the fatigue methodology.

After the run of the simulations, it was observed that the vessel offset exceeded the maximum offset limit (450 *m*) for some of the wind-wave combinations presented in the scatter diagram (from the COREWIND (2019) project).

More importantly, the fatigue life of the new design was found as 13 – 14 years, which is lower than the results found in the Base Model. The fatigue occurs around the upper connection between the upper chain and the polyester line segments, the same as in the previous cases. Therefore, the design is not feasible both in terms of economics and structure.

To find a feasible design, several corrections to the optimization problem description and objective function can be made to improve the solutions.

The major problem is the vessel offset (drift). A limitation over the strains over FE nodes on the whole length of the cable can be made, along with more strict bounds for the anchor position. An overall improvement is required for the input boundaries (lower and upper bounds). Therefore, detailed sensitivity analysis and DOE runs are needed, especially for the anchor position. Additionally, a candidate material library must be created that involves several sets of materials (e.g., chain of different grades, composites) must be introduced to the OrcaFlex software and included in the optimization problem in the modeFRONTIER software. There exists several software that can aid for the formation of such a library (for example, Granta EduPack by ANSYS). The overall process will require additional computational time.

In the optimization study, the end tensions were utilized since the whole cable length variates with each solution. However, the script can be improved in such a way as to analyze the whole cable by the FE nodes. More sensitivity studies for the number of FE are required to reach a certain accuracy in the segments. This will also lead to additional computational time.

The number of design evaluations was determined concerning the hardware. An overall increase in the number of design evaluations is required in general. However, the problem will get more complex with the improvements, and an increase in evaluations is inevitable.

All the presented improvements require more computational power and time. Thus, better hardware is required for a precise optimization study. Mooring optimization is a complex problem that requires further exploration and more complex analyses.

10 CONCLUSIONS

This thesis has been dedicated to presenting a complete preliminary design for the mooring system of a state-of-the-art floating offshore wind turbine structure that was placed in the Morro Bay wind energy area. The area has an average depth of 1046 *meters*.

The first few chapters cover the required data about the environmental conditions of the target location along with the precise information about the floating offshore wind turbine structures, and mooring systems.

Additionally, important theoretical aspects of the mooring analysis and vortex-induced vibrations have been presented. Available software (with their capabilities and limitations) have been concisely reported.

There exists several software that are capable of the assessment of the mooring analysis. Other software was introduced for vortex-induced vibrations and mooring optimization assessments. The OrcaFlex (by Orcina) was selected for it is advanced capabilities, broad theory, and software manuals that are publicly available online. Orcina Ltd. granted an academic license and engineering support for the required tasks. Mr. Paul Jacob (Orcina) guided the load case setup and simulation run.

The Workbench and AQWA (by ANSYS) were utilized for a basic demonstration of design and uncoupled time domain analyses for the mooring system of a reference spar-type floating offshore wind turbine. A chapter was dedicated to this study, which aims to cover the design process (initial sketch, stability calculations, materials, 3D modeling, key design, and simulation inputs) and key concepts of hydrodynamics (such as RAOs, diffraction and radiation, wave spectra, resonance) under the guidance of Dr. Xavier Castello (UFJR).

Afterward, coupled time domain simulations have been carried out for the reference 15 *MW* semi-submersible floating offshore wind turbine. An OrcaFlex base mooring system was created for the 15 *MW* semi-submersible FOWT by following the design methodology presented by Ma et al in *"Mooring System Engineering for Offshore Structures"* (2019).

The ABS, IEC and API guidelines have been followed for the assessment. IEC standards present design load cases (DLCs) for the floating offshore wind turbines. The IEC DLC table presents 10 cases for the DLCs. In addition to the IEC DLC table, ABS rules require a survival load case to calculate the survival limit state (SurLS).

To carry out a complete design process, one needs to run thousands of 3-*hour* time domain coupled simulations that cover all the required DLCs. These simulations are highly expensive in terms of computational effort.

However, for the preliminary design, one can use 10-*mins* simulations. As a result of the hardware limitations, critical DLCs have been selected from all the DLCs that are required by the ABS rules. The selection of these DLCs was based on the normal and extreme normal events that cover over 99% of the operational lifetime of the floating offshore wind turbines.

Then the data files were created with Excel tables and the OrcaFlex Excel add-in tool for pre-processing automation to create the simulation data files. Post-processing of the results has been made via Python scripts.

Limit state calculations (ultimate and accidental) have been carried out along with fatigue life calculations (T-N curves and rain flow counting method) for the created model. The base design passed the ULS check, however, all the IEC DLCs must be evaluated with simulations that have a period of three hours.

It was observed in the mooring loss simulations that the software could not capture the instantaneous effects due to the snap back of the mooring line. The platform simulates a smooth line release instead of a line snap. This issue should be further investigated for an appropriate ALS evaluation for platform safety.

A new model was developed that aims for better fatigue life by alteration of the initial dimensions of the mooring segments. The new model had better fatigue characteristics; however, further improvements were required that led to the optimization study.

Additionally, a 2D CFD simulation was demonstrated in Lily Pad CFD software (by Prof. Gabriel Weymouth, University of Southampton) to highlight the vortex-induced vibration (VIV) phenomenon under the guidance of Dr. Leixin Ma (MIT).

Vortex-induced vibrations are highly complex problems. This part of the study aimed to present vortex shedding that occurs behind the mooring cable. Vortex shedding is the main reason behind the VIV issue. A script in Java language has been developed in the Processing Development Environment (PDE). The current characteristic data (speed, direction, return periods) is limited in the target location. However, the data that was found in the earlier chapters (20 years maximum current speed) has been used.

Results show that significant vorticity occurred behind the cable cross-section. Therefore, the VIV (and the VIM) characteristics should be further assessed with more data and more complex 3D CFD simulations.

It should be noted that the current data that was used for the CFD simulation is conservative. More current data should be included in the simulations.

Lastly, a mooring fatigue life optimization study was carried out under the guidance of Dr. Matthew Hall (NREL) and Adarsh Elango (ESTECO SpA). This part of the study targeted to increase the fatigue life of the upwind mooring line. The modeFRONTIER software (by ESTECO SpA) was utilized for the optimization study. ESTECO SpA granted a sponsorship license and engineering support.

For a complete mooring system optimization, many parameters must be included in the problem description. Initially, 37 input variables were found that involve the materials, diameters, lengths, angles, and positions of the mooring lines.

The computational burden of such an optimization run exceeds the limits of the available hardware. The material characteristics and cost information are limited. Thus, the optimization study focused on the anchor and fairlead characteristics and minimization of the overall length of the upwind mooring line that bears the highest tensions. Therefore, the input variables were reduced to seven parameters: lengths of the three sections, angles and positions of the anchor, and the fairlead.

The HYBRID optimization algorithm that the modeFRONTIER software provides has been utilized. The aim was to determine the optimum position(s) and angle(s) for the anchor and the fairlead along, section lengths that minimize the length, and the effective tension acting on the upwind mooring line. Optimization runs are computationally expensive since many simulation runs are required for the fatigue load case. Some simplifications have been made to the OrcaFlex model.

The two software were coupled with a Python script. This script can pre-process, process and post-process the OrcaFlex simulations (automated parallel simulations) and couple the interfaces of the two software.

The first set of Pareto designs was found unfeasible since they resulted in great vessel offsets. These designs are not acceptable in terms of safety and power production.

Therefore, a second optimization run was set. The problem description has been improved. The downwind mooring lines were added to the objective function in the second run. After the run, a new set of Pareto designs were obtained. These designs presented lower offset values, and one of them was further analyzed for fatigue life.

However, the fatigue calculations presented that the new design was not feasible in terms of fatigue life, and it also violated the offset criteria. Several improvements have been suggested for the model, objective function, and the DOE runs.

To summarize, the mooring system design process of a floating offshore wind turbine involves several sets of computational procedures that require extremely powerful hardware. For the deep-water locations, environmental forces acting on the mooring system result in high tensions.

High-speed ocean currents at the target area can lead to harmful vortex-induced vibrations for the mooring systems in deep-water locations. The VIV contributes to fatigue damage; therefore, it must be included in the fatigue calculations as requested by the standards. Advanced 3D CFD simulations are required for precise VIV damage assessment on the mooring systems.

Two main goals are present for the mooring system design: the first (and the most important) one is to design a redundant mooring system that satisfies the classification society rules (limit states). The second one is to minimize the mooring system costs. By nature, these two goals conflict with each other.

However, a good compromise can be found by multi-objective or many-multi-objective optimizations for the mooring system. Mooring system optimization is a complex problem that involves many parameters, a complete optimization study exceeds the capabilities of the present hardware for this study. Several improvements have been proposed to improve the optimization results which lay the foundation for further research for a complete mooring system optimization for the reference floating offshore wind turbine.

10.1 Further Research

As explained in the earlier chapters, environmental data is important for the coupled analysis of offshore wind turbines. The raw datasets for the wave, wind, and current data have been found, however, intense data analysis through specific software is required to process the buoy data. New research has been initiated under the guidance of Prof. Dr. Ertugrul Taciroglu (UCLA) to create detailed site-specific environmental data that can be utilized in simulation software for the Morro Bay wind energy area.

It was observed in the mooring loss simulations that the software could not capture the instantaneous effects due to the snap back of the mooring line. The platform simulates a smooth line release instead of a line snap. This issue should be further investigated for an appropriate ALS evaluation that includes the snap loads for safety. The programming interface (OrcFxAPI) of the OrcaFlex can be utilized and modified to perform such research.

In addition to the presented work in this study, a weak point analysis or a mooring sensitivity analysis is recommended by API RP 2SK (Shu et al., 2018). Which aims to find the (probable) failure mode of the mooring lines.

Moreover, it should be acknowledged that the tensions and weights of the anchor and the power cable are not included in the study. The Anchor and the power cable should also be modeled and analyzed with respect to the guidelines.

The OrcaFlex simulations are computationally expensive in terms of memory and computation time. Model order reduction methods (e.g., Guyan-Irons, Craig-Bampton methods) can be applied to the OrcaFlex model to reduce the required computational effort.

As mentioned earlier, the VIV and VIM must be further investigated. Research has been initiated in collaboration with Dr. Leixin Ma (MIT) to investigate the VIV and the VIM phenomenon for the floating offshore wind turbine model that was created for this study. The 3D CFD simulations will be conducted in the OpenFOAM (by OpenCFD) software. Another research was also initiated in Lily Pad software that focuses on the flapping foils.

It was also observed during the VIV study that several research focuses on the cylinder tubes in a flow. However, ellipse cross sections have been rarely studied which can be considered a research gap.

Two more optimization topics have been considered. The first one focuses on the mooring and anchoring system costs, and the second one aims to analyze the relationship between the mooring system and the power production efficiency.

The literature involves several research that address the mooring and anchoring system cost optimization. Innovative mooring design solutions such as shared anchoring and mooring systems, clump weights, and buoys can be included in the base design to analyze the overall performance of these design solutions in deep water locations.

A more complex study can include the power production efficiency and the mooring system relationship. The transfer functions between the mooring system and the tower & nacelle assembly can be utilized for the formulation of the objective function. Those transfer functions can be minimized to investigate power production efficiency. This can present the relationship of the mooring system on the efficiency of power production.

Moreover, another research has been initiated regarding the seismic activity. California is an earthquake zone with high seismic activity in general. This research aims to investigate the reliability of the mooring system (and the structure) under seismic (and tidal) loads. Seismic analyses will be conducted on the created mooring system model for the reference floating offshore wind turbine under Taciroglu Research Group (UCLA).

REFERENCES

ABS. (2016). *Guidance Notes on Selecting Design Wave by Long Term Stochastic Method*. American Bureau of Shipping (ABS).

ABS. (2020). *Guide for Building and Classing Floating Offshore Wind Turbines (July 2020)*. American Bureau of Shipping.

ABS. (2022). *Guide for Position Mooring Systems*. American Bureau of Shipping (ABS).

Acteon. (2021, April 21). *Anchor types for floating wind* [Company Website]. Acteon. https://acteon.com/blog/anchor-types-for-floating-wind/

Allen, C., Viscelli, A., Dagher, H., Goupee, A., Gaertner, E., Abbas, N., Hall, M., & Barter, G. (2020). *Definition of the UMaine VolturnUS-S Reference Platform Developed for the IEA Wind 15-Megawatt Offshore Reference Wind Turbine* (NREL/TP--5000-76773, 1660012, MainId:9434; p. NREL/TP--5000-76773, 1660012, MainId:9434). https://doi.org/10.2172/1660012

Andre, J., Siarry, P., & Dognon, T. (2001). An improvement of the standard genetic algorithm fighting premature convergence in continuous optimization. *Advances in Engineering Software*, *32*(1), 49–60. https://doi.org/10.1016/S0965-9978(00)00070-3

ANSYS. (2012). *ANSYS AQWA Manual*. ANSYS.

Arany, L., & Bhattacharya, S. (2018). Simplified load estimation and sizing of suction anchors for spar buoy type floating offshore wind turbines. *Ocean Engineering*, *159*, 348–357. https://doi.org/10.1016/j.oceaneng.2018.04.013

Audot, D. A. G., Banks, J., & Hudson, D. (2019). 2D Numerical Simulations of Human Underwater Undulatory Swimming. *22nd Numerical Towing Tank Symposium*.

Azcona Armendáriz, J. (2015). *Computational and Experimental Modelling of Mooring Lines Dynamics for Offshore Floating Wind Turbines.* [Doctoral Dissertation]. E.T.S.I. Navales (UPM).

Azcona, J., Munduate, X., González, L., & Nygaard, T. A. (2017). Experimental validation of a dynamic mooring lines code with tension and motion measurements of a submerged chain. *Ocean Engineering*, *129*, 415–427. https://doi.org/10.1016/j.oceaneng.2016.10.051

Beiter, P., Musial, W., Duffy, P., Cooperman, A., Shields, M., Heimiller, D., & Optis, M. (2020). *The Cost of Floating Offshore Wind Energy in California Between 2019 and*

2032 (NREL/TP--5000-77384, 1710181, MainId:26330; p. NREL/TP--5000-77384, 1710181, MainId:26330). https://doi.org/10.2172/1710181

Bennett, N. J. (2019). Marine Social Science for the Peopled Seas. *Coastal Management*, *47*(2), 244–252. https://doi.org/10.1080/08920753.2019.1564958

BOEM. (n.d.). *BOEM Homepage | Bureau of Ocean Energy Management* [Governmental]. Retrieved April 18, 2022, from https://www.boem.gov/

BOEM, & NOAA. (n.d.-a). *Marine Cadastre: California Call Area - Morro Bay OceanReports: Oceanographic and Biophysical*. BOEM/NOAA. Retrieved April 18, 2022, from https://marinecadastre.gov/oceanreports

BOEM, & NOAA. (n.d.-b). *MarineCadastre: California Call Area—Morro Bay OceanReports: Energy and Minerals*. BOEM/NOAA. Retrieved April 18, 2022, from https://marinecadastre.gov/oceanreports

Britannica. (n.d.). *Continental Slope*. Retrieved April 18, 2022, from https://www.britannica.com/science/continental-slope

Britannica. (n.d.). *Ocean current | Distribution, Causes, & Types | Britannica*. Retrieved August 30, 2022, from https://www.britannica.com/science/ocean-current

BSEE. (2015). *Fatigue Design Methodologies Applicable to Complex Fixed and Floating Offshore Wind Turbines*. Bureau of Safety and Environmental Enforcement.

Castello, X. (Director). (2021, October 23). *Floating Offshore Wind Turbine in Ansys Aqwa—From a sketch to numerical model*. https://www.youtube.com/watch?v=XthkX7pqfew

Cevasco, D., Collu, M., Rizzo, C., & Hall, M. (2018). On mooring line tension and fatigue prediction for offshore vertical axis wind turbines: A comparison of lumped mass and quasi-static approaches. *Wind Engineering*, *42*(2), 97–107. https://doi.org/10.1177/0309524X18756962

Christensen, P. W., & Klarbring, A. (2009). *An introduction to structural optimization*. Springer.

Chuang, T.-C., Yang, W.-H., & Yang, R.-Y. (2021). Experimental and numerical study of a barge-type FOWT platform under wind and wave load. *Ocean Engineering*, *230*, 109015. https://doi.org/10.1016/j.oceaneng.2021.109015

Cooperman, A., Duffy, P., Hall, M., Lozon, E., Shields, M., & Musial, W. (2022). *Assessment of Offshore Wind Energy Leasing Areas for Humboldt and Morro Bay Wind Energy Areas, California* (NREL/TP-5000-82341, 1865877, MainId:83114; p. NREL/TP-5000-82341, 1865877, MainId:83114). https://doi.org/10.2172/1865877

COREWIND. (2019). Publications. *COREWIND*. http://corewind.eu/publications/

da Silveira, L. M. Y., Martins, C. de A., Cunha, L. D., & Pesce, C. P. (2007). An Investigation on the Effect of Tension Variation on VIV of Risers. *Volume 1: Offshore Technology; Special Symposium on Ocean Measurements and Their Influence on Design*, 267–275. https://doi.org/10.1115/OMAE2007-29247

Davidson, J., & Ringwood, J. (2017). Mathematical Modelling of Mooring Systems for Wave Energy Converters—A Review. *Energies*, *10*(5), 666. https://doi.org/10.3390/en10050666

Du, A. (2021). *Floating Wind. Semi-Submersible, Spar, TLP - Empire engineering*. https://www.empireengineering.co.uk/semi-submersible-spar-and-tlp-floating-wind-foundations/

ESTECO Resource Library. (n.d.). ESTECO SpA. Retrieved August 27, 2022, from https://engineering.esteco.com/resources?page=1

ESTECO SpA. (n.d.). *ModeFRONTIER | Simulation process automation and design optimization*. Retrieved August 30, 2022, from https://engineering.esteco.com/modefrontier/

Felix-Gonzalez, I., & Mercier, R. S. (2016). Optimized design of statically equivalent mooring systems. *Ocean Engineering*, *111*, 384–397. https://doi.org/10.1016/j.oceaneng.2015.11.002

Flow Science. (2019). *FLOW-3D*. FLOW-3D. https://www.flow3d.com/

Fujarra, A. L. C., Rosetti, G. F., de Wilde, J., & Gonçalves, R. T. (2012). State-of-Art on Vortex-Induced Motion: A Comprehensive Survey After More Than One Decade of Experimental Investigation. *Volume 4: Offshore Geotechnics; Ronald W. Yeung Honoring Symposium on Offshore and Ship Hydrodynamics*, 561–582. https://doi.org/10.1115/OMAE2012-83561

Gaertner, E., Rinker, J., Sethuraman, L., Zahle, F., Anderson, B., Barter, G., Abbas, N., Meng, F., Bortolotti, P., Skrzypinski, W., Scott, G., Feil, R., Bredmose, H., Dykes, K., Shields, M., Allen, C., & Viselli, A. M. (2020). *Definition of the IEA Wind 15-Megawatt Offshore Reference Wind Turbine Technical Report* [Technical Report].

GWEC. (2021). *Global wind report 2021*. GWEC.

Ha, K., Truong, H. V. A., Dang, T. D., & Ahn, K. K. (2021). Recent Control Technologies for Floating Offshore Wind Energy System: A Review. *International Journal of Precision Engineering and Manufacturing-Green Technology*, *8*(1), 281–301. https://doi.org/10.1007/s40684-020-00269-5

Hall, M., & Goupee, A. (2015). Validation of a lumped-mass mooring line model with DeepCwind semisubmersible model test data. *Ocean Engineering*, *104*, 590–603. https://doi.org/10.1016/j.oceaneng.2015.05.035

Hanania, J., Sheardown, A., Stenhouse, K., & Donev, J. (2019). *Prevailing Winds*. Energy Education. https://energyeducation.ca/encyclopedia/Prevailing_winds#cite_note-env-1

Hankins, J. (2021, June 5). Floating offshore wind project to power 1.6 million homes. *Sierra Club*. https://www.sierraclub.org/los-padres/blog/2021/06/floating-offshore-wind-project-power-16-million-homes

Hartman, L. (2021). Top 10 Things You Didn't Know About Offshore Wind Energy. *Energy.Gov*. https://www.energy.gov/eere/wind/articles/top-10-things-you-didnt-know-about-offshore-wind-energy

Hasanvand, E., & Edalat, P. (2021). Evaluation of the Safe and Failure Zones of Mooring and Riser Systems in a CALM Oil Terminal. *Journal of Marine Science and Application*, *20*(4), 751–766. https://doi.org/10.1007/s11804-021-00240-z

Hodgson, M. (2022). Public critical of environmental analysis for Morro Bay Wind Energy Area. *Santa Maria Times*. https://santamariatimes.com/news/local/govt-and-politics/public-critical-of-environmental-analysis-for-morro-bay-wind-energy-area/article_3485a12e-6bc6-553e-9814-c6114e656e0f.html

IBERDROLA. (n.d.). *Floating offshore wind power: A milestone to boost renewables through innovation*. Iberdrola. Retrieved April 18, 2022, from https://www.iberdrola.com/innovation/floating-offshore-wind

Ibinabo, I., & Tamunodukobipi, D. T. (2019). Determination of the Response Amplitude Operator(s) of an FPSO. *Engineering*, *11*(09), 541–556. https://doi.org/10.4236/eng.2019.119038

IEC. (2005). *Wind turbines – Part 1: Design requirements*.

Iman, R. L., & Conover, W. J. (1982). A distribution-free approach to inducing rank correlation among input variables. *Communications in Statistics - Simulation and Computation*, *11*(3), 311–334. https://doi.org/10.1080/03610918208812265

InterMoor. (n.d.). *Home—InterMoor*. Retrieved August 30, 2022, from https://intermoor.com/

IPCC. (2022). *Global Warming of 1.5°C: IPCC Special Report on impacts of global warming of 1.5°C above pre-industrial levels in context of strengthening response to climate change, sustainable development, and efforts to eradicate poverty* (1st ed.). Cambridge University Press. https://doi.org/10.1017/9781009157940

IRENA. (2016). *Floating Foundations: A Game Changer for Offshore Wind Power*. International Renewable Energy Agency.

Ishihara, T., Phu, P., & Sukegawa, H. (2007). *A numerical study on the dynamic response of a floating offshore wind turbine system due to resonance and nonlinear wave*.

Ja'e, I. A., Osman Ahmed Ali, M., Yenduri, A., Nizamani, Z., & Nakayama, A. (2022). Optimisation of mooring line parameters for offshore floating structures: A review paper. *Ocean Engineering*, *247*, 110644. https://doi.org/10.1016/j.oceaneng.2022.110644

Johansson, P. I. (1976). *A Finite Element Model for Dynamic Analysis of Mooring Cables* [Doctoral Dissertation]. Massachusetts Institute of Technology.

Johnson, J. M., & Rahmat-samii, Y. (1994). Genetic algorithm optimization and its application to antenna design. *Proceedings of IEEE Antennas and Propagation Society International Symposium and URSI National Radio Science Meeting*, *1*, 326–329. https://doi.org/10.1109/APS.1994.407746

Jonkman, B., Mudafort, R. M., Platt, A., E. Branlard, Sprague, M., Jjonkman, HaymanConsulting, Vijayakumar, G., Buhl, M., Ross, H., Bortolotti, P., Masciola, M., Shreyas Ananthan, Schmidt, M. J., Rood, J., Rdamiani, Nrmendoza, Sinolonghai, Hall, M., … Rcorniglion. (2022). *OpenFAST/openfast: OpenFAST v3.1.0* (v3.1.0). Zenodo. https://doi.org/10.5281/ZENODO.6324288

Jonkman, J. (2010). *Definition of the Floating System for Phase IV of OC3* (NREL/TP-500-47535, 979456; p. NREL/TP-500-47535, 979456). https://doi.org/10.2172/979456

Jonkman, J., Butterfield, S., Musial, W., & Scott, G. (2009). *Definition of a 5-MW Reference Wind Turbine for Offshore System Development* (NREL/TP-500-38060, 947422; p. NREL/TP-500-38060, 947422). https://doi.org/10.2172/947422

Jonkman, J. M. (2007). *Dynamics Modeling and Loads Analysis of an Offshore Floating Wind Turbine* (NREL/TP-500-41958, 921803; p. NREL/TP-500-41958, 921803). https://doi.org/10.2172/921803

Journée, J. M. J., & Massie, W. W. (2001). *Offshore Hydromechanics* (First). Delft University of Technology.

Lifes50+. (2015). *Lifes50+—Results*. Lifes50+. https://lifes50plus.eu/results/

Ma, K.-T., Luo, Y., Kwan, C.-T. T., & Wu, Y. (2019). *Mooring System Engineering for Offshore Structures*. Elsevier. https://doi.org/10.1016/C2018-0-02217-3

Madsen, F. J., Pegalajar-Jurado, A., & Bredmose, H. (2019). *Performance study of the QuLAF pre-design model for a 10MW floating wind turbine* [Preprint]. Aerodynamics and hydrodynamics. https://doi.org/10.5194/wes-2019-20

Madsen, P., Pierce, K., & Buhl, M. (1999, January 11). Predicting ultimate loads for wind turbine design. *37th Aerospace Sciences Meeting and Exhibit*. 37th Aerospace Sciences Meeting and Exhibit, Reno,NV,U.S.A. https://doi.org/10.2514/6.1999-69

Maertens, A. P., & Weymouth, G. D. (2015). Accurate Cartesian-grid simulations of near-body flows at intermediate Reynolds numbers. *Computer Methods in Applied Mechanics and Engineering*, *283*, 106–129. https://doi.org/10.1016/j.cma.2014.09.007

Masciola, M., Jonkman, J., & Robertson, A. (2014). Extending the Capabilities of the Mooring Analysis Program: A Survey of Dynamic Mooring Line Theories for Integration Into FAST. *Volume 9A: Ocean Renewable Energy*, V09AT09A032. https://doi.org/10.1115/OMAE2014-23508

Masciola, M., Robertson, A., Jonkman, J., & Driscoll, F. (2011). *Investigation of a FAST-OrcaFlex Coupling Module for Integrating Turbine and Mooring Dynamics of Offshore Floating Wind Turbines: Preprint*. 12.

Matha, D., Schlipf, M., & Stuttgart, U. (2011). *Challenges in Simulation of Aerodynamics, Hydrodynamics, and Mooring-Line Dynamics of Floating Offshore Wind Turbines*. 10.

McCloy, J. (2019). Onshore vs Offshore Wind: What Are the Differences and Facts? *Green Coast*. https://greencoast.org/onshore-vs-offshore-wind/

McKay, M. D., Beckman, R. J., & Conover, W. J. (1979). Comparison of Three Methods for Selecting Values of Input Variables in the Analysis of Output from a Computer Code. *Technometrics*, *21*(2), 239–245. https://doi.org/10.1080/00401706.1979.10489755

Natarajan, A., Hansen, M., & Wang, S. (2016). *Design Load Basis for Offshore Wind turbines DTU Wind Energy Report No. E-0133*.

National Geographic Society. (n.d.). *Ocean Currents*. Retrieved April 18, 2022, from http://www.nationalgeographic.org/topics/resource-library-ocean-currents/

Neisi, A., Ghassemi, H., Iranmanesh, M., & He, G. (2022). Effect of the multi-segment mooring system by buoy and clump weights on the dynamic motions of the floating platform. *Ocean Engineering*, *260*, 111990. https://doi.org/10.1016/j.oceaneng.2022.111990

Newman, J. N. (2017). *Marine hydrodynamics* (40th anniversary edition). MIT press.

Orcina. (n.d.). *OrcaFlex—Dynamic analysis software for offshore marine systems*. Orcina. Retrieved April 18, 2022, from https://www.orcina.com/orcaflex/

Pan, Q., Mahfouz, M. Y., & Lemmer, F. (2021). Assessment of mooring configurations for the IEA 15MW floating offshore wind turbine. *Journal of Physics: Conference Series*, *2018*(1), 012030. https://doi.org/10.1088/1742-6596/2018/1/012030

Petracca, E., Faraggiana, E., Ghigo, A., Sirigu, M., Bracco, G., & Mattiazzo, G. (2022). Design and Techno-Economic Analysis of a Novel Hybrid Offshore Wind and Wave Energy System. *Energies*, *15*(8), 2739. https://doi.org/10.3390/en15082739

Pillai, A. C., Gordelier, T. J., Thies, P. R., Dormenval, C., Wray, B., Parkinson, R., & Johanning, L. (2022). Anchor loads for shallow water mooring of a 15 MW floating wind turbine — Part I: Chain catenary moorings for single and shared anchor scenarios. *Ocean Engineering*, 111816. https://doi.org/10.1016/j.oceaneng.2022.111816

Rodríguez Luis, Á., Armesto, J. A., Guanche, R., Barrera, C., & Vidal, C. (2020). Simulation of Marine Towing Cable Dynamics Using a Finite Elements Method. *Journal of Marine Science and Engineering*, *8*(2), 140. https://doi.org/10.3390/jmse8020140

Shafieefar, M., & Rezvani, A. (2007). Mooring optimization of floating platforms using a genetic algorithm. *Ocean Engineering*, *34*(10), 1413–1421. https://doi.org/10.1016/j.oceaneng.2006.10.005

Shu, H., Yao, A., Ma, K.-T., Ma, W., & Miller, J. (2018). API RP 2SK 4th Edition—An Updated Stationkeeping Standard for the Global Offshore Environment. *Day 1 Mon, April 30, 2018*, D011S004R001. https://doi.org/10.4043/29024-MS

Skandali, D., Lourens, E., & Ogink, R. H. M. (2020). Calibration of response amplitude operators based on measurements of vessel motions and directional wave spectra. *Marine Structures*, *72*, 102774. https://doi.org/10.1016/j.marstruc.2020.102774

Sound and Sea Technologies. (2009). *Advanced Anchoring and Mooring Study* [Technical Report]. Sound and Sea Technologies.

Tacx, J. (2019, November 30). Floating Wind Structures and Mooring Types. *Energy Facts*. https://www.energyfacts.eu/floating-wind-structures-and-mooring-types/

Thomsen, J., Ferri, F., & Kofoed, J. (2017). Screening of Available Tools for Dynamic Mooring Analysis of Wave Energy Converters. *Energies*, *10*(7), 853. https://doi.org/10.3390/en10070853

Turco, A. (2011a). *HYBRID - Benchmark Tests (Technical Report)* (No. 2011–004).

Turco, A. (2011b). *HYBRID - Description (Technical Report)* (No. 2011–003).

Vanegas-Cantarero, M. M., Pennock, S., Bloise-Thomaz, T., Jeffrey, H., & Dickson, M. J. (2022). Beyond LCOE: A multi-criteria evaluation framework for offshore renewable energy projects. *Renewable and Sustainable Energy Reviews*, *161*, 112307. https://doi.org/10.1016/j.rser.2022.112307

Viselli, A. M., Goupee, A. J., & Dagher, H. J. (2015). Model Test of a 1:8-Scale Floating Wind Turbine Offshore in the Gulf of Maine1. *Journal of Offshore Mechanics and Arctic Engineering*, *137*(4), 041901. https://doi.org/10.1115/1.4030381

Wang, F.-S., & Chen, L.-H. (2013). Heuristic Optimization. In W. Dubitzky, O. Wolkenhauer, K.-H. Cho, & H. Yokota (Eds.), *Encyclopedia of Systems Biology* (pp. 885–885). Springer New York. https://doi.org/10.1007/978-1-4419-9863-7_411

Wang, X., Zeng, X., Li, J., Yang, X., & Wang, H. (2018). A review on recent advancements of substructures for offshore wind turbines. *Energy Conversion and Management*, *158*, 103–119. https://doi.org/10.1016/j.enconman.2017.12.061

Weebly. (n.d.). Anchoring Systems. *Floating Wind Turbines*. Retrieved April 18, 2022, from http://floatingwindfarm.weebly.com/anchoring-systems.html

Wendland, E., & Schulz, H. (2005). Numerical experiments on mass lumping for the advection-diffusion equation. *Pesquisa e Tecnologia Minerva*, *2*, 227–233.

Weymouth, G. D. (2015). *Lily Pad: Towards Real-time Interactive Computational Fluid Dynamics*. https://doi.org/10.48550/ARXIV.1510.06886

Weymouth, G. D., & Yue, D. K. P. (2011). Boundary data immersion method for Cartesian-grid simulations of fluid-body interaction problems. *Journal of Computational Physics*, *230*(16), 6233–6247. https://doi.org/10.1016/j.jcp.2011.04.022

Williamson, C. H. K., & Govardhan, R. (2004). Vortex-Induced Vibrations. *Annual Review of Fluid Mechanics*, *36*(1), 413–455. https://doi.org/10.1146/annurev.fluid.36.050802.122128

Wiser, R., Jenni, K., Seel, J., Baker, E., Hand, M., Lantz, E., & Smith, A. (2016). Expert elicitation survey on future wind energy costs. *Nature Energy*, *1*(10), 16135. https://doi.org/10.1038/nenergy.2016.135

Woellwarth, L. (2020, November 3). Floating wind: What are the mooring options? *Energy Global*. https://www.energyglobal.com/special-reports/03112020/floating-wind-what-are-the-mooring-options/

Xue, X., & Chen, N.-Z. (2017). Fracture mechanics analysis for a mooring system subjected to tension and out-of-plane bending. *IOP Conference Series: Materials Science and Engineering*, *276*, 012036. https://doi.org/10.1088/1757-899X/276/1/012036

Zhu, H., Du, Z., Wu, J., & Sun, Z. (2022). Innovation environment and opportunities of offshore wind turbine foundations: Insights from a new patent analysis approach. *World Patent Information*, *68*, 102092. https://doi.org/10.1016/j.wpi.2021.102092

APPENDIX A1

WEIGHT AND STABILITY CALCULATIONS FOR 5 *MW* SPAR (EXCEL SHEET)

Spar Hull Size		
Do	15.00	m
Area,o	176.71	m^2
Length	100.00	m
Freeboard	15.00	m
Draft	85.00	m
Porosity	0.98	
Di (eqv)	14.70	m
Area,i	169.72	m^2
∇	15020.74	m^3
Δ	1.54E+07	kg
CoB	**-42.50**	**m**
$\rho_{seawater}$	1025.00	kg/m^3
$\rho_{magnetite}$	5000.00	kg/m^3

Fixed Ballast		
Magnetite	8.00	m
Mass	6.79E+06	kg
CoG	-81.00	m
Ixx, Iyy	1.28E+08	kg*m^2
Iz	1.83E+08	kg*m^2

Variable Ballast		
Seawater	30.51	m
Mass	5.31E+06	kg
CoG	-61.74	m
Ixx, Iyy	4.83E+08	kg*m^2
Iz	1.43E+08	kg*m^2
Seawater	30.51	m

Hull Mass		
Linear Mass	10000	kg/m
Bulkheads #	5	
Bulkhead Mass	80000	kg
Sec. Eqp. (Steel)	10000	kg/m
Mass	2400000	kg
CoG	-35.00	m
Ixx, Iyy	2.03E+09	kg*m^2
Iz	6.75E+07	kg*m^2

Mass Summary			
Part	Mass, kg	CoG, m	Moment, kg*m
Hull	2.40E+06	-35.00	-8.40E+07
Var. Ballast	5.31E+06	-61.74	-3.28E+08
Fixed Ballast	6.79E+06	-81.00	-5.50E+08
NLE+Rotor	2.30E+05	100.00	2.30E+07
Tower	6.70E+05	56.50	3.79E+07
Total	1.54E+07		-9.01E+08

WTG - 5MW		
Hub Height	100.00	m
NLE Mass	150000	kg
Rotor Mass	80000	kg
NLE to Tower	2.00	m
Mass	230000	kg
CoG	100.00	m
Ixx, Iyy	1.70E+09	kg*m^2
Iz	4.50E+06	kg*m^2
Tower Diameter	7.50	m
Tower Height	83.00	m
Tower Mass	670000	kg
Tower CoG	56.50	m

Balance of Mass		
Δ	1.54E+07	kg
Weight	1.54E+07	kg
Net	**0.00E+00**	**kg**

Stability of the Hull		
CoG	-58.50	m
CoB	-42.50	m
BG	**16.00**	**m**

APPENDIX A2

MOORING AND ANCHOR POSITION FOR 5 *MW* SPAR (EXCEL SHEET)

Mooring		
Water Depth	-1000	m
# lines	3	
Fairlead Depth	34	m
Angle to vert.	45	deg
Line Depth	-966	m
Length	1366.13	m
Radius	966	m

Chain and Polyester		
Chain Length Top	50	m
Chain Length Bottom	50	m
Poly Length	1266.13	m
Tension Factor	0.15	
Top Tension	1.98E+06	N
Poly EA/L	124789.68	N/m
Poly Stretch	15.84	m

Power Cable		
Connection Depth	-85.00	m
Angle to Vert.	45	deg
Line Depth	-1085.00	m
Length	1534.42	m
Radius	1085	m
Tension Factor	0.15	
Top Tension	7.50E+05	N

Cable and Mooring Properties							
Type	DN, in	De, m	Deqv, m	A_{eqv}, m2	Dry mass, kg/m	MBL, N	EA, N
Chain	4.7	0.12	0.24	0.0448	315	1.36E+07	1.03E+09
Polyesther	8.4	0.21	0.16	0.0201	44	1.32E+07	1.58E+08
Power Cable	4	0.10		0.0081	150	5.00E+06	5.00E+08

Vertical Forces			
Type	# Lines	Total Top Tension, N	Vert Force, kg
Mooring	3	5.93E+06	6.05E+05
Power Cable	1	7.50E+05	7.65E+04
Total		6.68E+06	6.81E+05

Coordinates				
Azimuth	X	Y	Z	
	R	7.5	m	
0	7.5	0	-34	Fairleads
120	-3.75	6.5	-34	
240	-3.75	-6.5	-34	
0	973.5	0	-1000	Anchors
120	-483	836.58	-1000	
240	-483	-836.58	-1000	

APPENDIX B

MODIFIED ANCIENT SWIMMER CLASS (LILY PAD)

```
class AncientSwimmer extends BodyUnion{
  float x0,y0,L,s,lead,St,pamp;

  AncientSwimmer( float x0, float y0, float L, float s, float lead, float St, Window view){
//  make geometry
    super(new EllipseBody(x0,y0,L,0.707213578,view),      // front foil
        new CircleBody(x0+s,y0,0.000001,view));    // back foil

// save parameters
    this.L = L;                  // Foil coord
    this.x0 = x0; this.y0 = y0;          // Starting position of front foil
    this.s = s; this.lead = lead;         // Spacing and phase lag
    this.St = St;                 // Strouhal number of motion

// set pitch amplitude to get 10 degree AOA
  // pamp = atan(PI*St)-PI/18.;

// set initial state
    bodyList.get(0).follow(kinematics(0,0,0),new PVector());
    bodyList.get(1).follow(kinematics(s,lead,0),new PVector());

// set color
    bodyColor=color(255);
  }

// define the foil motion
  PVector kinematics(float s, float lead, float t){
    float phase = PI*St*t/L+lead;        // phase
    return new PVector(x0+s,            // x position
            y0-L*sin(phase),    // y position
```

```
              pamp*cos(phase));   // pitch position
  }
  PVector dkinematics(float lead, float t, float dt){
    float phase = PI*St*t/L+lead;         // phase
    return new PVector(0,                // dx
               -cos(phase)*PI*St*dt,   // dy
               -pamp*sin(phase)*PI*St/L*dt); // dphi
  }


// get pressure force of both foils
  PVector[] pressForces(Field p){
    PVector f0 = bodyList.get(0).pressForce(p);
    return new PVector[]{f0};
  }
}
```

APPENDIX C

COMPLETE OPTIMIZATION SCRIPT

```
# <fmiModelDescription fmiVersion="2.1" modelName="orcapy-preprocess2" guid="">
#    <ModelVariables>

#       <Variable name="UPP_L" valueReference="0" causality="parameter">
#          <Real/>
#       </Variable>

#       <Variable name="UPC1_L" valueReference="1" causality="parameter">
#          <Real/>
#       </Variable>

#       <Variable name="UPC2_L" valueReference="2" causality="parameter">
#          <Real/>
#       </Variable>

#       <Variable name="AZEnd1" valueReference="3" causality="parameter">
#          <Real/>
#       </Variable>

#       <Variable name="BXEnd1" valueReference="4" causality="parameter">
#          <Real/>
#       </Variable>

#       <Variable name="ADec1" valueReference="5" causality="parameter">
#          <Real/>
#       </Variable>

#       <Variable name="BDec1" valueReference="6" causality="parameter">
#          <Real/>
#       </Variable>
```

```python
#    </ModelVariables>

# </fmiModelDescription>

import OrcFxAPI
import os
import pandas as pd
import numpy as np
import multiprocessing
import logging
import sys
import glob


# Processing Phase
class Worker(multiprocessing.Process):
    myJobs = []
    def setJobs(self, jobList):
        self.myJobs = jobList
    @staticmethod
    def changedExtensionFileName(oldFileName, newExtension):
        return '.'.join((os.path.splitext(oldFileName)[0], newExtension))
    def run(self):
        model = OrcFxAPI.Model(threadCount=1)
        for job in self.myJobs:
            try:
                print('%s starting' % job)
                sys.stdout.flush()
                model.LoadData(job)
                model.CalculateStatics()
                model.RunSimulation()
                model.SaveSimulation(self.changedExtensionFileName(job, 'sim'))
                print('%s completed' % job)
                sys.stdout.flush()
            except OrcFxAPI.DLLError as err:
```

```python
                print('%s ERROR: %s' % (job, err))
                sys.stdout.flush()
                with open(self.changedExtensionFileName(job, 'FAIL'), 'w') as f:
                    f.write('%s error: %s' % (job, err))
                    f.close()
if __name__ =='__main__':
    # Pre-processing Phase
    directory = os.getcwd()
    for files in os.listdir(directory):
        if files.endswith('.dat') & files.startswith('OPT'):
            path = os.path.join(directory,files)
            model = OrcFxAPI.Model()
            model.LoadData(path)
            line = model['Mooring1']
            line.NumberOfSections = 3
            line.Length[0] = UPC1_L
            line.Length[1] = UPP_L
            line.Length[2] = UPC2_L
            line.EndAZ = AZEnd1
            line.EndBX = BXEnd1
            line.EndADeclination = ADec1
            line.EndBDeclination = BDec1
            model.SaveData(path)
        else:
            continue
    multiprocessing.log_to_stderr()
    logger = multiprocessing.get_logger()
    logger.setLevel(logging.INFO)
    corecount = 32 # edit this value to the number of cores you want to use on your computer
    fileList = []
    workers = []
    for datfile in glob.glob('*.dat'): # edit this to *.sim, *.dat, *.yml or other filter to select the
files you want to run
        fileList.append(datfile)
```

```python
        chunkSize = int(len(fileList) / corecount)
        chunkRemainder = int(len(fileList) % corecount)
        print('%s jobs found, dividing across %s workers - %s each remainder %s' %
(str(len(fileList)), str(corecount), chunkSize, chunkRemainder))
        start = 0
        for coreNum in range(0, corecount):
            worker = Worker()
            workers.append(worker)
            end = start + chunkSize
            if chunkRemainder>0:
                chunkRemainder -= 1
                end += 1
            if end>len(fileList):
                end = len(fileList)
            worker.setJobs(fileList[start:end])
            worker.start()
            start = end
            if start>=len(fileList):
                break
        for worker in workers:
            worker.join()
        print('Done...')


        # # Post-Processing Phase
        meanEffListA = np.zeros(505)
        meanEffListB = np.zeros(505)
        hours = np.array([#add the hours/year here])
        gen = (files for files in (os.listdir(directory)) if files.endswith('.sim') &
files.startswith('OPT'))
        i=0
        for files in gen:
            try:
                path = os.path.join(directory,files)
```

```
        model1 = OrcFxAPI.Model(path)
        model1.LoadSimulation
        line1 = model1['Mooring1']
        ResultsEndA = line1.TimeHistory('Effective Tension',
OrcFxAPI.SpecifiedPeriod(0.0,600.0), OrcFxAPI.oeEndA)
        meanEffTenA = np.mean(ResultsEndA)
        meanEffListA[i] = meanEffTenA
        ResultsEndB = line1.TimeHistory('Effective Tension',
OrcFxAPI.SpecifiedPeriod(0.0,600.0), OrcFxAPI.oeEndB)
        meanEffTenB = np.mean(ResultsEndB)
        meanEffListB[i] = meanEffTenB
        i=i+1
    except:
        print(files)
  opt1 = sum(meanEffListA*hours)
  opt2 = sum(meanEffListB*hours)
```